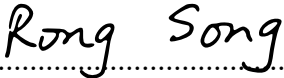




Universitetet  
i Stavanger

Faculty of Science and Technology

## MASTER'S THESIS

Study program/ Specialization : <b>Offshore Technology/ Marine and Offshore Technology</b>	Spring semester, 2019 <b>Open / <del>Restricted access</del></b>
Writer: <b>Rong Song</b>	 ..... (Writer's signature)
Faculty Supervisor: <b>Dr. Charlotte Obhrai</b> Co-Supervisor(s): <b>Dr. Rieska Mawarni Putri</b>	
Thesis title: <b>The Impact of Non-Surface Layer Wind Profiles on the Loads and Motions of Offshore Wind Turbines</b>	
Credit (ECTS) : <b>30</b>	
Keywords: <i>Atmosphere Boundary Layer; Wind Profiles; Damage Equivalent Load (DEL); Offshore Floating Wind Turbine Motion</i>	Pages : 124 Stavanger, 15 <sup>th</sup> July 2019

## **Acknowledgement**

I would like to express my deepest gratitude to my supervisor Dr. Charlotte Obhrai who had provided me support and guidance. She taught me how to write a thesis correctly and efficiently and answered my every question patiently. This thesis could not reach its present form without her consistent and illuminating instruction.

Furthermore, I would also like to appreciate Dr. Rieska Mawarni Putri for helping me with doing simulation by SIMA software as well as for the quick responses whenever I needed.

Finally, I am grateful to all my friends who have helped me with this thesis.

# **Abstract**

This master thesis analyzes the influence of wind speed and variation in mean wind profiles on the loads and motions of offshore wind turbine. Primarily, fully-scale measurement data from the research platform FINO3 in North Sea is collected and analyzed, to derive exponent coefficients which are then used to simulate mean wind profiles under different stability conditions. Thereinto, stability classification is classified by the Richardson number and exponent coefficients are calculated by the power law following IEC standards. The SIMA software is used to simulate the loads and motions of a 5MW spar floating wind turbine. The dependence of the fatigue load (damage equivalent load) of several turbine components and the motions of wind turbine for varying wind profile is assessed.

**Key words: Atmosphere Boundary Layer; Wind Profiles; Damage Equivalent Load (DEL); Offshore Floating Wind Turbine Motion**

# Contents

<b>List of Abbreviations .....</b>	<b>iv</b>
<b>Symbols .....</b>	<b>v</b>
<b>List of Figures .....</b>	<b>viii</b>
<b>List of Tables .....</b>	<b>xii</b>
<b>1. Introduction .....</b>	<b>1</b>
<b>1.1 Background.....</b>	<b>1</b>
<b>1.2 Research Platform.....</b>	<b>3</b>
<b>2. Theoretical Background.....</b>	<b>7</b>
<b>2.1 Atmospheric Boundary Layer .....</b>	<b>7</b>
<b>2.2 Atmospheric Stability .....</b>	<b>8</b>
2.2.1 Monin-Obukhov Length .....	10
2.2.2 Richardson Number .....	11
<b>2.3 Turbulence .....</b>	<b>13</b>
2.3.1 Turbulence Intensity .....	13
2.3.2 Turbulence Model.....	15
<b>2.4 Wind Profile .....</b>	<b>16</b>
2.4.1 Power Law Wind Profile .....	16
2.4.2 Logarithmic Wind Profile .....	17
2.4.3 Extended Surface Layer Wind Profile .....	19
<b>2.5 Wind Turbine Load .....</b>	<b>22</b>

2.5.1 The Tower Base Fore-Aft Loads .....	27
2.5.2 The Blade Loads .....	27
2.5.3 Rotor Loads .....	28
<b>3. Modelling of Floating Wind Turbine by SIMA .....</b>	<b>29</b>
<b>3.1 SIMA Software .....</b>	<b>29</b>
3.1.1 Defining Coordinate System.....	30
<b>3.2 Turbulence Wind Field Input .....</b>	<b>32</b>
<b>4. Coupled RIFLEX-SIMO Simulation for Floating Wind Turbine .....</b>	<b>34</b>
<b>4.1 General .....</b>	<b>34</b>
<b>4.2 Wave Inputs .....</b>	<b>34</b>
<b>4.3 Offshore Wind Turbine Properties .....</b>	<b>35</b>
<b>4.4 Wind Turbulence Inputs .....</b>	<b>36</b>
<b>4.5 Wind Input.....</b>	<b>37</b>
4.5.1 Wind Input – Turbulence Box .....	40
<b>4.6 Simulation Results.....</b>	<b>41</b>
4.6.1 Eigenfrequencies.....	41
4.6.2 Damage Equivalent Loads .....	43
4.6.3 Tower Base Fore-Aft Loads and Moment .....	43
4.6.4 Blades Root Flapwise Loads and Moment .....	48
4.6.5 Blades Root Edgewise Loads and Moment .....	53
4.6.6 Tower Top Torsion and Yaw Moment .....	57
4.6.7 Rotor Loads and Moment .....	62
4.6.8 Translational Motion .....	66
4.6.9 Rotational Motion .....	72

<b>5. Discussion and Conclusion</b> .....	<b>78</b>
<b>5.1 Discussion</b> .....	<b>78</b>
5.1.1 Wind Turbine Damage Equivalent Loads .....	78
5.1.2 Wind Turbine Motions .....	86
<b>5.2 Conclusion</b> .....	<b>89</b>
<b>5.3 Future Work</b> .....	<b>90</b>
<b>Reference</b> .....	<b>91</b>
<b>Appendix A</b> .....	<b>A-1</b>
<b>A.1 Mooring Lines Loads</b> .....	<b>A-1</b>
<b>A.2 The Results of Simulation without Turbulence</b> .....	<b>A-11</b>
A.2.1 Damage Equivalent loads .....	A-11
A.2.2 Comparison of Tower Base Fore-Aft Moment.....	A-15

## List of Abbreviations

ABL	Atmospheric Boundary Layer
DALR	Dry Adiabatic Lapse Rate
DEL	Damage Equivalent Load
ELR	Environmental Lapse Rate
FINO	Forschungsplattformen in Nord-und Ostsee
GL	Germanischer Lloyd
LiDAR	Light Detection and Ranging
MABL	Marine Atmospheric Boundary Layer
MOST	Monin-Obukhov similarity theory
NORCOWE	Norwegian Center for Offshore Wind Energy
NREL	National Renewable Energy Laboratory
OBLEX-F1	Offshore Boundary Layer Experiment at FINO1
OC3	Offshore Code Comparison Collaboration
PBL	Planetary Boundary Layer
PDF	Probability Density Function
SL	Surface Layer
TI	Turbulence Intensity
Univ. Kiel	The R&D Centre Fachhochschule Kiel University of Applied Sciences GmbH

## Symbols

$\overline{u}_*$	Mean friction velocity
$\overline{z}_0$	Mean roughness length
$\frac{\Delta u}{\Delta z}$	Vertical gradient of the horizontal wind speed
$\frac{\Delta \theta}{\Delta z}$	Vertical density gradient
$A_c$	Charnock constant
$I_{15}$	Average value of hub height turbulence intensity
$l_{MBL}$	The length scale of the middle boundary layer
$l_{SL}$	Length scale in the surface layer
$l_{UBL}$	The length scale of the upper boundary layer
$L_x$	The length of turbulence box in the long direction
$L_y$	The length of turbulence box in the cross wind direction
$L_z$	The length of turbulence box in the vertical wind direction
$M_{edgewise}$	The edge-wise bending moment
$M_{flapwise}$	The flap-wise bending moment
$m_n$	The spectral moments
$M_x$	The moment along the x-axis
$M_y$	The moment along the y-axis
$M_z$	The moment along the z-axis
$N_F$	The number of cycles at failure
$N_x$	The number of grid points in the long wind direction
$N_y$	The number of grid points in the cross wind direction
$N_z$	The number of grid points in the vertical wind direction
$Q_0$	Surface heat flux

$Ri_b$	Bulk Richardson Number
$T_{air}$	Absolute virtual temperature and
$\bar{T}$	Mean temperature
$u_*$	Friction velocity
$u_*$	Surface friction velocity
$u_{*0}$	Friction velocity near the ground
$U_{air,z}$	The change in horizontal wind components across that same layer
$\bar{U}$	Average longitudinal wind speed
$V_{hub}$	Wind speed at the hub height
$x_m$	A mean frequency
$z_0$	Roughness length
$z_{hub}$	Hub height
$z_i$	Boundary-layer depth
$\alpha_c$	Charnock's parameter
$\sigma_1$	Standard deviation
$\phi_m$	Atmospheric stability correction
$\Psi_m$	Stability-dependent function
$\Delta u_*$	Friction velocity deviation of each wind speed profile from the mean value
$\Delta \theta_v$	Virtual potential temperature
a	Empirical constant defined for each wind turbine class
$dx$	The grid spacing in the long wind direction
$dy$	The grid spacing in the cross wind direction
$dz$	The grid spacing in the vertical wind direction
$E[D]$	The expected amount of accumulated damage
$E[N]$	The expected number of cycles

$E[P]$	The expected number of peaks per unit time
$g$	Acceleration of gravity
$g/T_0$	Buoyancy parameter
$H_s$	Significant Wave Height (m)
$I$	Turbulence Intensity
$K$	The second material parameter which is proportional to the number of cycles
$k$	Von Kármán constant
$l$	Length scale
$L$	Monin-Obukhov Length
$m$	Wöhler coefficient
$N_b$	Number of blades
$N_b P$	The Blade Passing Frequency
$R_i$	Gradient Richardson Number
$S$	Each cycle of a constant stress range amplitude
$T$	Seconds
$T_0$	Virtual reference temperature
$T_p$	Peak Period
$u$	Horizontal wind velocity
$V(z)$	Wind speed at height $z$
$z$	Height over the ground
$Z$	A normalized stress range
$\alpha$	Power law exponent
$\gamma$	The expected ratio of zero-crossings to peaks
$\theta$	Potential temperature

## List of Figures

Figure 1.1 FINO Platforms in the North Sea and Baltic Sea [2] .....	2
Figure 1.2 The Top View of Met-mast on FINO1 and FINO3 [2].....	4
Figure 1.3 Mast Design and Measurement System DistributionFINO1 (a) and FINO3 (b) .....	5
Figure 2.1 The Schematic of Atmospheric Stabilities. [9] .....	9
Figure 3.1 Modelling of Floating Wind Turbine in SIMA Software .....	29
Figure 3.2 Coordinate System of Floating Wind Turbine [21] .....	30
Figure 3.3 Blades Coordinate System [22].....	31
Figure 3.4 A 3D Turbulence Box [22] .....	32
Figure 4.1 Normalized Mean Wind Speed Profile for Each Stability Class .....	37
Figure 4.2 The Eigenfrequencies for the OC3-Hywind System [23] .....	42
Figure 4.3 Tower Base Fore-Aft Damage Equivalent Loads under Each Stability Class for 8 m/s, 11.4 m/s and 15 m/s.....	44
Figure 4.4 Normalized Tower Base Fore-Aft Damage Equivalent Loads under Each Stability Class for 8 m/s, 11.4 m/s and 15 m/s .....	45
Figure 4.5 Tower Base Fore-Aft Moment Spectral Densities at 8 m/s (a), 11.4 m/s (b) and 15 m/s (c).....	47
Figure 4.6 Blade Root Flapwise Damage Equivalent Loads under Each Stability Class for 8 m/s, 11.4 m/s and 15 m/s.....	48
Figure 4.7 Normalized Blade Root Flapwise Damage Equivalent Loads under Each Stability Class for 8 m/s, 11.4 m/s and 15 m/s .....	49
Figure 4.8 Blades Root Flapwise Spectral Densities at 8 m/s (a), 11.4 m/s (b) and 15 m/s (c) .....	52
Figure 4.9 Blades Root Edgewise Damage Equivalent Loads under Each Stability Class for 8 m/s, 11.4 m/s and 15 m/s.....	53

Figure 4.10 Normalized Blades Root Edgewise Damage Equivalent Loads under Each Stability Class for 8 m/s, 11.4 m/s and 15 m/s ..... 54

Figure 4.11 Blades Root Edgewise Spectral Densities at 8 m/s (a), 11.4 m/s (b) and 15 m/s (c) ..... 56

Figure 4.12 Tower Top Torsion Damage Equivalent Loads under Each Stability Class for 8 m/s, 11.4 m/s and 15 m/s ..... 57

Figure 4.13 Normalized Tower Top Torsion Damage Equivalent Loads under Each Stability Class for 8 m/s, 11.4 m/s and 15 m/s ..... 58

Figure 4.14 Tower Top Yaw Moment Spectral Densities at 8 m/s (a), 11.4 m/s (b) and 15 m/s (c) ..... 61

Figure 4.15 Rotor Damage Equivalent Loads under Each Stability Class for 8 m/s, 11.4 m/s and 15 m/s ..... 62

Figure 4.16 Normalized Rotor Damage Equivalent Loads under Each Stability Class for 8 m/s, 11.4 m/s and 15 m/s ..... 63

Figure 4.17 Rotor Spectral Densities at 8 m/s (a), 11.4 (b) and 15 m/s (c)4.6.8  
Mooring Lines Loads and Moment ..... 65

Figure 4.18 Surge Motion Spectral Densities at 8 m/s, 11.4 m/s and 15 m/s ..... 67

Figure 4.19 Comparison of Maximum and Minimum Surge Rotation under Each Stability for 8m/s, 11.4 m/s and 15 m/s ..... 67

Figure 4.20 Sway Motion Spectral Densities at 8 m/s, 11.4 m/s and 15 m/s ..... 68

Figure 4.21 Comparison of Maximum and Minimum Sway Rotation under Each Stability for 8m/s, 11.4 m/s and 15 m/s ..... 69

Figure 4.22 Heave Motion Spectral Densities at 8 m/s, 11.4 m/s and 15 m/s ..... 71

Figure 4.23 Comparison of Maximum and Minimum Heave Motion under Each Stability for 8m/s, 11.4 m/s and 15 m/s ..... 71

Figure 4.24 Roll Motion Spectral Densities at 8 m/s, 11.4 m/s and 15 m/s ..... 73

Figure 4.25 Comparison of Maximum and Minimum Roll Rotation under Each Stability for 8 m/s, 11.4 m/s and 15 m/s .....	73
Figure 4.26 Yaw Motion Spectral Densities at 8 m/s, 11.4 m/s and 15 m/s .....	75
Figure 4.27 Comparison of Maximum and Minimum Yaw Rotation under Each Stability for 8m/s, 11.4 m/s and 15 m/s .....	75
Figure 4.28 Pitch Motion Spectral Densities at 8 m/s, 11.4 m/s and 15 m/s .....	76
Figure 4.29 Comparison of Maximum and Minimum Pitch Rotation under Each Stability for 8 m/s, 11.4 m/s and 15 m/s .....	77
Figure 5.1 Tower Base Fore-Aft Damage Equivalent Loads without Turbulence under Each Stability for 8 m/s, 11.4 m/s and 15 m/s .....	80
Figure 5.2 Comparison of Tower Base Fore-Aft Moment Spectral Densities with Turbulence and without Turbulence under Each Stability for 11.4 m/s .....	80
Figure 5.3 Tower Top Damage Equivalent Loads without Turbulence under Each Stability for 8 m/s, 11.4 m/s and 15 m/s .....	83
Figure 5.4 Comparison of Tower Top Spectral Densities with Turbulence and without Turbulence at 8 m/s (a), 11.4 m/s (b) and 15 m/s (c) .....	85
Figure 5.5 Yaw Motion Spectral Densities under Each Stabilities at 8 m/s (a), 11.4 m/s (b) and 15 m/s (c) .....	88
Figure A.1 Mooring Line 1 Damage Equivalent Loads under Each Stability Class for 8 m/s, 11.4 m/s and 15 m/s .....	A-1
Figure A.2 Mooring Line 2 Damage Equivalent Loads under Each Stability Class for 8 m/s, 11.4 m/s and 15 m/s .....	A-2
Figure A.3 Mooring Line 3 Damage Equivalent Loads under Each Stability Class for 8 m/s, 11.4 m/s and 15 m/s .....	A-2
Figure A.4 Normalized Mooring Line 1 Damage Equivalent Loads under Each Stability Class for 8 m/s, 11.4 m/s and 15 m/s .....	A-3

Figure A.5 Normalized Mooring Line 2 Damage Equivalent Loads under Each Stability Class for 8 m/s, 11.4 m/s and 15 m/s ..... A-4

Figure A.6 Normalized Mooring Line 3 Damage Equivalent Loads under Each Stability Class for 8 m/s, 11.4 m/s and 15 m/s ..... A-4

Figure A.7 Mooring Line 1 Tension Spectral Densities at 8 m/s (a), 11.4 m/s (b) and 15 m/s (c) ..... A-7

Figure A.8 Mooring Line 2 Tension Spectral Densities at 8 m/s (a), 11.4 m/s (b) and 15 m/s (c) ..... A-9

Figure A.9 Mooring Line 3 Tension Spectral Densities at 8 m/s (a), 11.4 m/s (b) and 15 m/s (c) ..... A-10

Figure A.10 Blades Root Flapwise Damage Equivalent Loads without Turbulence under Each Stability for 8 m/s, 11.4 m/s and 15 m/s ..... A-11

Figure A.11 Blades Root Edgewise Damage Equivalent Loads without Turbulence under Each Stability for 8 m/s, 11.4 m/s and 15 m/s ..... A-12

Figure A.12 Rotor Damage Equivalent Loads without Turbulence under Each Stability for 8 m/s, 11.4 m/s and 15 m/s ..... A-12

Figure A.13 Mooring Line 1 Damage Equivalent Loads without Turbulence under Each Stability for 8 m/s, 11.4 m/s and 15 m/s ..... A-13

Figure A.14 Mooring Line 2 Damage Equivalent Loads without Turbulence under Each Stability for 8 m/s, 11.4 m/s and 15 m/s ..... A-13

Figure A.15 Mooring Line 3 Damage Equivalent Loads without Turbulence under Each Stability for 8 m/s, 11.4 m/s and 15 m/s ..... A-14

Figure A.16 Comparison of Tower Base Fore-Aft Moment Spectral Densities with Turbulence and without Turbulence under Each Stability for 8 m/s ..... A-15

Figure A.17 Comparison of Tower Base Fore-Aft Moment Spectral Densities with Turbulence and without Turbulence under Each Stability for 15 m/s ..... A-15

## List of Tables

Table 1.1 Specification of Research Platforms FINO1 and FINO3 [2] .....	3
Table 1.2 Measurement Devices Installed at FINO1 and FINO3 [4, 5].....	6
Table 2.1 Classification of Stability According to Obukhov Lengths [10].....	10
Table 2.2 Classification of Stability According to Gradient Richardson Number [5] .....	11
Table 2.3 Classification of Stability According to Bulk Richardson Number [12]	12
Table 4.1 Wave Input Parameters.....	34
Table 4.2 Summary of Properties for the NREL 5-MW Baseline Wind Turbine [23].....	35
Table 4.3 Turbulence Input Parameters form IEC Standard [13].....	36
Table 4.4 The Power Law Exponent for Each Stability Class .....	38
Table 4.5 Mean Speed Factors (Normalized Wind Speeds) Imported in SIMA Software .....	39
Table 4.6 3D Turbulence Box Input .....	40
Table 4.7 Frequencies of the Rotating Blades .....	41
Table 4.8 The Natural Frequency of the Platform Motions .....	43
Table 4.9 Percentages of Tower Base Fore-Aft Damage Equivalent Loads Relative to Neutral Stability at 8 m/s .....	45
Table 4.10 Percentages of Blades Root Flapwise Damage Equivalent Loads Relative to Neutral Stability .....	50
Table 4.11 Percentages of Blade Root Edgewise Damage Equivalent Loads Relative to Neutral Stability .....	54
Table 4.12 Percentages of Tower Top Torsion Damage Equivalent Loads Relative to Neutral Stability.....	59

Table 4.13 Percentages of Rotor Damage Equivalent Load Relative to Neutral Stability .....	63
Table A.1 Percentages of Mooring Line Damage Equivalent Loads Relative to Neutral Stability .....	A-5

# 1. Introduction

## 1.1 Background

With the development of technology and economy, wind energy has played a significant role in the renewable energy field in Europe. Especially, offshore wind power, which has greater potential than onshore but more challenges due to the hostile environment. Capturing the higher wind speeds is the primary purpose to develop offshore wind energy to produce more power. However, there is no rich experience of state of the art offshore wind turbines (0-300 m) designed in the MABL (Marine Atmosphere Boundary Layer) nowadays.

In the North Sea, the German federal government decided to establish two research platforms (FINO1 and FINO3) which aim to investigate conditions for offshore wind energy generation and research since January 2002. FINO1 is located 45 kilometers north of Borkum and FINO3 is situated at 80 km west of Sylt, shown in *Figure 1.1* [1]. Further, to enhance our understanding of the complex interaction between wind shear, atmospheric stability and turbulence characteristics offshore, the offshore measurement campaign OBLEX-F1 (Offshore Boundary Layer Experiment at FINO1) was also initiated. NORCOWE (Norwegian Center for Offshore Wind Energy) and several international partner institutions conducted on this campaign and the data obtained from marine and atmospheric instruments. Meanwhile, the campaign took an intensive and detailed study of the MABL under various synoptic conditions including modelling the wind loads by characteristic wind profiles and determining the impact on the motions and fatigue of offshore wind turbines. Furthermore, a large number of FINO3 research projects have followed, leading to

the expectations of new and available results, especially in wave propagation, wind shear and other areas of innovation. [1]

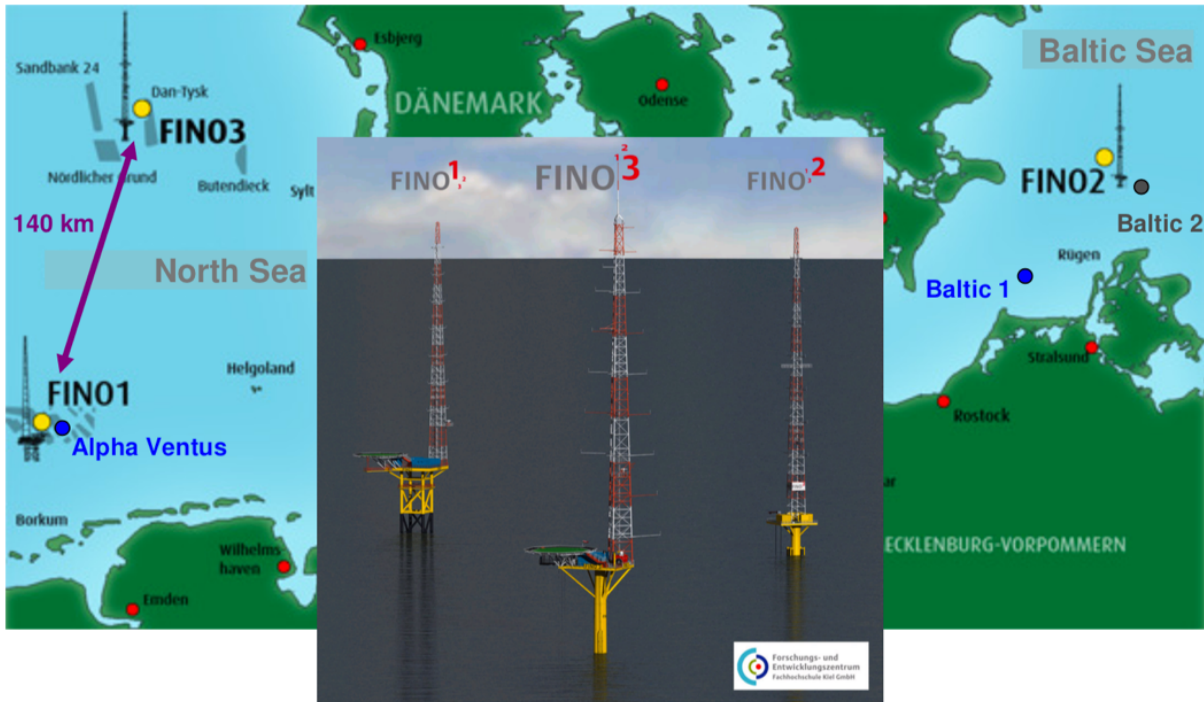


Figure 1.1 FINO Platforms in the North Sea and Baltic Sea [2]

## 1.2 Research Platform

Research platform FINO1 was operated by Germanischer Lloyd (GL) from 2003 to 2011. Then, the R&D Centre Fachhochschule Kiel University of Applied Sciences GmbH has taken over its operation and maintenance since 2012, which has also been the operator for FINO3 since the end of August 2009. [1] The specification of both research platforms illustrates at *Table 1.1*.

*Table 1.1 Specification of Research Platforms FINO1 and FINO3 [2]*

Research Platform	O&M	In Service	Mast Shape	Height	Water Depth	Distance To Coast	Foundation	Platform size	Heli Pad
FINO 1	GL Univ. Kiel	Sep 2003	Square	101m	28m	45km	Jacket	16×16m	yes
FINO 3	Univ. Kiel	Sep 2009	Triangular	106m (120m)	23m	80km	Monopile	13×13m	yes

Obviously, FINO3 is set up much further from the coast than FINO1, increasing the meteorological mast size due to increasing modern wind turbine hub height, and changing the shape of met-mast into the triangular base with three booms where three cup anemometers are installed at the end of the booms so as to minimize the significant flow distortion (shown in *Fig 1.2*), compared to FINO1. Furthermore, the location of cup anemometers relative to the mast is recommended in an International Electrotechnical Committee (IEC) standard so that the accuracy of measurement data on the platform can be ensured. Fabre et al. (2014) suggested

much shorter boom lengths are arranged for the triangular mast to place the anemometers outside the flow distortion created by the met-mast structure [3].

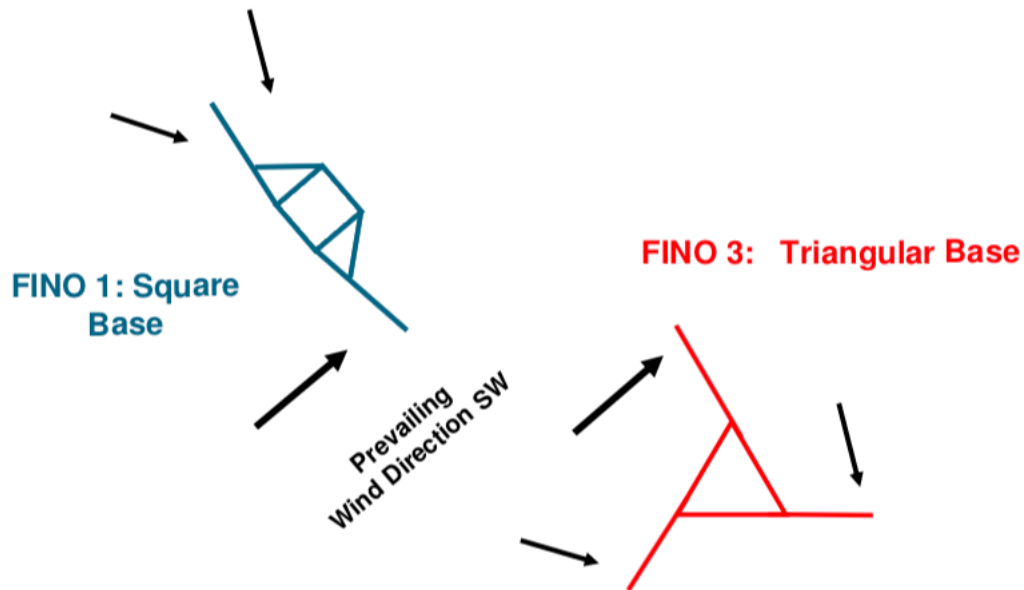


Figure 1.2 The Top View of Met-mast on FINO1 and FINO3 [2]

Different measurement equipment installed at research platforms in several heights for wind speed, wind direction, humidity, air pressure, air temperature and precipitation, as *Figure 1.3* shown, such as cup anemometer, wind vane, sonic anemometer, 3D scanning LiDAR and radiometer. The exact position, heights and accuracy of these devices on the platform FINO1 and FINO3 are shown in *Table 1.2*.

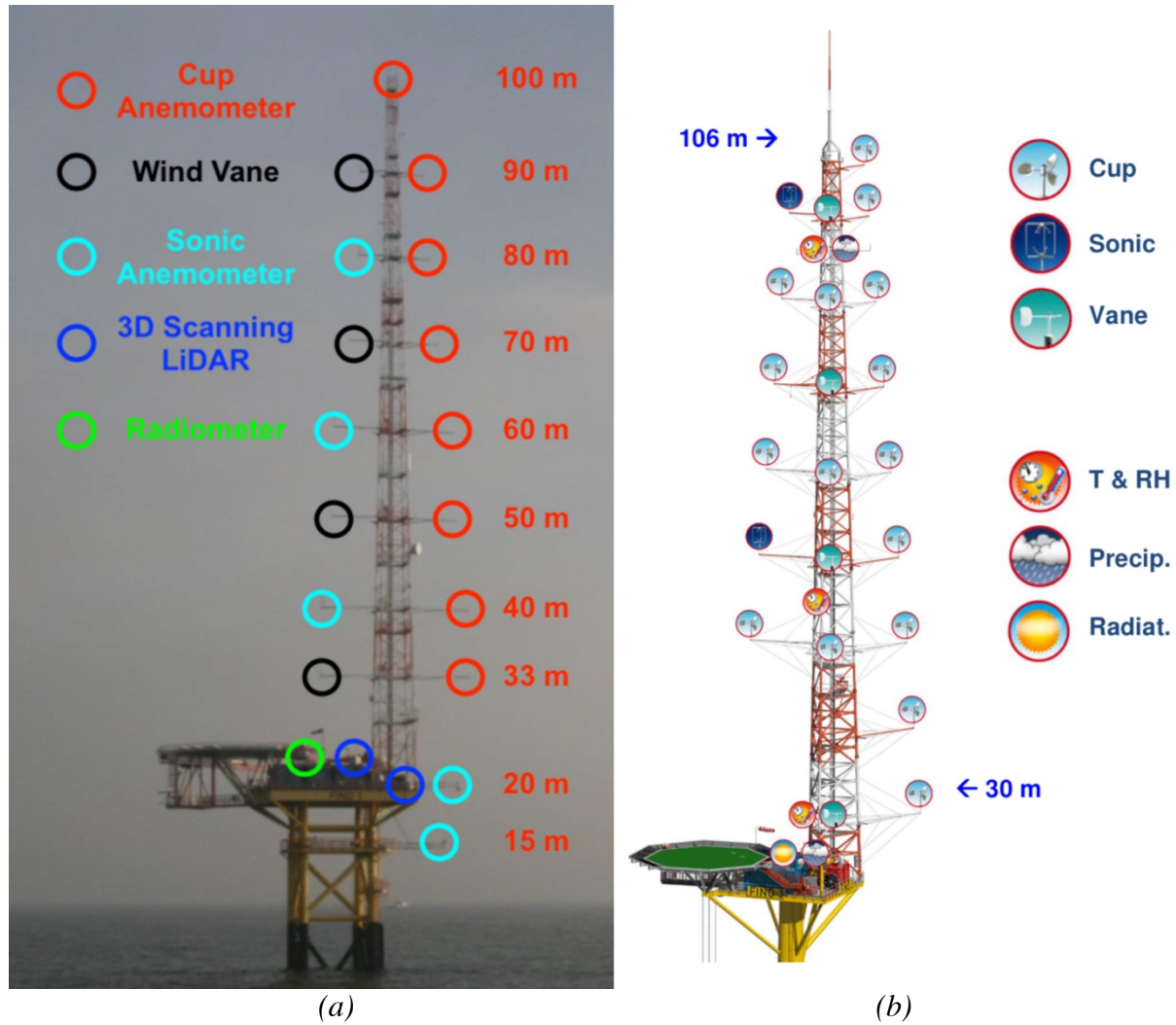


Figure 1.3 Mast Design and Measurement System Distribution FINO1 (a) and FINO3 (b)

Table 1.2 Measurement Devices Installed at FINO1 and FINO3 [4, 5]

Measurement Device	Position and Height		Accuracy	
	FINO1	FINO3	FINO1	FINO3
Cup Anemometer	135° - 143° from 100 m to 30 m Every 10 m	From 90m to 30m Every 10 m 106m also	± 0.1 m/s	A variation in u of more than 10%
Wind Vane	307° - 315° 90m, 70m, 50m, 33m	100m, 80m, 60m, 30m	± 2°	More than 10° between consecutive values
Sonic Anemometer	308° - 311° 80m, 60m, 40m, 20m, 15m	100m, 60m	± 0.01 m/s	A variation in u of more than 10%
3D Scanning LiDAR (Leosphere Windcube 100S)	On platform 25 m	On platform 25 m	± 0.2 m/s	A variation in u of more than 10%
Humidity Probe	Inside met-mast 101m, 52m, 34.5m	Inside met-mast 95m, 55m, 30m	± 2%	
Pressure Sensor	On Platform 25m	On Platform 25m	± 0.1 hPa	
Radiometer (HATPRO-RG3)	On platform 25m	On platform 25m	Temperature ± 6 K ... ± 1 K Absolute Humidity ±0.4 g/m <sup>3</sup>	A variation in temperature of more than 0.5°

## 2. Theoretical Background

### 2.1 Atmospheric Boundary Layer

Encyclopedia of Britannica defines that the atmospheric boundary layer (ABL), also called planetary boundary layer (PBL), where the surface influences temperature, moisture and wind through the turbulent transfer of air mass. As a result of surface friction, wind in the ABL is usually weaker and tends to blow toward areas of low pressure. [6]

The whole atmosphere entirely has more than 100 km thickness. A layer called troposphere hardly take up more than the bottom 10km where weather systems, including storms and hurricanes, happen. Unlike the quiet stratosphere distributes only from 10 to 50 km altitude, the troposphere is in a permanent state of turmoil. The Atmospheric boundary layer (ABL), lies within the troposphere and nearest Earth's surface, with around 1 km thickness (30 to 1000 m) and the remainder of the air in troposphere is called Free Atmosphere [7]. The interaction between the air and the ground presents in mechanical and thermal ways. The former is caused by the friction, exerted by the surface, results in wind shear which creates turbulence. The latter arises from the solar radiation, and there is diurnal intermittency of thermal contact because of day and night alternation.

The lowest part of 10% of the ABL is Surface Layer (SL) where the variables of turbulence fluxes and stress are less than 10% of their magnitude and they can be assumed to be relatively constant [7]. Marine Atmospheric Boundary Layer (MABL) literally means the boundary layer over oceans. Certainly, the MABL is the major research field for offshore wind turbines in this paper.

## 2.2 Atmospheric Stability

Atmospheric stability is a valuable property to describe the ABL and the base of the derivation of different wind profiles and simulations, having a significant influence on the wind energy and the fatigue load calculation as well. The basic concept of atmospheric stability is that an air parcel, with a higher temperature than the surrounding environment, will continue to rise. Conversely, the temperature of the surrounding environment is higher than the air parcel which will continue to sink. That is, atmospheric stability refers to the tendency for air parcels to move vertically.

The atmospheric stability can be divided into two types: (a) static stability and (b) dynamic stability. The static stability is the ability of air masses at rest to become turbulent or laminar (the atmospheric flow with stable stratification) due to the effect of buoyancy. The dynamic stability is the ability of air masses to resist or recover from finite disturbance of a stable state [8].

Based on the basic concept, buoyancy-generated turbulence regards as the turbulence due to atmospheric stability which is classified into three states (shown in *Figure 2.1*):

- Stable

An atmosphere where the environmental temperature is smaller than an air parcel's temperature. This air parcel is heavier and forced to sink down again, although it tries to rise up because of the lower temperature. In this condition, the air parcel under an equilibrium state and atmospheric stability is stable.

- Neutral

An atmosphere where the environmental temperature is equal to an air parcel's temperature. This air parcel remains at that height due to net buoyancy. In this condition, atmospheric stability is neutral.

- Unstable

An atmosphere where the environmental temperature is higher than an air parcel's temperature. This air parcel moves out of its equilibrium position and tends to rise or fall due to buoyancy. In this condition, atmospheric stability is unstable.

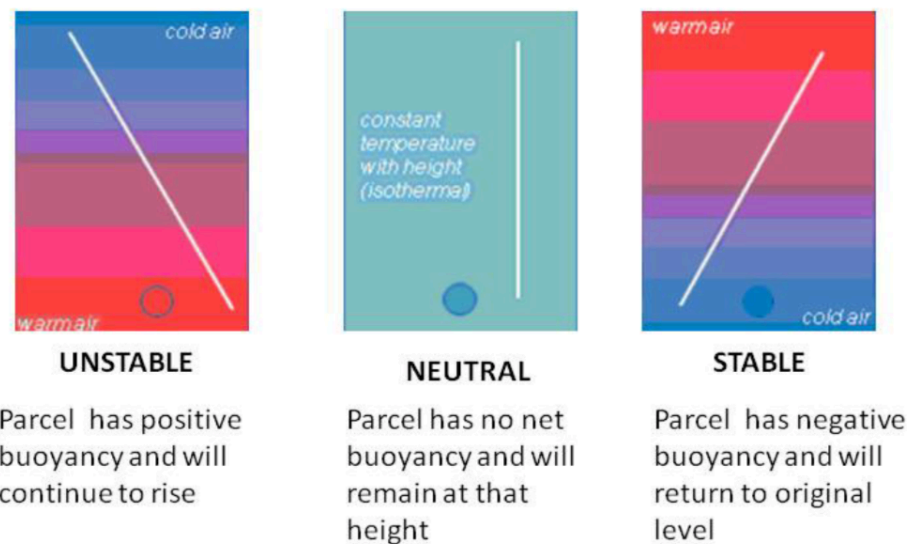


*Figure 2.1 The Schematic of Atmospheric Stabilities. [9]*

There are some parameters that can determine the atmospheric stability classification, which explained in the following.

## 2.2.1 Monin-Obukhov Length

The atmospheric stability classes also can be defined by Monin-Obukhov length which scales the height above the ground (*Table 2.1*).

*Table 2.1 Classification of Stability According to Obukhov Lengths [10]*

Monin-Obukhov length (L)	Stability Class
$10\text{m} \leq L \leq 50\text{m}$	Very stable
$50\text{m} \leq L \leq 200\text{m}$	Stable
$200\text{m} \leq L \leq 500\text{m}$	Near neutral stable
$ L  \geq 500\text{m}$	Neutral
$-500\text{m} \leq L \leq -200\text{m}$	Near neutral unstable
$-200\text{m} \leq L \leq -100\text{m}$	Unstable
$-100\text{m} \leq L \leq -50\text{m}$	Very unstable

Where  $L$  is defined that

$$L = \frac{-u_*^3}{kQ_0(g/T_0)} \quad (1)$$

- $u_*$  is the surface friction velocity
- $Q_0$  is the surface heat flux
- $k$  is the von Kármán constant
- $T_0$  is a virtual reference temperature
- $g$  is the gravitational acceleration
- $g/T_0$  is the buoyancy parameter [11]

## 2.2.2 Richardson Number

One of the measurements of atmospheric stability is according to the Richardson number. It expresses the ratio of buoyancy term to shear term and combines the concept both the static stability and the dynamic stability. [8]

### Gradient Richardson Number

The gradient Richardson number denotes the ratio of the buoyancy term to the wind shear term. Referring to the Richardson number, atmospheric stability is similarly cataloged (*Table 2.2*).

$$R_i = \frac{g \left( \frac{\Delta\theta}{\Delta z} \right)}{\bar{T} \left( \frac{\Delta u}{\Delta z} \right)^2} \quad (2)$$

Where  $g$  is the acceleration of gravity,  $\theta$  is the potential temperature,  $\bar{T}$  is the mean temperature,  $\frac{\Delta\theta}{\Delta z}$  is the vertical density gradient and  $\frac{\Delta u}{\Delta z}$  is the vertical gradient of the horizontal wind speed.

*Table 2.2 Classification of Stability According to Gradient Richardson Number [5]*

<b>Gradient Richardson Number <math>R_i</math></b>	<b>Stability Class</b>
$R_i \geq 0.49$	Very Stable
$0.196 \leq R_i < 0.49$	Stable
$0.083 \leq R_i < 0.196$	Weakly Stable
$-0.569 \leq R_i < 0.083$	Neutral
$-2.26 \leq R_i < -0.569$	Weakly Unstable
$-5.34 \leq R_i < -2.26$	Unstable
$R_i < -5.34$	Very Unstable

## Bulk Richardson Number

When the data is unavailable for gradient Richardson number under with infinitesimal measurement values, a bulk Richardson number will be an approximation instead of  $R_i$  (Table 2.3).

$$Ri_b = -\frac{gz}{T_{air}} \frac{\Delta\theta_v}{U_{air,z}^2} \quad (3)$$

Where  $z$  is the height over the ground,  $\Delta\theta_v$  is the virtual potential temperature,  $T_{air}$  is absolute virtual temperature and  $U_{air,z}$  is the change in horizontal wind components across that same layer.

Table 2.3 Classification of Stability According to Bulk Richardson Number [12]

<b>Bulk Richardson Number <math>Ri_b</math></b>	<b>Stability Class</b>
$Ri_b \geq 0.25$	Strongly Stable
$0.05 \leq Ri_b < 0.25$	Stable
$-0.05 \leq Ri_b < 0.5$	Neutral
$-10 \leq Ri_b < -0.05$	Unstable
$Ri_b < -10$	Strongly Unstable

## 2.3 Turbulence

The occurrence of turbulence has two mechanisms: temperature and shear friction. As sector 2.2 mentions, the tendency of air parcels is sinking or rising, which depends on its temperature relative to its surroundings. This vertical motion of air parcels makes for thermal instability in the atmospheric boundary layer. In this case, the turbulence is called buoyant turbulence. For another, the obstructions in the surface layer create friction when the wind blows near the surface, with wind shear generation. This shear causes turbulence referred as mechanically generated turbulence, also called mechanical turbulence. The wind shear production depends only on the surface roughness under the assumption that it is independent of the atmospheric conditions concerning onshore, whereas offshore conditions where surface roughness goes up with wind speed and hence increasing wave height [5].

### 2.3.1 Turbulence Intensity

The turbulence intensity (TI) is a normalized representation of the variance in the wind field, and it is also an essential measure of atmospheric turbulence, defined by

$$I = \frac{\sigma_1}{\bar{U}} \quad (4)$$

where  $\sigma_1$  is the standard deviation and  $\bar{U}$  is average longitudinal wind speed.

At present, all the standards state about external wind conditions in the offshore regime define in guidelines by Det Norske Veritas (DNV), International Electrotechnical Committee (IEC) and Germanischer Lloyd (GL). All of the standards give different characteristic value for  $\sigma_1$ . The DNV standard states the

standard deviation  $\sigma_U$  is a measure of the variability of the wind speed about the mean at height 10 m. In the GL standard, the standard deviation is

$$\sigma_1 = \frac{I_{15} \times (15 \times aV_{hub})}{(a + 1)} \quad (5)$$

where  $I_{15}$  is the average value of hub height turbulence intensity determined at  $V_{hub} = 15 \text{ m/s}$ , and parameter  $a$  is an empirical constant defined for each wind turbine class. This equation assumes that the standard deviation is invariant with altitude.

However, the IEC standard gives the following expression for  $\sigma_1$  :

$$\sigma_1 = \frac{V_{hub}}{\ln\left(\frac{z_{hub}}{z_0}\right)} + 1.28 \times 1.44 \times I_{15} \quad (6)$$

where  $z_{hub}$  is the hub height (reference height) and  $z_0$  is the roughness length. This equation also assumes that the standard deviation is invariant with height.

The turbulence intensity is frequently in the range of 0.1 to 0.4. Generally, maximum turbulence intensity occurs at minimum wind speeds, but the lower limitation at a given location will depend on specific topographic features and surface conditions at the site.

## **2.3.2 Turbulence Model**

The IEC 16400-1 standard gives two turbulence models for design load calculation, the Mann uniform shear model and the Kaimal spectral and exponential coherence model respectively. The former is a model of a three-dimensional velocity spectral tensor for atmospheric SL turbulence. A decomposition of the spectral tensor and an approximate value which is from the discrete Fourier transform determine the velocity components. [13] Moreover, the numerical integration of the three-dimensional spectral tensor is required, resulting in greater computing power for Mann uniform shear model. The Kaimal spectral and exponential coherence model is simpler than the former model as it uses a one-dimensional fast Fourier transform to generate time histories and spectra for each turbulence component. [5] Both turbulence models are described in the IEC 16400-1 standard in which the turbulence velocity fluctuations are assumed to be a stationary, random vector field, based on neutral stability and Gaussian wind speed distribution.

## 2.4 Wind Profile

Wind profile is a sort of diagram that presents the relationship between mean wind speed and various elevations above the ground, commonly, affected by friction velocity, atmospheric stability, turbulence and roughness length. Likewise, the DNV, the IEC and the GL recommend what kinds of wind profile model that is more suitable to determine the vertical structure of the ABL and derive wind shear profiles. The wind shear is one of principal elements that influences wind turbine fatigue loads, given by the power law and logarithmic law. [14] Sathe et al. study shows the atmospheric stability has a significant impact on wind shear. [15]

Following Gryning et al. [16], the starting point for wind shear profile derivation is that

$$\frac{\partial u}{\partial z} = \frac{u_*}{kl} \quad (7)$$

where  $u$  is the horizontal wind velocity at a given height  $z$ ,  $u_*$  is the local friction velocity,  $k = 0.4$  is the von Karman constant and  $l$  is the local length scale.

### 2.4.1 Power Law Wind Profile

$$\frac{u_z}{u_{z_r}} = \left(\frac{z}{z_r}\right)^\alpha \quad (8)$$

Where

- $u_z$  is the wind speed at height  $z$

- $u_{z_r}$  is the reference velocity
- $z_r$  is the reference height
- $\alpha$  is the power law exponent

This wind profile assumes neutral stability with a constant roughness length 0.002m under over the sea in the GL standards. Moreover, the power law exponent  $\alpha$  has the value of 0.14 for all wind speed. Similarly, the IEC standards prescribe the same  $\alpha = 0.14$  for all wind speed. However, it does not allow for the influence of surface roughness and thermal effects. [5] The power law is just a known function to fit logarithmic wind profile because of no specific theoretical basis. [5]

## 2.4.2 Logarithmic Wind Profile

In the surface layer and under neutral atmospheric condition, to integrate Eq. (7) with assumption that the mixing length increase with height,  $l = z$ :

$$u = \left(\frac{u_*}{k}\right) \ln\left(\frac{z}{z_0}\right) \quad (9)$$

In which

- $u_*$  is friction velocity
- $k$  is von Karman's constant, 0.4
- $z$  is the height
- $z_0$  is the roughness length

The roughness length  $z_0$  can be estimated based on the Charnock relation.

$$z_0 = \frac{A_c u_*^2}{g} \quad (10)$$

Where  $g$  is the gravity acceleration and  $u_*$  is friction velocity.  $A_c$  is the Charnock constant which by default ranges from 0.01 to 0.04, also, its maximum is for near-coastal condition and its minimum for open sea surface. [17] The  $z_0$  can be considered as the point where the wind speed becomes zero when extrapolated downwards from the surface layer using Monin-Obukhov theory. [7]

The influence of atmospheric stability on  $l$  is expressed as:

$$l = l_{SL} \phi_m^{-1} \quad (11)$$

where  $\phi_m$  is the atmospheric stability correction, also called the dimensionless wind shear according to Monin-Obukhov similarity theory (MOST). Moreover, Inserting Eq. 11 into Eq. 7 and replacing  $l_{SL}$  (the length scale in the surface layer) by  $z$ , based on the Most that the atmospheric stability can be described regarding stability parameter  $\frac{z}{L}$ , the surface layer wind profile can be shown below:

$$\bar{u} = \frac{u_*}{k} \left[ \ln \left( \frac{z}{z_0} \right) - \Psi_m \left( \frac{z}{L} \right) \right] \quad (12)$$

Where  $\Psi_m$  is a stability-dependent function and it is decided by the ratio the height  $z$  to the Monin-Obukhov length  $L$ .

The ratio is positive for stable conditions:

$$\Psi_m \left( \frac{z}{L} \right) = \frac{-4.7z}{L} \quad (13)$$

The ratio is negative for unstable conditions:

$$\Psi_m \left( \frac{z}{L} \right) = 2 \ln[1 + x] + \ln[1 + x^2] - 2 \tan^{-1}(x) \quad (14)$$

In which  $x = (1 - 19.3(z/L))^{1/4}$ .

For neutral conditions when the ratio is equal to zero, both functions above reduce to the logarithmic wind profile.

Eventually, the wind profile over sea can be parameterized as:

$$\frac{u}{u_*} + \frac{1}{k} \ln \left[ 1 + 2 \frac{\Delta u_*}{\bar{u}_*} + \left( \frac{\Delta u_*}{\bar{u}_*} \right)^2 \right] + \frac{1}{k} \Psi_m \left( \frac{z \bar{z}_0}{\bar{z}_0 L} \right) = \frac{1}{k} \ln \left[ \frac{z}{\bar{z}_0} \right] \quad (15)$$

where  $\Delta u_*$  is the friction velocity deviation of each wind speed profile from the mean value,  $\bar{u}_*$  can be computed in each stability class, and  $\bar{z}_0$  is the mean roughness length defined in the same as  $z_0$ . [18]

### 2.4.3 Extended Surface Layer Wind Profile

Wind profile plays an important role in fatigue loading among several factors. In stable conditions, loads induced by the wind profile are the larger due to increased

wind shear under diabatic states. [10] The wind profiles models used in wind energy are only valid in the surface layer. [19] The SL can be as low as 30-40m offshore especially under stable conditions. State of the art wind turbines can reach heights up to 200 m which is well above the surface layer, so it is necessary to extend, commonly, used wind profiles up to the height above the surface layer. [19] Furthermore, the diabatic wind profile model is investigated by using the theory by Gryning et al [16].

In the ABL,

$$u_* = u_{*0} \left(1 - \frac{z}{z_i}\right)^\alpha \quad (16)$$

where  $u_{*0}$  is the friction velocity near the ground,  $z_i$  is the boundary-layer height and  $\alpha$  depends on the state of the boundary layer [18]. Gryning et al. concluded that there is normally the interval of  $\alpha$  is between 1/2 and 3/2 based on different previous studies, but for simplicity the friction velocity is taken to decline linearly with height corresponding to  $\alpha = 1$  [16].

The length scale,  $l$ , is composed of three terms and which is modelled by inverse summation.

$$\frac{1}{l} = \frac{1}{l_{SL}} + \frac{1}{l_{MBL}} + \frac{1}{l_{UBL}} \quad (17)$$

I            II            III

where  $l_{SL}$  is the length scale in the surface layer,  $l_{MBL}$  is the length scale of the middle boundary layer and  $l_{UBL}$  is the length scale of the upper boundary layer.

$l_{MBL}$  is not proportional to  $z$  but varies with atmospheric stability, and  $l_{UBL}$  depends linearly on the distance to the top of the boundary layer:

$$l_{UBL} = (z_i - z) \quad (18)$$

Gyning et al. gives the expression for the entire boundary layer [16]. For neutral atmospheric conditions, to insert  $\alpha = 1$ , the wind profile derivation equation changes to:

$$\frac{\partial u}{\partial z} = \frac{u_{*0}}{k} \left(1 - \frac{z}{z_i}\right) \left(\frac{1}{z} + \frac{1}{l_{MBL}} + \frac{1}{(z_i - z)}\right) \quad (19)$$

After integrating with  $z$  for  $z \gg z_0$ ,

$$u = \frac{u_{*0}}{k} \left[ \ln\left(\frac{z}{z_0}\right) + \frac{z}{l_{MBL}} - \frac{z}{z_i} \left(\frac{z}{2l_{MBL}}\right) \right] \quad (20)$$

In the same way, for unstable conditions,

$$u = \frac{u_*}{k} \left[ \ln\left(\frac{z}{z_0}\right) - \Psi_m\left(\frac{z}{l}\right) + \frac{z}{l_{MBL}} - \frac{z}{z_i} \left(\frac{z}{2l_{MBL}}\right) \right] \quad (21)$$

and for stable conditions,

$$u = \frac{u_*}{k} \left[ \ln\left(\frac{z}{z_0}\right) - \Psi_m\left(\frac{z}{l}\right) \left(1 - \frac{z}{2z_i}\right) + \frac{z}{l_{MBL}} - \frac{z}{z_i} \left(\frac{z}{2l_{MBL}}\right) \right] \quad (22)$$

## 2.5 Wind Turbine Load

The state of art wind turbine expects to produce more wind energy and reduce fatigue loads simultaneously with the location in very deep water or long distances from the coast. Thus, it is vital that the fatigue loads are calculated and analyzed.

The atmospheric stability and atmospheric turbulence are two important factors which influence wind turbine loads. The study by Ragan et al. shows there are three ways to estimate wind turbine fatigue loads (the Miner's rule, the Rainflow Cycle-Counting Algorithm and Dirlik's method, respectively. [20] Sathe et al. analyzed the influence of atmospheric stability on wind turbine loads by using the Rainflow Cycle-Counting Algorithm method. [10] After that, Sathe and Bierbooms did fatigue load simulation using the Miner's rule but only for neutral stability conditions and neglected turbulent winds. [14]

### Miner's Rule

The Miner's rule is an empirical design method describes how fatigue damage accumulates on a structural component is given by Wohler's equation:

$$N_F S^m = K \quad (23)$$

or given by a log-log relationship which defines Wöhler curve (or the stress-number of cycles, S-N curve):

$$\log S = (\log K - \log N_F)/m \quad (24)$$

where  $S$  is each cycle of a constant stress range amplitude,  $N_F$  is the number of cycles at failure,  $K$  is the second material parameter which is proportional to the number of cycles and  $m$  is a material parameter called Wöhler coefficient. In Ragan et al.'s and Sathe et al.'s studies,  $m$  is equal to 3 for the turbine blade loads while the different values of  $m$  for the tower loads in both studies,  $m = 10$  in former study and  $m = 12$  in the latter. [10, 20]

If  $N$  is the number of stress cycles before failure, the damage fraction can be that

$$D = \frac{NS^m}{K} \quad (25)$$

where  $D$  is a number which has an interval between zero and unity. Failure is reached when  $D$  is equal to 1. [20]

### **Rainflow Counting for Variable Stress Cycle Amplitudes**

Normally, it is difficult to obtain the S-N curve of a component material when quantifying the fatigue damage. Therefore, the concept of fatigue damage equivalent load (DEL) is used instead of using the log-log relationship. Primarily, to use the Rainflow Cycle-Counting Algorithm, a variable amplitude cyclic stress time series are separated into individual load ranges ( $S_i$ ) and the corresponding number of cycles ( $N$ ). Then, Eq.(25) becomes:

$$D = \frac{\sum_{i=1}^N S_i^m}{K} \quad (26)$$

In terms of the DEL, the constant amplitude stress range would cause an equivalent amount of damage.

$$DEL = \left( \sum_{i=1}^N \frac{S_i^m}{N} \right)^{\frac{1}{m}} \quad (27)$$

combining Eq.(26) and Eq.(27), we obtain

$$D = \frac{N(DEL)^m}{K} \quad (28)$$

### Dirlik's Method

The Dirlik's method is a kind of spectral techniques to estimate stress range probability distributions based on spectral moments of fatigue loads in the frequency domain. Ragan and Manuel introduced that the formula for Dirlik's stress range probability density function (PDF), which is a weighted combination of an exponential and two Rayleigh distributions regarding the 0<sup>th</sup>, 1<sup>st</sup>, 2<sup>nd</sup> and 4<sup>th</sup> spectral moments. [20]

$$p(S) = \frac{\frac{D_1}{Q} e^{-z/Q} + \frac{D_2 Z}{R^2} e^{-(z^2/2R^2)} + D_2 Z e^{-z^2/2}}{2\sqrt{m_0}} \quad (29)$$

where  $Z = \frac{s}{2\sqrt{m_0}}$  (30) is a normalized stress range,  $m_n = \int_0^\infty f^n P_s(f) df$  (31) are the spectral moments. Here, there are two parameters which are needed. The One is A regularity factor  $\gamma = \frac{m_2}{\sqrt{m_0 m_4}}$  (32), meaning the expected ratio of zero-crossings to peaks, and the another one is a mean frequency  $x_m = \frac{m_1}{m_0} \sqrt{\frac{m_2}{m_4}}$  (33). Thus, the rest parameters are defined below,

$$D_1 = \frac{2(x_m - \gamma^2)}{1 + \gamma^2} \quad (34)$$

$$D_2 = \frac{1 - \gamma - D_1 + D_1^2}{1 - R} \quad (35)$$

$$D_3 = 1 - D_1 - D_2 \quad (36)$$

$$Q = \frac{1.25(\gamma - D_3 - D_2 R)}{D_1} \quad (37)$$

$$R = \frac{\gamma - x_m - D_1^2}{1 - \gamma - D_1 + D_1^2} \quad (38)$$

The Eq.(27) can be rewritten by using this spectral approach,

$$EFL = (E[S^m])^{1/m} \quad (39)$$

where

$$E[S^m] = \int_0^\infty S^m p(S) dS \quad (40)$$

The expected number of peaks per unit time

$$E[P] = \sqrt{\frac{m_4}{m_2}} \quad (41)$$

and the expected number of cycles in T seconds is

$$E[N] = T \cdot E[P] \quad (42)$$

Finally, the amount of accumulated damage predicted in this Dirlik's approach:

$$E[D] = \frac{E[N] \cdot E[S^m]}{K} = \frac{T}{K} E[P] E[S^m] = \frac{E[N] \cdot (EFL)^m}{K} \quad (43)$$

## 2.5.1 The Tower Base Fore-Aft Loads

In the study of Sathe et al., the tower base fore-aft load is defined as the bending moment at the base of the tower along the x-axis in the tower coordinate system. [10] The wind profile on the tower base exerts an asymmetrical thrust force on a rotor with three symmetrical blades. This results in different tower loads with respect to varying atmospheric stabilities and mean wind speeds. The much larger tower base fore-aft loads occur under the unstable as well as the smaller loads occur under stable conditions. The tower base fore-aft loads are affected mostly by turbulence under diabatic conditions. [10]

## 2.5.2 The Blade Loads

The blade loads can be estimated by calculating two bending moments ( the flap-wise bending moment  $M_{flapwise}$  and the edge-wise bending moment  $M_{edgewise}$ ) at the root of the blade along the x-axis and y-axis in the blade coordinate system. In comparison to the loads on the tower base, the blade loads will be influenced by both wind profile and turbulence under diabatic conditions. [10] The result from the study by Sathe et al. indicates that the wind profile under stable condition will exert a larger cyclic loading on the blades than under unstable condition while turbulence is lower under stable condition than under unstable condition. [10] The blade loads in the aspects of the variation in mean wind speeds and atmospheric stability have a slightly increasing trend from unstable to stable under diabatic conditions. It is worth noting that variations in atmospheric turbulence has least influence on the blade loads because the gravity forces of the blades take up more dominant proportion in producing the blade loads than wind loads. Hence the influence of wind shear is

more significant when determining the fatigue damage and extreme loads on the blades.

### 2.5.3 Rotor Loads

The rotor loads which are denoted by the moments  $M_x$  (experiencing the rotor yaw loads based on the azimuth position),  $M_y$  and  $M_z$  (experiencing the rotor tilt loads based on the azimuth position) along the x-axis, y-axis and z-axis, respectively, in the rotating hub coordinate system. By contrast with the tower loads and the blades loads, the rotor loads will be mainly influenced by wind profile under diabatic condition. [10] The variation of the rotor  $M_x$  loads in terms of mean wind speeds and atmospheric stability increases significantly from unstable to stable. The surface layer wind profile model can induce larger rotor  $M_x$  loads in contrast with the beyond surface layer wind profile model by Gryning et al. [10] [16] However, the rotor  $M_y$  loads are not influenced by atmospheric stability compared to the effect of gravity, which is similar to blade loads. The  $M_z$  loads are also not strongly influenced by atmospheric stability, varying non-linearly with respect to the wind speed.

### 3. Modelling of Floating Wind Turbine by SIMA

#### 3.1 SIMA Software

The SIMA is a powerful tool for modeling and analysis of tasks within the marine technology field. There are three supported programs in SIMA, SIMO, RIFLEX and SIMO & RIFLEX coupled. In this paper, the SIMO & RIFLEX coupled program is used to a model slender, elastic structure(s) of a floating wind turbine. Generally, locations and environmental conditions, body and slender system are three major elements composing this modelling. A scheme of modelling a spar floating wind turbine is shown in *Figure 3.1*. The locations give general information about physical constants including acceleration due to gravity, water density and water depth, etc. In this study, the environment is set into seven parts referring to atmospheric stability classified by Gradient Richardson Number shown in *Table 2.2*, also, in our simulations it was set no swell and no current.

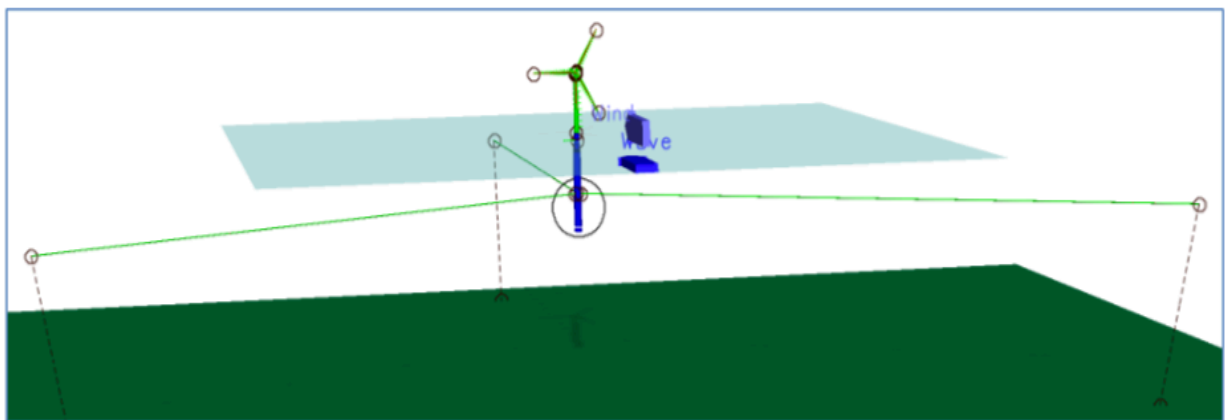


*Figure 3.1 Modelling of Floating Wind Turbine in SIMA Software*

### 3.1.1 Defining Coordinate System

The Coordinate system used in SIMA for spar floating wind turbine includes the global coordinate ( $X_G Y_G Z_G$ ), the local coordinate ( $xyz$ ) and the wind coordinate system ( $U_{wind} V_{wind} W_{wind}$ ). The motion of floating wind turbine is also a key parameter including three translational components (surge, sway and heave) and three rotational components (roll, pitch and yaw) as shown in *Figure 3.2*.

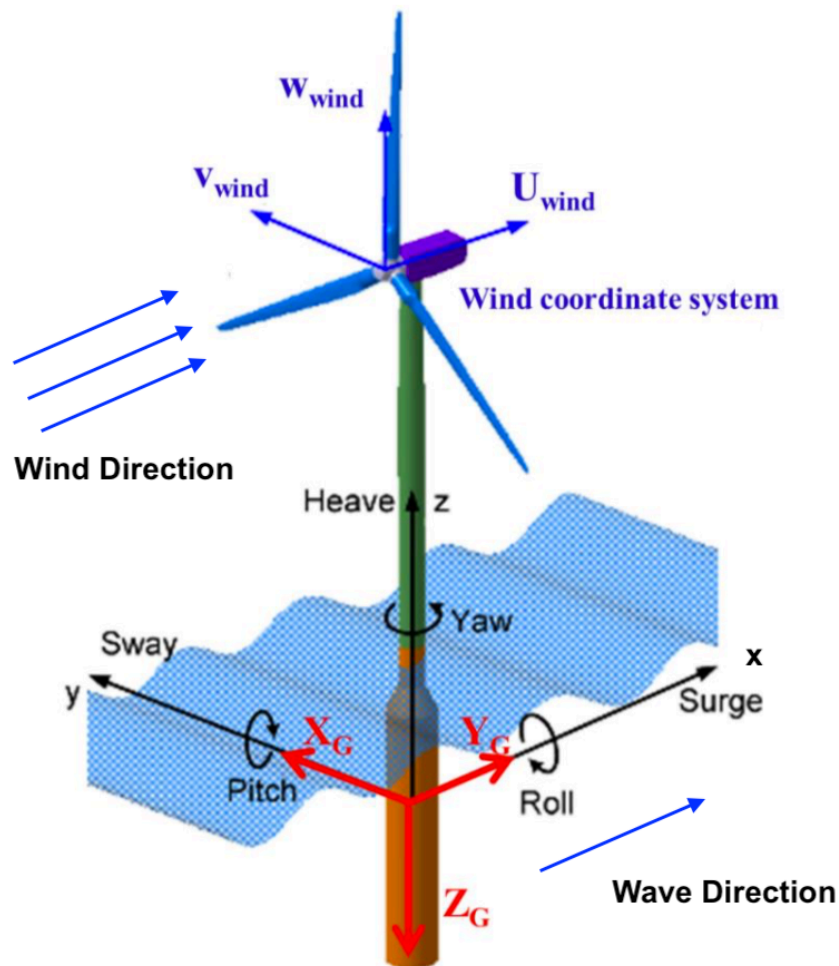
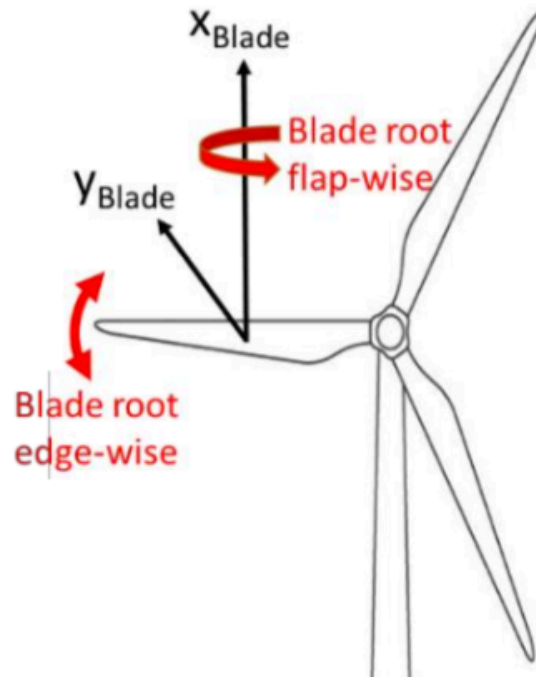


Figure 3.2 Coordinate System of Floating Wind Turbine [21]

The blades coordinate system is shown in *Figure 3.3*. The blades flapwise load happens around  $x_{blade}$  axial and the blades edge-wise load is around  $y_{blade}$ .



*Figure 3.3 Blades Coordinate System [22]*

## 3.2 Turbulence Wind Field Input

Assuming a 3D box of vector field consisting of grid points as the synthetic wind field, the turbulence wind field simulates real wind field condition in SIMA software as shown in *Figure 3.4*. Where  $dx$  is grid spacing in the long wind direction;  $dy$  is the grid spacing in the cross wind direction;  $dz$  is grid spacing in the vertical wind direction;  $L_x$  is the length of turbulence box in the long direction;  $L_y$  is length of turbulence box in the cross wind direction;  $L_z$  is the length of turbulence box in the vertical wind direction. [22] Each grid point is seen as a spatial location in the box and provides information about the local wind speed for  $u$ ,  $v$  and  $w$  components and local wind direction. The number of grid points in the long wind direction  $N_x$  can be calculated by the function  $L_x = N_x dx$ . In the same way,  $N_y$  ( the number of grid points in the cross wind direction) =  $L_y / y dy$  and  $N_z$  (the number of grid points in the vertical wind direction) =  $L_z / z dz$ . [22] The grid spacing =  $\frac{T U_{hub}}{N_x}$ , where  $T$  is simulation time length and  $U_{hub}$  is mean wind speed at hub height.

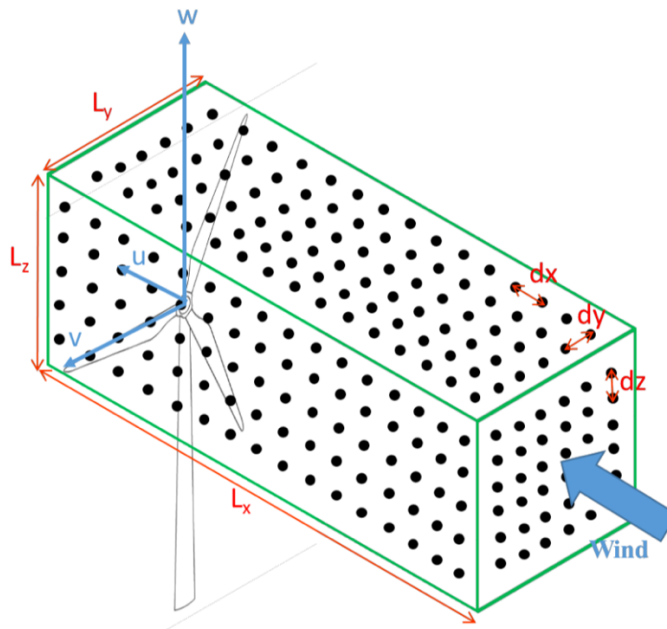


*Figure 3.4 A 3D Turbulence Box [22]*

This 3D vector field box only covers the rotor swept area, because the rotor swept area of the wind turbine relative to the rest of wind turbine is the most important regarding the turbulent wind exposure. Furthermore, the mean wind speed in all simulations is specified by the wind speed at hub height. In this thesis, the IEC Kaimal spectral and exponential coherence model is utilized, derived based on measurements in Kansas under adiabatic atmospheric stability conditions (ref). However, the  $w$  component is derived under the neutral conditions,  $u$  and  $v$  components fits stable condition. [22]

## 4. Coupled RIFLEX-SIMO Simulation for Floating Wind Turbine

### 4.1 General

The overall simulation length is 10 min, i.e., 600s and the simulation time step is 0.02s in all simulations. Thus, the total number of simulation data is 30000.

### 4.2 Wave Inputs

The wave input parameters for all simulations in SIMA software are shown in *Table 4.1* where the wave direction (degree) is equal to zero, which means the wave direction is same with wind direction.

*Table 4.1 Wave Input Parameters*

Parameter	Value
Wave Type	Irregular Airy Wave
Significant Wave Height $H_s$ (m)	6
Peak Period $T_p$ (s)	10
Wave Direction (degree)	0
Spectrum	JONSWAP

### 4.3 Offshore Wind Turbine Properties

The wind turbine used is an offshore floating wind turbine in Offshore Code Comparison Collaboration (OC3) phase IV. The floater is a spar-buoys whose concept called ‘Upwind’ and developed by Equinor. [23] The characteristics of the turbine are summarized in *Table 4.2*.

*Table 4.2 Summary of Properties for the NREL 5-MW Baseline Wind Turbine [23]*

Rating	5 MW
Rotor orientation, configuration	Upwind, 3 blades
Control	Variable speed, collective pitch
Drivetrain	High speed, multiple-stage gearbox
Rotor, hub diameter	126 m, 3 m
Hub height	90 m
Cut-in, rated, cut-out wind speed	3 m/s, 11.4m/s, 25 m/s
Cut-in, rated rotor speed	6.9 rpm, 12.1 rpm
Rated tip speed	80 m/s
Overhang, shaft tilt, precone	5 m, 5°, 2.5°
Rotor mass	110,000 kg
Nacelle mass	240,000 kg
Tower mass	347,500 kg
Coordinate location of overall center of mass (CM)	(-0.2 m, 0.0 m, 64.0 m)

## 4.4 Wind Turbulence Inputs

The turbulence is generated from IEC Kaimal spectral and exponential coherence model only for neutral condition. The turbulence input parameters including the turbulence intensity (TI) and two random seed numbers for each simulation are summarized in *Table 4.3*. The seed numbers are set as constant for different stability conditions (environment in SIMA software).

*Table 4.3 Turbulence Input Parameters form IEC Standard [13]*

Parameter	IEC Kaimal spectral & exponential coherence model		
	8 m/s	11.4 m/s	15 m/s
Turbulence Intensity	Class C (0.12)	Class C (0.12)	Class C (0.12)
Seed no.1	227638, RanLux	227638, RanLux	227638, RanLux
Seed no.2	2703, 1992	2703, 1992	2703, 1992
Seed no.3	8797, 15509022	8797, 15509022	8797, 15509022

## 4.5 Wind Input

Three mean wind speed cases used in this study correspond to different regions of operation: 8 m/s (below rated wind speed) 11.4 m/s (rated wind speed) and 15 m/s (above rated wind speed). The air density is 1.225 kg/m<sup>3</sup> and TI is 0.12 when there is no scaling ratio for the generated turbulence. There are several steps following in order to get normalized wind speed (mean speed factors which are inputted in SIMA software).

Firstly, the mean wind profiles are normalized taking the velocity measured at 52 m for the FINO 3 platform under each stability class from the period 01/10/2009 to 01/10/2011 (*Figure 4.1*). we observe that there is marked wind shear under very stable conditions, which is in accordance with theory like subchapter 2.4.3 mentioned.

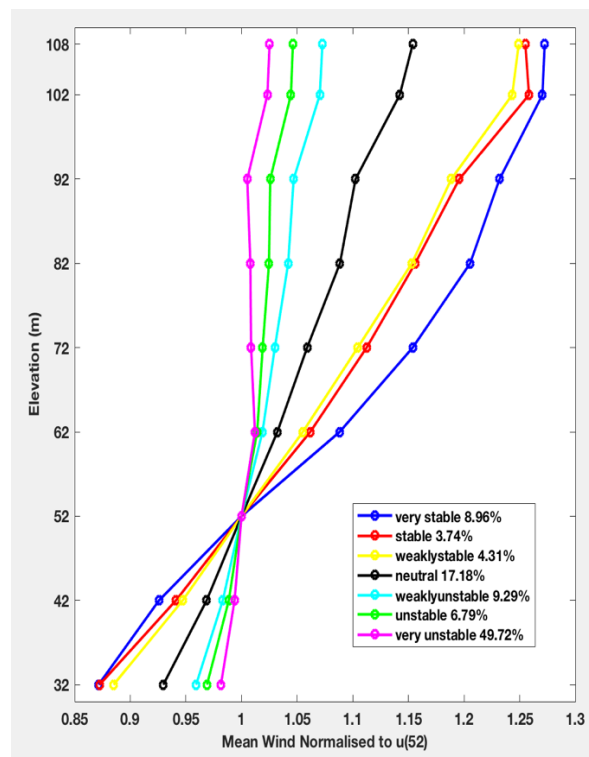


Figure 4.1 Normalized Mean Wind Speed Profile for Each Stability Class

The power law exponents  $\alpha$  can be approximately estimated for each stability class from the trendline of normalized wind profiles by the power law and are given in *Table 4.4*.

*Table 4.4 The Power Law Exponent for Each Stability Class*

Stability Class	Power Law Exponent		
	8 m/s	11.4 m/s	15 m/s
Very Stable	0.1298		
Neutral	0.0797		
Very Unstable	0.0383		

As subchapter 2.4.1 and subchapter 3.2 mentioned, the power law gives the wind profiles, taking the wind turbine hub height (90m) as the reference height for simulation in SIMA software.

Therefore, the mean wind speed factors (normalized wind speed) in the shear profile levels input of simulation SIMA software can be figured out corresponding to different elevations, as presented in *Table 4.5*.

Table 4.5 Mean Speed Factors (Normalized Wind Speeds) Imported in SIMA Software

Elevation	Normalized Wind Speeds under Each Stability Class for 8m/s, 11.4 m/s and 15 m/s				
	Very Stable $\alpha = 0.16$	Very Stable $\alpha = 0.14$	Very Stable $\alpha = 0.1298$	Neutral $\alpha = 0.0797$	Very Unstable $\alpha = 0.0383$
0	0	0	0	0	0
12.5	0.729166656	0.758531203	0.77395951	0.85441842	0.92718024
25	0.814688526	0.835829413	0.84682162	0.9029479	0.95212422
37.5	0.869293038	0.88464785	0.89258294	0.93260376	0.96702546
50	0.910241012	0.921004706	0.92654311	0.95423377	0.97773928
62.5	0.943326427	0.950231124	0.95377196	0.97135618	0.98613124
75	0.97124993	0.974797991	0.97661249	0.98557404	0.99304141
87.5	0.995502802	0.996063844	0.9963501	0.9977573	0.99892164
90	1	1	1	1	1
100	1.017000575	1.014859797	1.01376974	1.00843259	1.00404346
112.5	1.036347972	1.03173319	1.02938757	1.01794363	1.00858302
125	1.053966484	1.047064536	1.04356197	1.02652753	1.01266119
137.5	1.070162257	1.061129593	1.05655233	1.03435495	1.01636454
150	1.085165055	1.074134893	1.06855275	1.04155293	1.01975726
162.5	1.099151956	1.086239321	1.0797124	1.04821866	1.02288826
167.5	1.104494527	1.090857752	1.08396796	1.05075352	1.02407621

### 4.5.1 Wind Input – Turbulence Box

The input to the turbulence box for the Kaimal spectral and exponential coherence model is presented in *Table 4.6*.

*Table 4.6 3D Turbulence Box Input*

	Mean Wind Speed at Hub (m/s)		
	8 m/s	11.4 m/s	15 m/s
Nx	32768		
Ny	32		
Nz	32		
dx	0.879	1.252	1.648
dy	5		
dz	5		
dt	0.02		
Analysis Time (s)	600		
Lx (m)	28800	41040	54000
Ly (m)	160		
Lz (m)	160		

## 4.6 Simulation Results

This chapter will demonstrate the simulation results of fatigue loads and motions of floating wind turbine (the OC3-Hywind) following a standard which is served by the OC3 project and verify the validity of offshore spar-buoys wind turbine structure model.

### 4.6.1 Eigenfrequencies

#### Eigenfrequencies of the Rotating Rotor

The eigenfrequencies of the rotating blades and the excitations of wind and wave are important parameters determining the dynamics of the OC3-Hywind. The  $N_b P$  represents the blade passing frequency, in which  $N_b$  is the number of blades. That is, 1P is the constant rotor rotational speed, and the blade passing frequency for the 3-bladed OC3-Hywind is 3P. *Table 4.7* shows the frequencies of the rotating blades at each wind speed.

*Table 4.7 Frequencies of the Rotating Blades*

Operating region	Wind speed (m/s)	Rotor rotational frequency (rpm)	1P Frequency (Hz)	2P Frequency (Hz)	3P Frequency (Hz)
Below rated	8	9.995	0.17	0.33	0.50
Rated	11.4	12.1	0.20	0.40	0.60
Above rated	15	12.1	0.20	0.40	0.60

## Eigenfrequencies of the Environmental Loads

The environmental loads involve the turbulence wind and wave in the simulation. Regarding to the wave environment, the wave eigenfrequency  $f_p = \frac{1}{T_p}$  is equal to 0.1 Hz.

## Eigenfrequencies of the OC3-Hywind Modes

The lowest 19 eigenfrequencies whose results were obtained from all codes except FAST by POSTECH and Bladed, calculated for stationary OC3-Hywind system are shown at *Figure 4.2*. [23] It is found that the eigenfrequencies which is in agreement with our SIMA free decay tests where the values of six platform motions read below in *Table 4.8*.

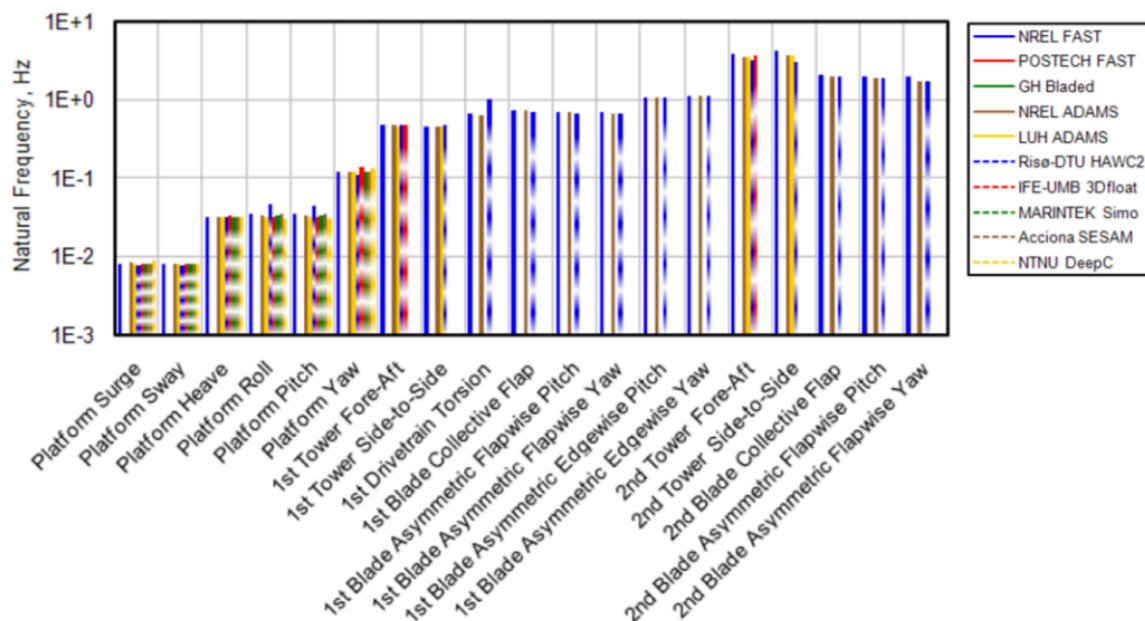


Figure 4.2 The Eigenfrequencies for the OC3-Hywind System [23]

Table 4.8 The Natural Frequency of the Platform Motions

Platform Motions	Surge	Sway	Heave	Roll	Pitch	Yaw
Natural Frequency (Hz)	0.00714	0.0073	0.045	0.033	0.033	0.1

### 4.6.2 Damage Equivalent Loads

The fatigue damage equivalent load (DEL) is a significant parameter for the analysis of floating wind turbine loads. Therefore, the lifetime fatigue loads are converted to equivalent loads by Miner’s rule in this study. Rainflow Counting method with Miner’s rule as mentioned at subchapter 2.5, assuming the wind turbine will operate for 20 years with the number of cycles  $N = 10^7$  which approaches the fatigue limit for typical steel material types. [24] The Wöhler coefficient  $m$  is equal to 3 for tower base and tower top which are made from steel and  $m=12$  is for the blades since they are made from fiberglass. [10]

### 4.6.3 Tower Base Fore-Aft Loads and Moment

Figure 4.3 presents the calculated result for the fatigue damage equivalent loads of the tower base fore-aft under three stability classes (very stable, neutral and very unstable) as well as two additional stable conditions with exponents  $\alpha = 0.14$  and  $\alpha = 0.16$ . Comparing the tower base fore-aft DELs of different wind speeds, the rated

wind speed (11.4 m/s) results in the largest damage equivalent load. The tower base damage loads at below rated wind speed in neutral conditions have the largest DEL than the other two stability classes, whereas the very stable conditions cause more damage loads when the wind speed at rated wind speed.

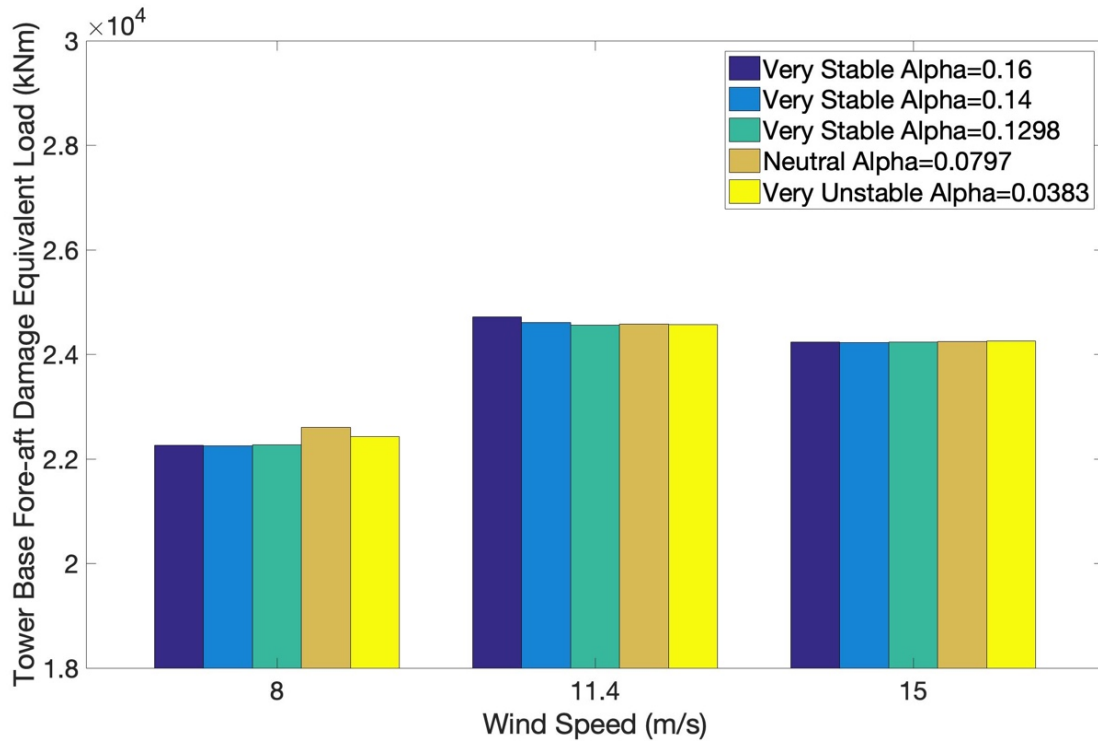


Figure 4.3 Tower Base Fore-Aft Damage Equivalent Loads under Each Stability Class for 8 m/s, 11.4 m/s and 15 m/s

Figure 4.4 demonstrates the normalized tower base fore-aft damage equivalent loads relative to neutral conditions at 8 m/s, and the percentages are shown in Table 4.9. Comparing different wind speed, it is found that the variation of the normalized tower base fore-aft damage loads at 11.4 m/s is up to 9% and 7% for 15 m/s. In terms of different stability conditions, the differences of the normalized tower base fore-aft loads are less 2% at each mean wind speed.

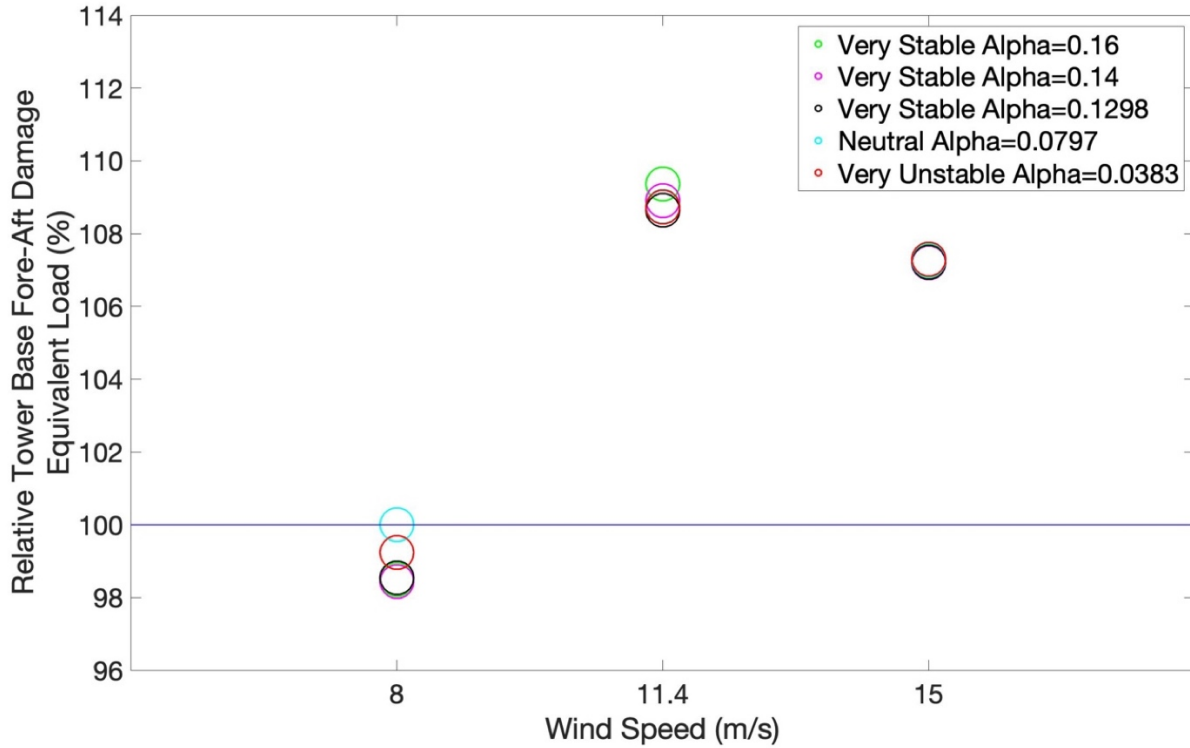
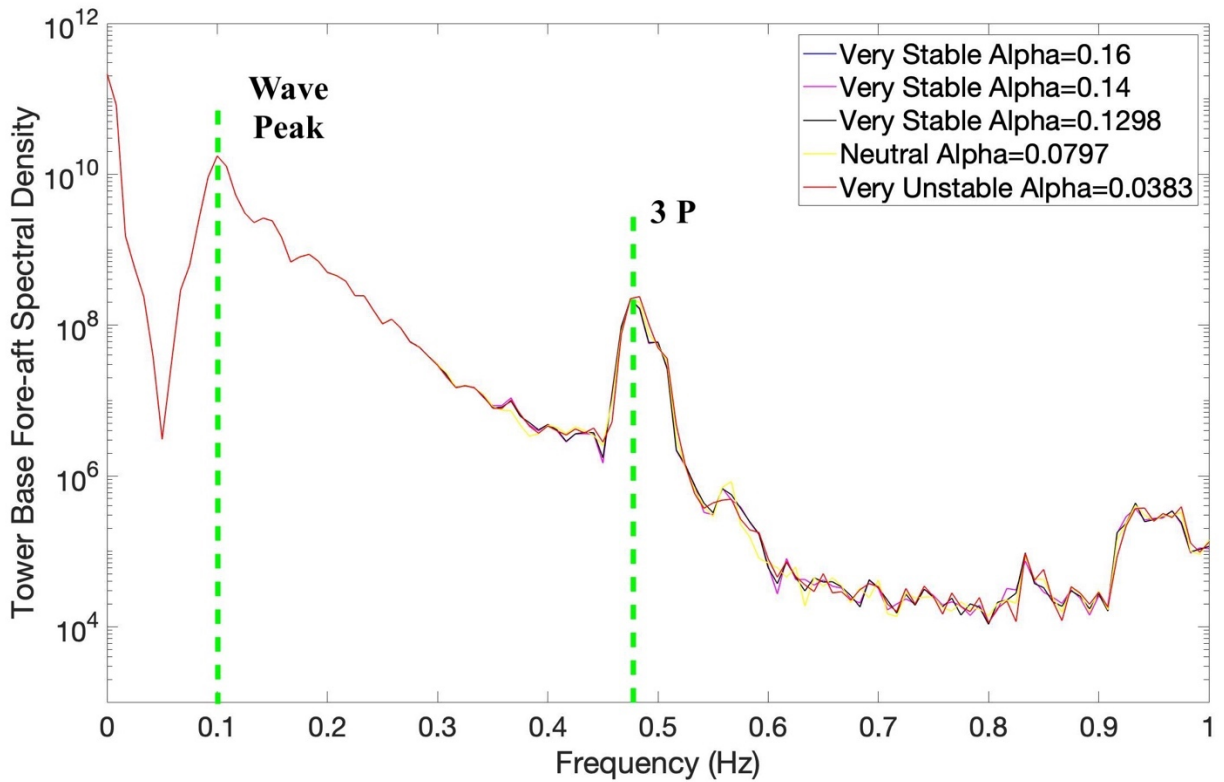


Figure 4.4 Normalized Tower Base Fore-Aft Damage Equivalent Loads under Each Stability Class for 8 m/s, 11.4 m/s and 15 m/s

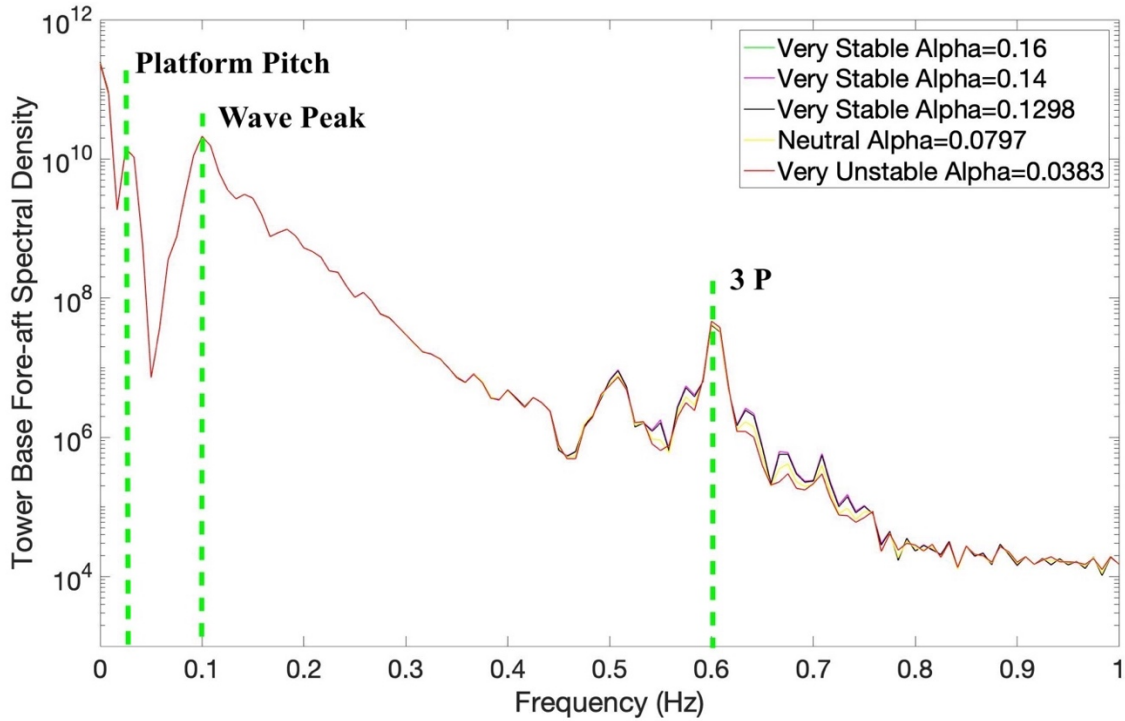
Table 4.9 Percentages of Tower Base Fore-Aft Damage Equivalent Loads Relative to Neutral Stability at 8 m/s

Atmospheric Stability	Tower Base Fore-Aft (%)		
	8 m/s	11.4 m/s	15 m/s
Very Stable $\alpha = 0.16$	98.497	109.365	107.237
Very Stable $\alpha = 0.14$	98.441	108.900	107.199
Very Stable $\alpha = 0.1298$	98.549	108.646	107.213
Neutral $\alpha = 0.0797$	100	108.740	107.268
Very Unstable $\alpha = 0.0383$	99.239	108.725	107.298

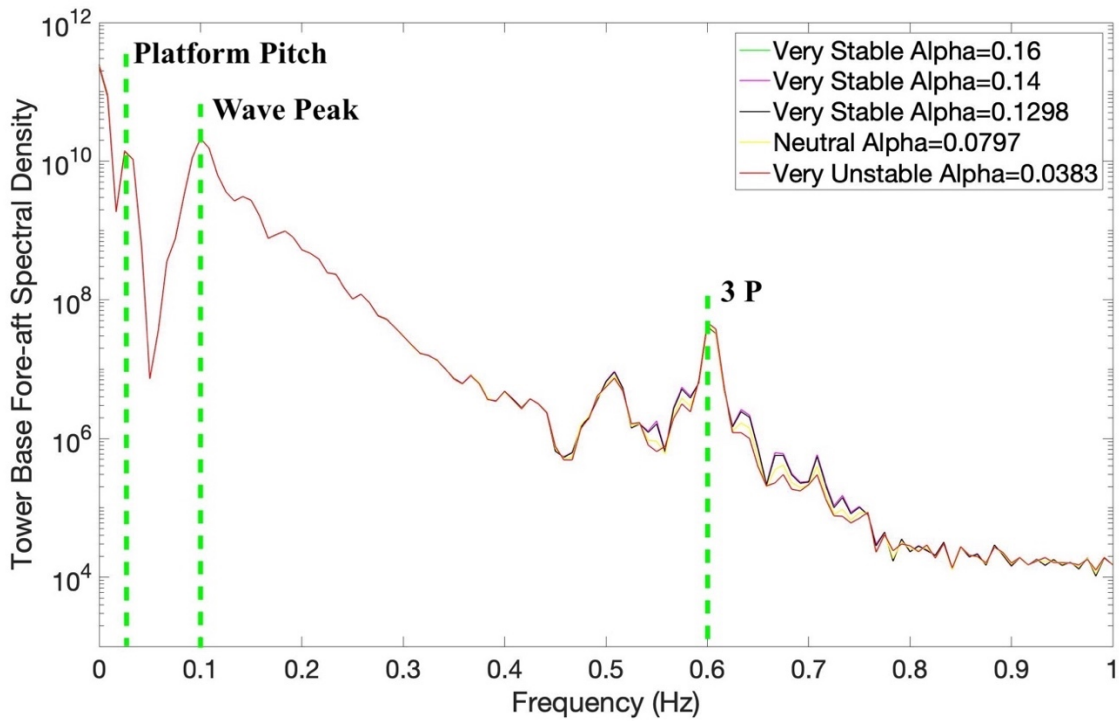
The spectral density plots of tower base fore-aft moment are given in *Figure 4.5* for different wind speeds. We observe that there are platform pitch excitations at the tower base fore-aft moment spectral densities at 11.4 m/s and 15 m/s in *Figure 4.5* (b) and (c). Our findings are consistent with (A Sathe et al.) study that a decline of tower base fore-aft loads is induced by the pitching of the three blades above 12 m/s, meanwhile, the turbine starts to pitch. [10] The wave spectral peak gives the maximum excitation of tower base fore-aft moment energy amongst other primary excitations. The results in from *Figure 4.3* to *Figure 4.5* suggest that wind profile has very little influence on the tower base fore-aft loads, although there are some fluctuations in the tower base fore-aft damage equivalent loads for higher frequency under different stability classes.



(a)



(b)



(c)

Figure 4.5 Tower Base Fore-Aft Moment Spectral Densities at 8 m/s (a), 11.4 m/s (b) and 15 m/s (c)

### 4.6.4 Blades Root Flapwise Loads and Moment

The blades root flapwise damage equivalent loads with respect to varying wind shear due to atmospheric stability is shown below in *Figure 4.6*. The highest DELs occur for a combination of very stable conditions and the largest wind speed. Although there are some studies which show unstable conditions increased DELs of blades root flapwise in Ref. [27] and in Ref. [10] at lower wind speed due to the contrasting influence of wind profiles and turbulence, in this study very stable conditions induce higher loads because of fixed turbulence intensity input. It is seen from our results that the variations in wind shear influence the DELs of blade root flapwise slightly at below rated wind speed, while the influence at above rated (15 m/s) wind speed more significantly.

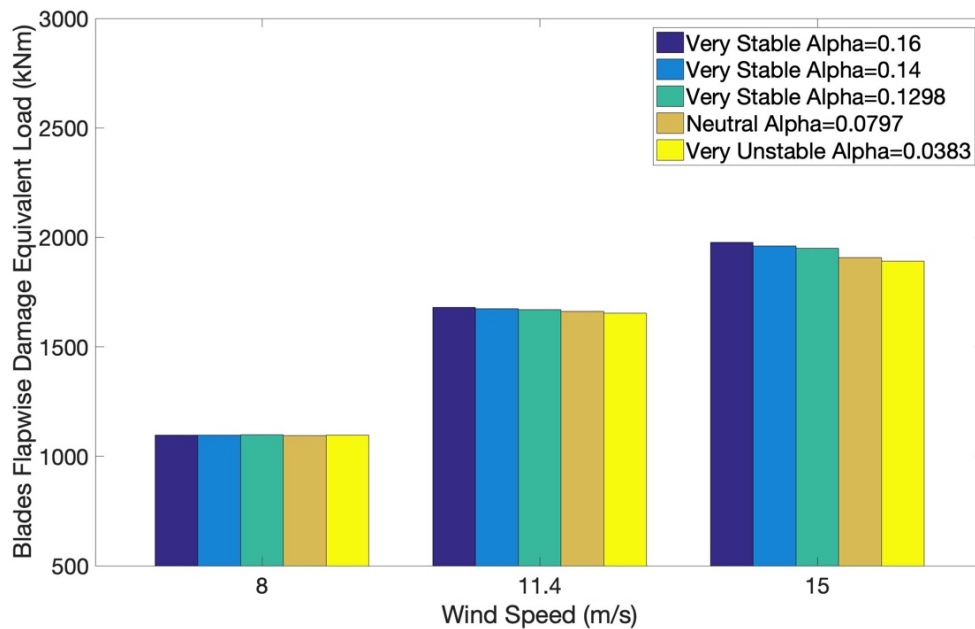


*Figure 4.6 Blade Root Flapwise Damage Equivalent Loads under Each Stability Class for 8 m/s, 11.4 m/s and 15 m/s*

The blade root flapwise damage equivalent load is normalized by neutral conditions at 8 m/s. Comparing different wind speed, the largest percentages appear at very stable ( $\alpha=0.16$ ) stratifications by respectively 53% at 11.4 m/s and 81% at 15 m/s (see *Figure 4.7* and *Table 4.10*). At 8 m/s, the blade root flapwise loads are the least affected by the five different stability classes, where differences are less than 1%. This corresponds to the results from the spectra of blade root flapwise bending moment (see *Figure 4.8*).

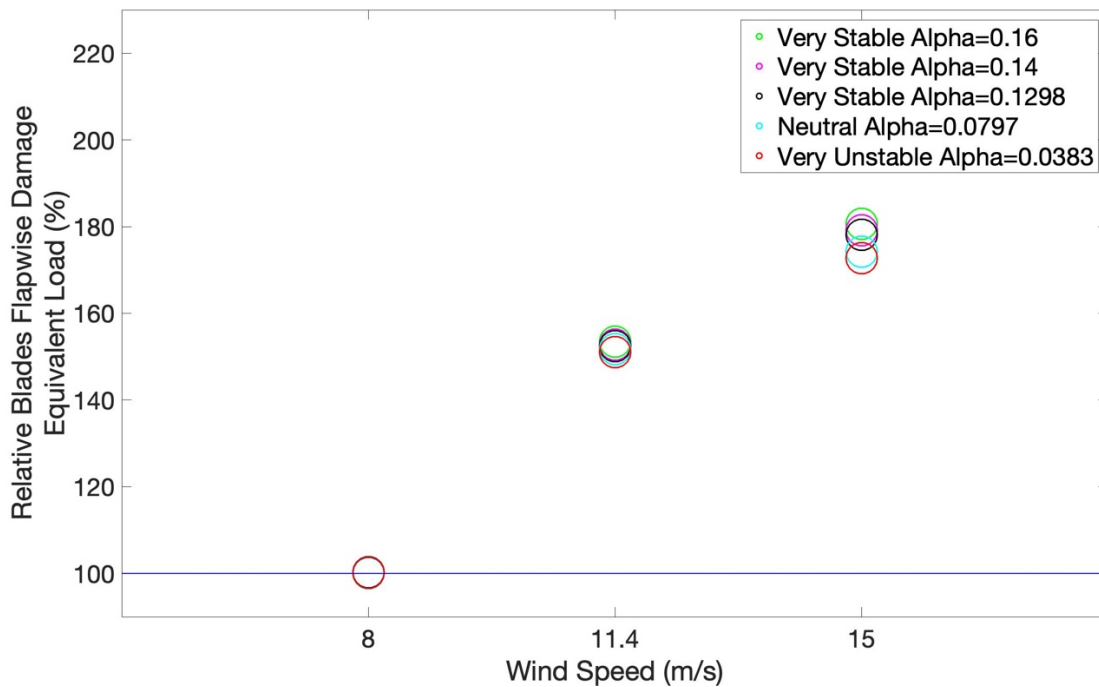
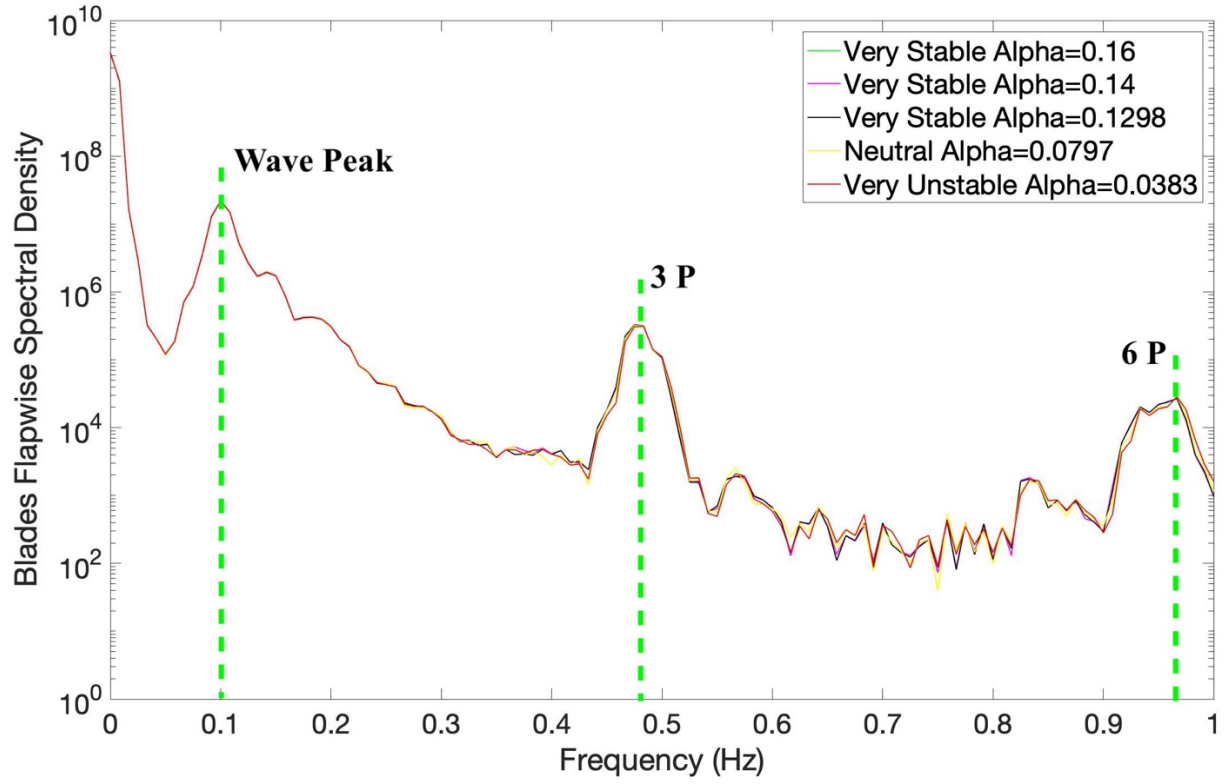


*Figure 4.7 Normalized Blade Root Flapwise Damage Equivalent Loads under Each Stability Class for 8 m/s, 11.4 m/s and 15 m/s*

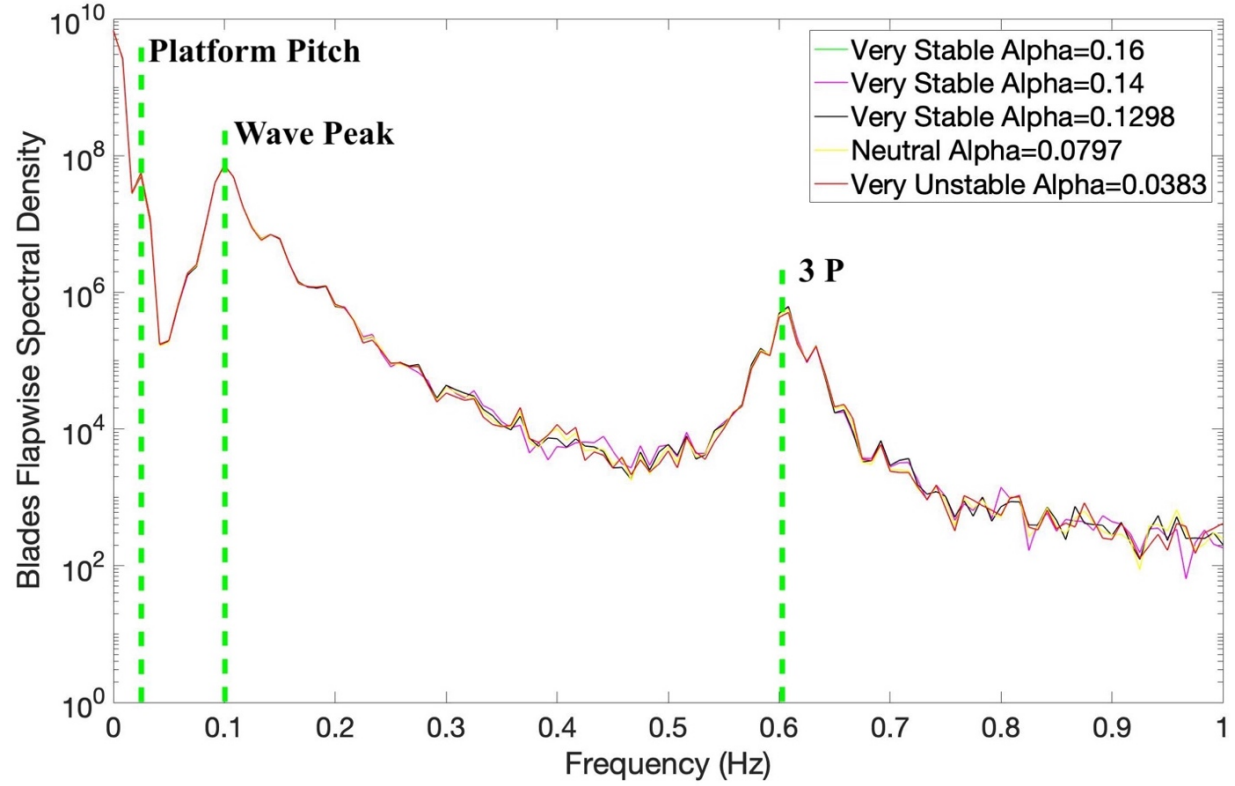
*Table 4.10 Percentages of Blades Root Flapwise Damage Equivalent Loads Relative to Neutral Stability*

Atmospheric Stability	Blade Root Flapwise (%)		
	8 m/s	11.4 m/s	15 m/s
Very Stable $\alpha = 0.16$	100.183	153.443	180.586
Very Stable $\alpha = 0.14$	100.220	152.831	179.146
Very Stable $\alpha = 0.1298$	100.275	152.443	178.096
Neutral $\alpha = 0.0797$	100	151.760	174.184
Very Unstable $\alpha = 0.0383$	100.179	151.026	172.700

The various wind profiles impact on blade root flapwise energy which are presented in *Figure 4.8*. Very stable conditions have slightly more energy at 3P frequency for the three wind speeds considered. The 6P frequency is observed at below rated wind speed. Each main excitations frequency corresponding to each wave spectral peak of blades flapwise is agreement with the blade passing frequencies (in *Table 4.7*). Likewise, the wave eigenfrequency gives the highest excitation of the blades boot flapwise loads compared with 1P, 2P and 3P rotational frequencies. As the mean wind speed increases to 11.4 m/s, a new excitation induced by platform pitch at 0.033 Hz frequency is observed, this wave spectral peak generates significant blade root flapwise moment energy as well.



(a)



(b)

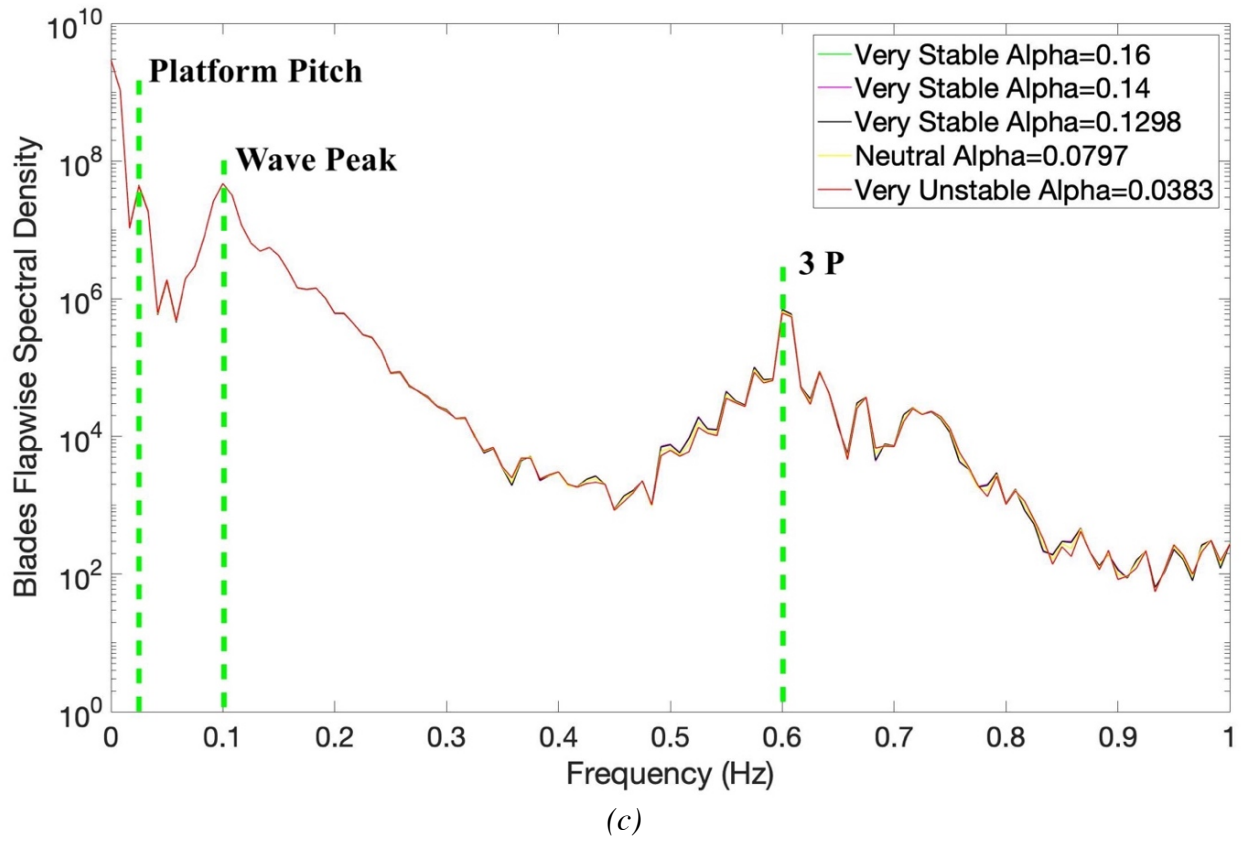


Figure 4.8 Blades Root Flapwise Spectral Densities at 8 m/s (a), 11.4 m/s (b) and 15 m/s (c)

### 4.6.5 Blades Root Edgewise Loads and Moment

Figure 4.9 presents the blade root edgewise damage equivalent loads at 8 m/s, 11.4 m/s and 15 m/s. A small difference (up to 6%) is among the three mean wind speeds of the normalized blade root edgewise equivalent loads relative to neutral conditions at 8 m/s is observed. The more unstable atmospheric stability results in higher loads especially for the higher wind speed, but it is not noticeable for lower wind speed. Comparing three very stable conditions with three different alpha values ( $\alpha = 0.1298$ , 0.14 and 0.16), the blades root edgewise damage equivalent loads do not have much differences, i.e. the wind shear influences the loads very little.

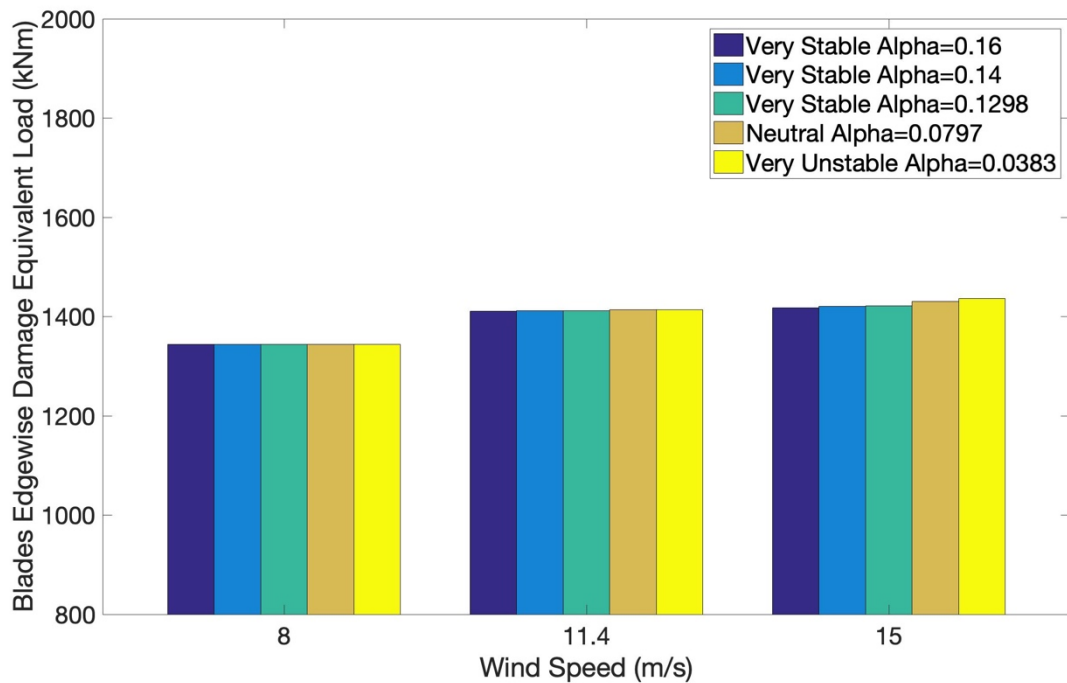


Figure 4.9 Blades Root Edgewise Damage Equivalent Loads under Each Stability Class for 8 m/s, 11.4 m/s and 15 m/s

We observed all percentages of blade edgewise loads amongst different stability classes are normalized to neutral conditions at 8 m/s where all differences are less than 1% from Figure 4.10 and Table 4.11. A. Sathe et al. and M. C. Holtslag et al.

[27] both mention that this is because the gravitational forces resulting from the mass of blades have the dominant contribution to the blade edgewise loads.

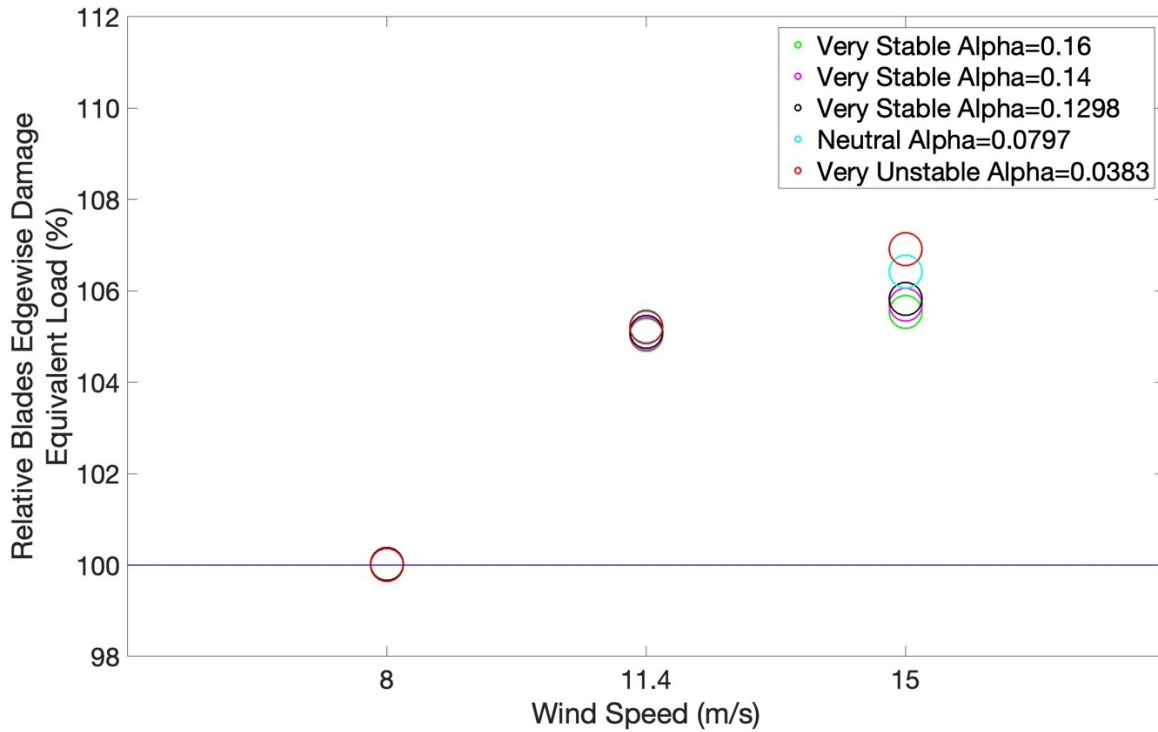
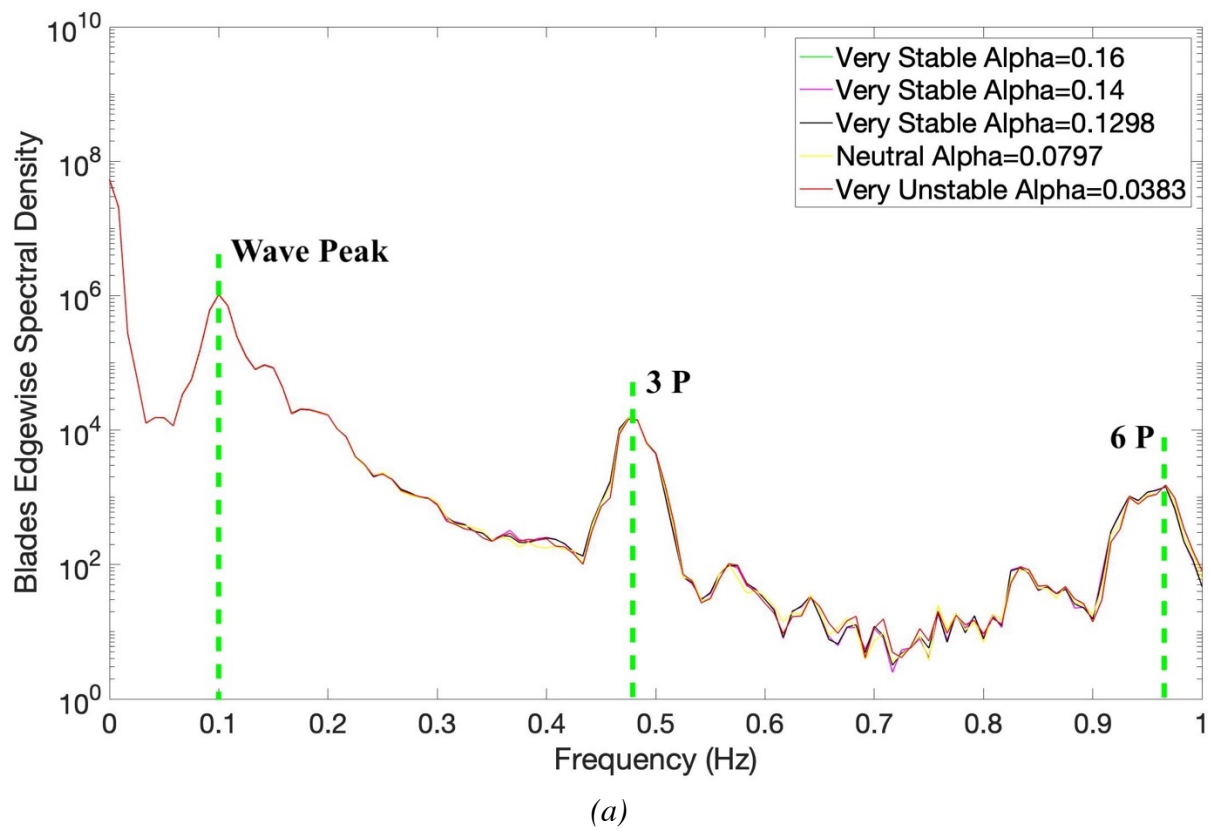


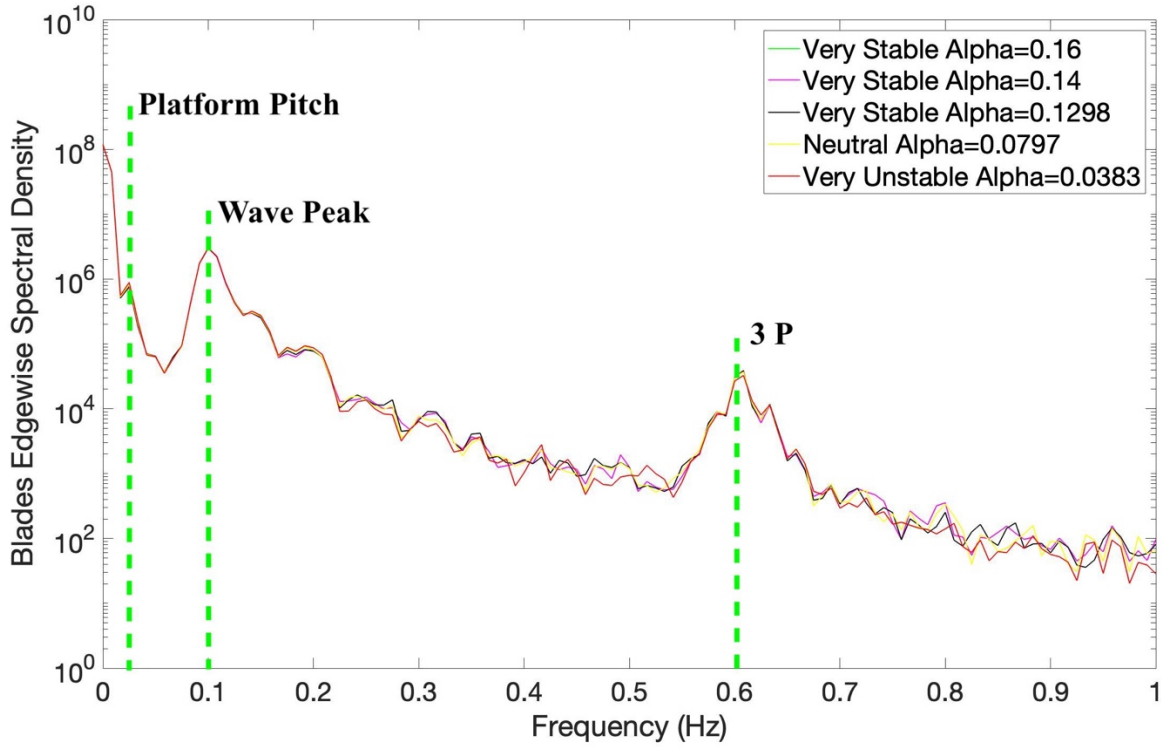
Figure 4.10 Normalized Blades Root Edgewise Damage Equivalent Loads under Each Stability Class for 8 m/s, 11.4 m/s and 15 m/s

Table 4.11 Percentages of Blade Root Edgewise Damage Equivalent Loads Relative to Neutral Stability

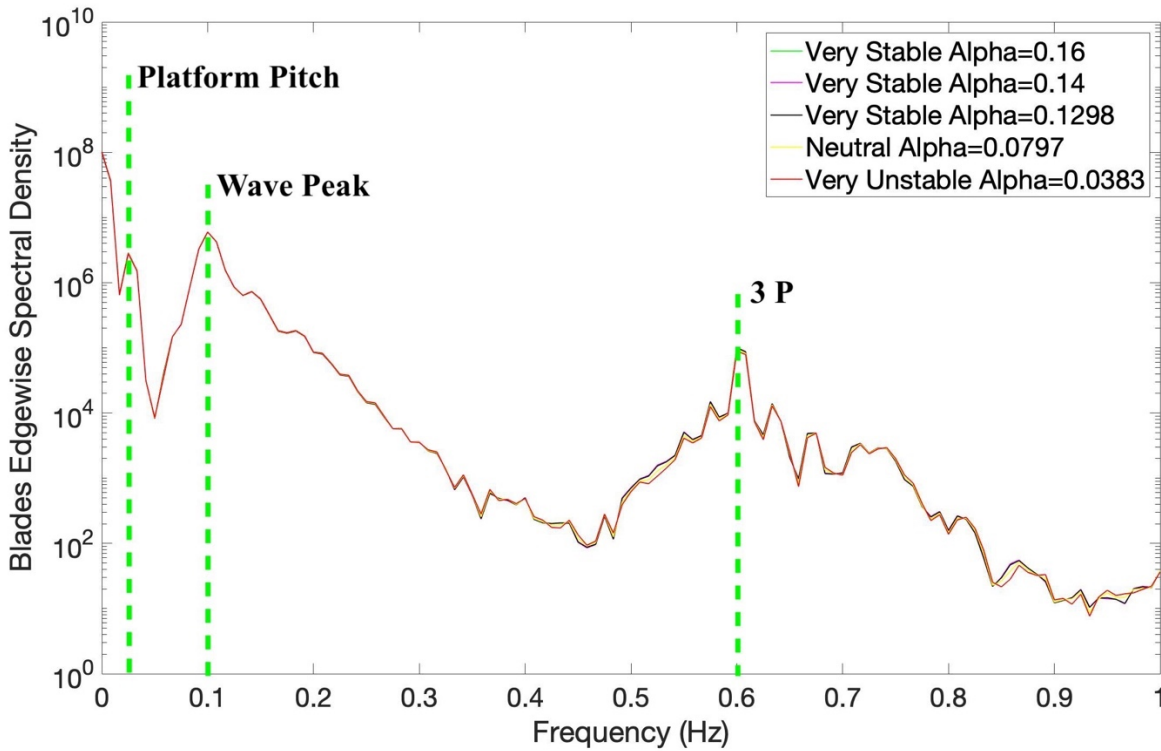
Atmospheric Stability	Blade Root Edgewise (%)		
	8 m/s	11.4 m/s	15 m/s
Very Stable $\alpha = 0.16$	100.005	105.034	105.542
Very Stable $\alpha = 0.14$	100.008	105.059	105.699
Very Stable $\alpha = 0.1298$	100.020	105.098	105.824
Neutral $\alpha = 0.0797$	100	105.225	106.427
Very Unstable $\alpha = 0.0383$	100.001	105.212	106.919

Figure 4.11 shows the blade root edgewise spectral densities for variation mean wind speeds. An additional 6P frequency is observed at below rated wind speed. The increase in the wind speed affects the blade root edgewise energy content in a similar way to the blade root flapwise. Moreover, the wind shear does not appear to influence the blade root edgewise energy content too much. The maximum excitations of blades root edgewise moment spectral densities for these three velocities are at wave peak frequency.





(b)



(c)

Figure 4.11 Blades Root Edgewise Spectral Densities at 8 m/s (a), 11.4 m/s (b) and 15 m/s (c)

### 4.6.6 Tower Top Torsion and Yaw Moment

The variation of tower top torsion damage equivalent loads at 8 m/s, 11.4 m/s and 15 m/s with regard to various stability classifications is elaborated in *Figure 4.12*. There is a notable increase in the DELs from very stable to very unstable. Additionally, there is an increasing trend from lower wind speed to higher wind speed. It is fascinating to note that in *Figure 4.12*, the tower top DELs are significantly influenced by mean wind profiles and mean wind speeds, since there is a bigger difference between very stable and very unstable at 15 m/s which is up to 30% (*Table 4.12*). However, we do not observe much difference in tower top torsion under the three very stable conditions, this is same with blade root edgewise loads. To verify this consequence in detail, tower top torsion damage equivalent loads under various stability classifications are normalized to neutral condition at 8 m/s as shown in *Figure 4.13* and percentages are shown in *Table 4.12*.

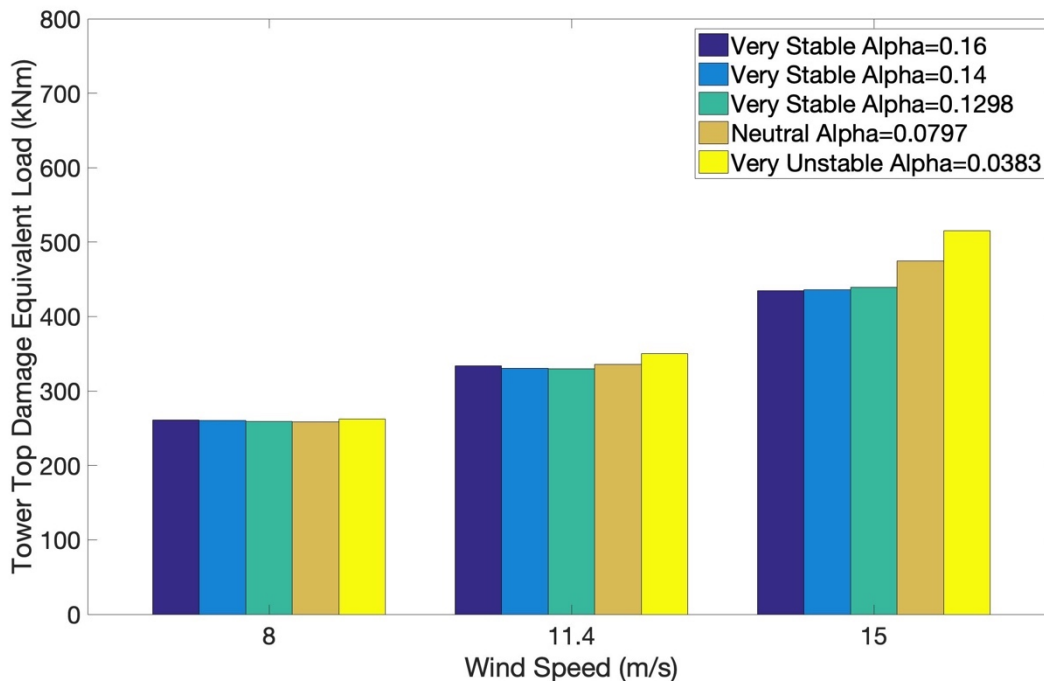


*Figure 4.12 Tower Top Torsion Damage Equivalent Loads under Each Stability Class for 8 m/s, 11.4 m/s and 15 m/s*

When the mean wind speed increases from 8 m/s to 15 m/s, the normalized tower top torsion damage loads relative to neutral conditions at 8 m/s increase by about 78% under very unstable, especially at above rated wind speed (15 m/s) where the percentage is the largest (up to 99%). In terms of various wind profiles, the variations between normalized tower top torsion damage loads under very unstable and neutral conditions are significant, which are up to 16% at above rated wind speed (15 m/s), 6% at rated wind speed (11.4 m/s) and 2% at below rated wind speed (8 m/s). Likewise, the difference of 14% is between very stable and neutral conditions at 15 m/s while the differences are less 2% at 8 m/s and 11.4 m/s. The combination of very unstable conditions and a larger wind speed resulted in the largest tower top torsion DEL.

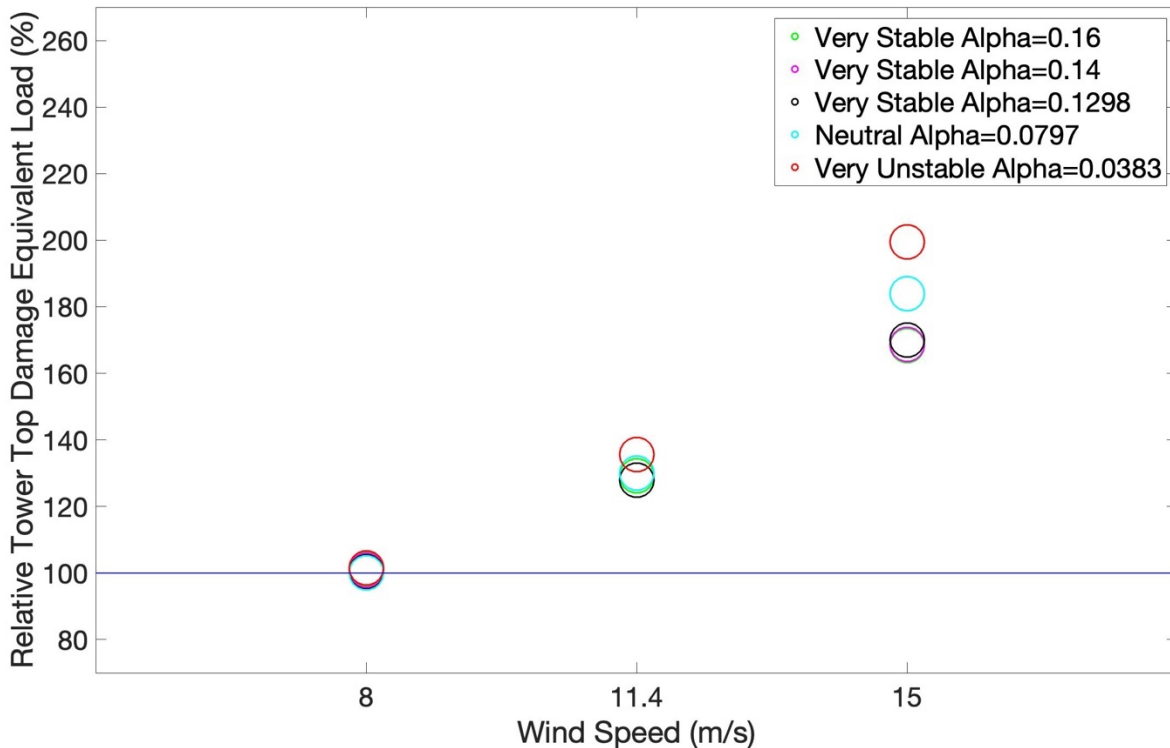


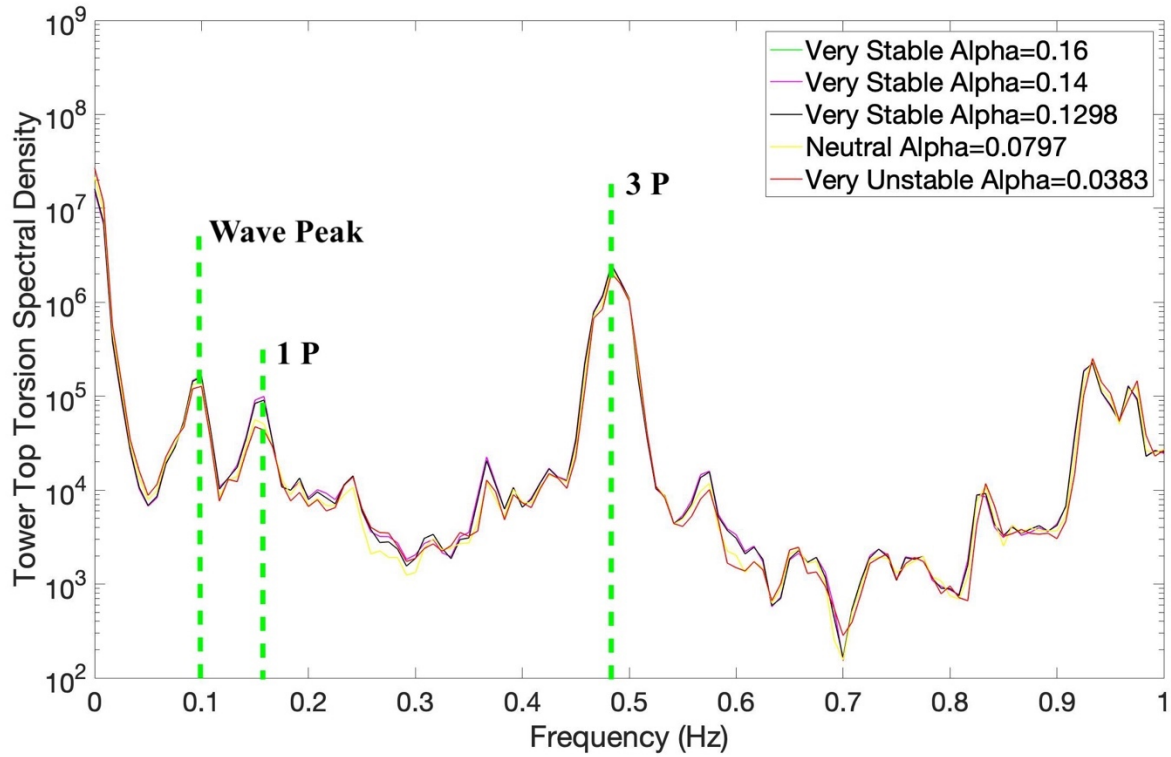
Figure 4.13 Normalized Tower Top Torsion Damage Equivalent Loads under Each Stability Class for 8 m/s, 11.4 m/s and 15 m/s

Table 4.12 Percentages of Tower Top Torsion Damage Equivalent Loads Relative to Neutral Stability

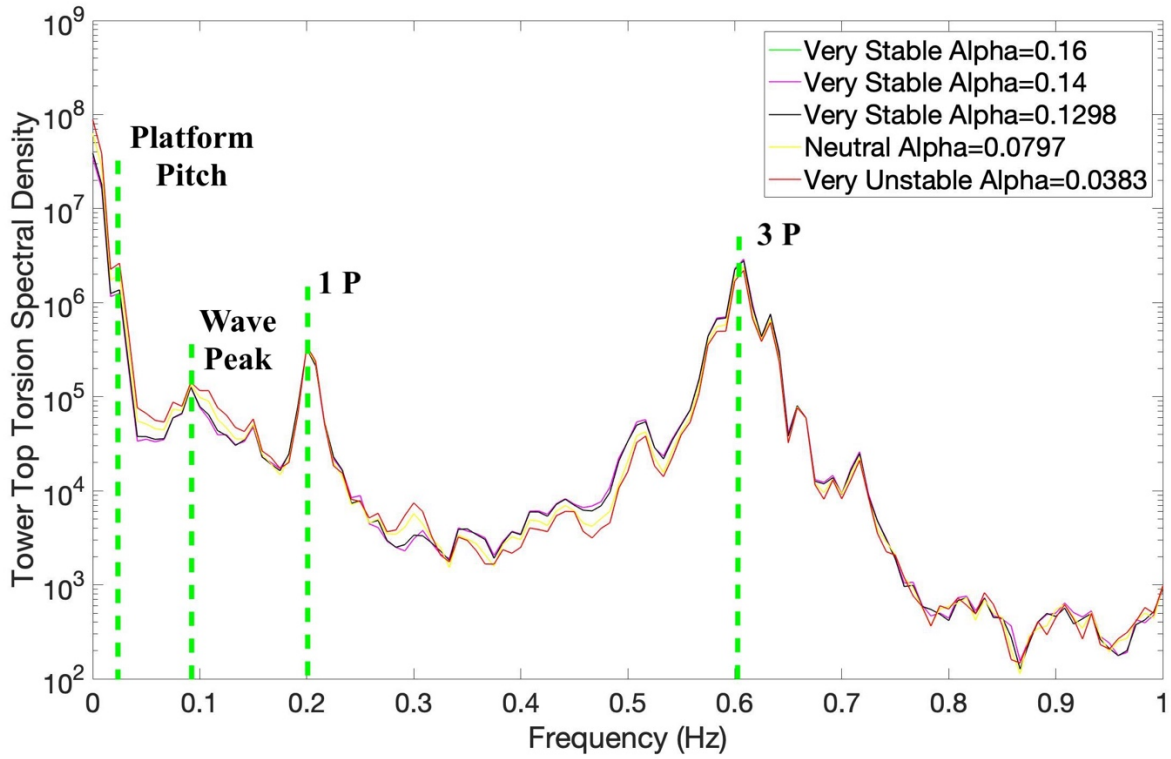
Atmospheric Stability	Tower Top (%)		
	8 m/s	11.4 m/s	15 m/s
Very Stable $\alpha = 0.16$	100.967	129.295	168.375
Very Stable $\alpha = 0.14$	100.826	127.948	168.711
Very Stable $\alpha = 0.1298$	100.340	127.822	170.049
Neutral $\alpha = 0.0797$	100	130.080	183.885
Very Unstable $\alpha = 0.0383$	101.547	135.620	199.566

Figure 4.14 shows the tower top yaw moment spectral densities at below rated, rated and above rated mean wind speeds. The tower top yaw moment spectral density at the three wind speeds indicates a notable variation depending on variation in wind shear across the rotor. A maximum excitation in energy at a frequency of around 0.5 Hz (at 8 m/s) and around 0.6 Hz (at 11.4 m/s and 15 m/s) is respectively generated for the tower top torsion, which is the third excitation frequency of the rotor 3P. Thus, the tower top yaw moment depended strongly on the 3P excitation for various mean wind speeds (see Figure 4.14). The wave and rotation of the rotor also result in tower top yaw moment spectral energy because of the excitations of wave eigenfrequency and 1P (particularly at above rated wind speed). In terms of various stability classifications, there are no very obvious differences at below rated wind speed (8 m/s) except neutral and very unstable which have lower energy content at 1P. Nevertheless, very unstable condition has the highest energy at lower frequency (0-0.2Hz) at 11.4 m/s and 15 m/s. However, the very stable conditions have the lowest energy content at 3P, and at the frequency of 1P, negligible differences can be seen.

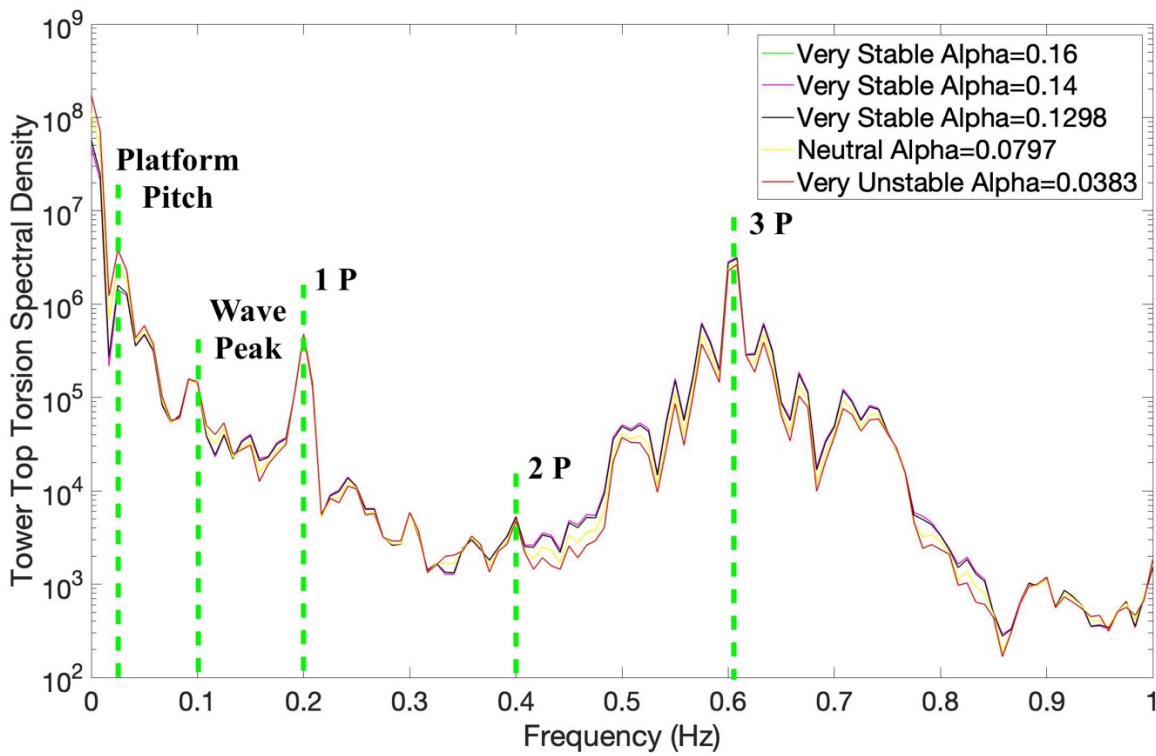
Overall, the tower top torsion shows a dependence on varying wind shear due to different stability classes with highest energies observed under unstable conditions.



(a)



(b)



(c)

Figure 4.14 Tower Top Yaw Moment Spectral Densities at 8 m/s (a), 11.4 m/s (b) and 15 m/s (c)

### 4.6.7 Rotor Loads and Moment

The x-direction aerodynamic forces  $F_x$  in shaft system are selected and analyzed. In terms of rotor damage equivalent load, larger wind speeds will generate more pronounced DELs as shown in *Fig 4.15*. The rotor loads at rated and above rated wind speeds are almost twice the value of below rated wind speed. In terms of variation in wind shear, there is negligible differences among these three power law exponents. Normalizing rotor damage loads to neutral condition at 8 m/s is done to indicate how much differences under a combination of the effects of different wind shear and mean wind speeds (see *Figure 4.16* and *Table 4.13*).

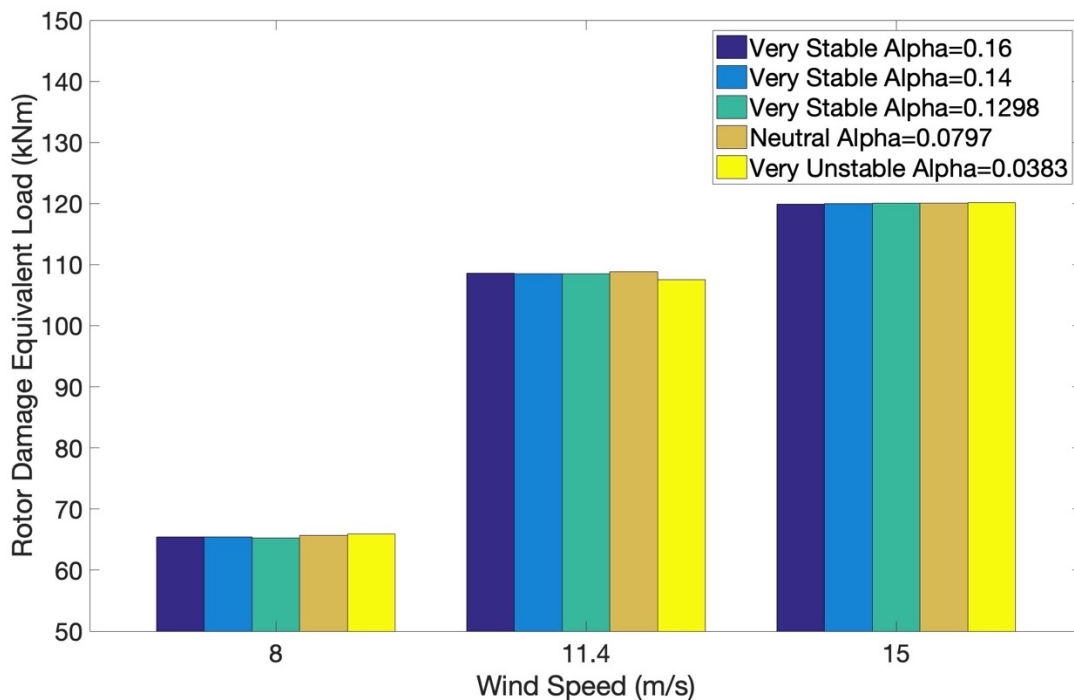


*Figure 4.15 Rotor Damage Equivalent Loads under Each Stability Class for 8 m/s, 11.4 m/s and 15 m/s*

As *Table 4.13* shown, there are no significant differences amongst distinct stability classifications for steady mean wind speed because all of them are less than 1%. It is concluded that wind shear (wind profile) contributes only minor influence on rotor

loads in contrast to mean wind speed, which is in line with previous paper from M. C. Holtslag et al.. [27]

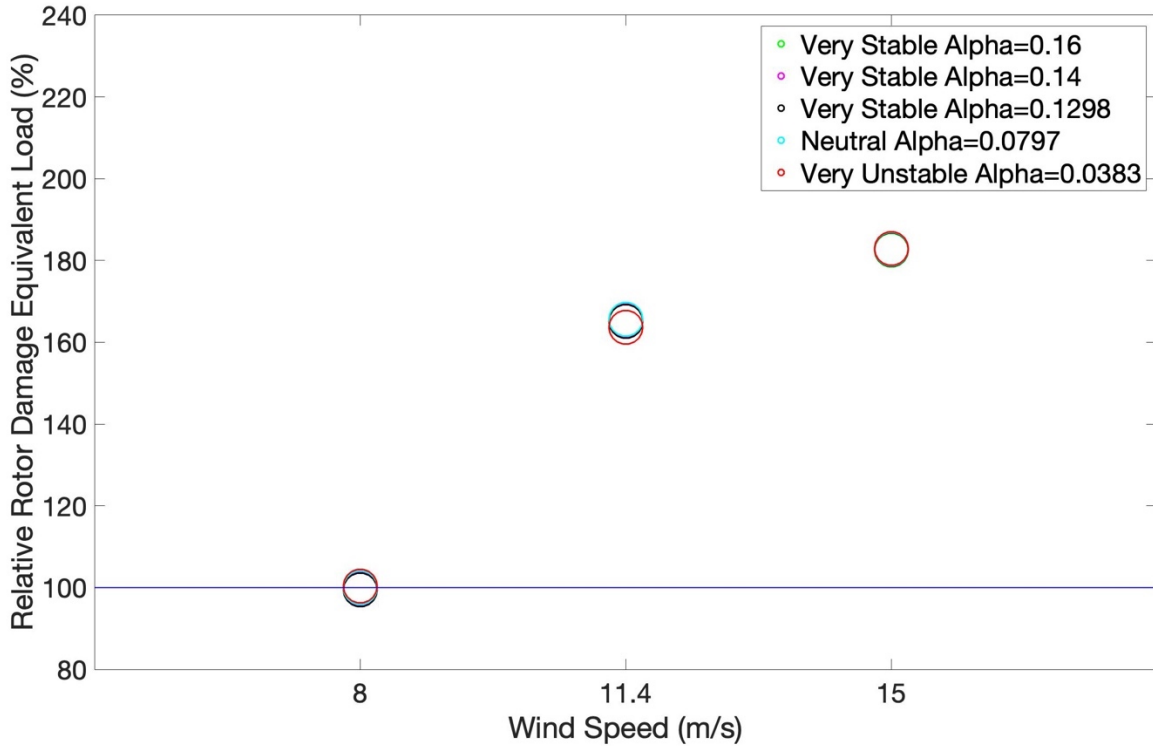
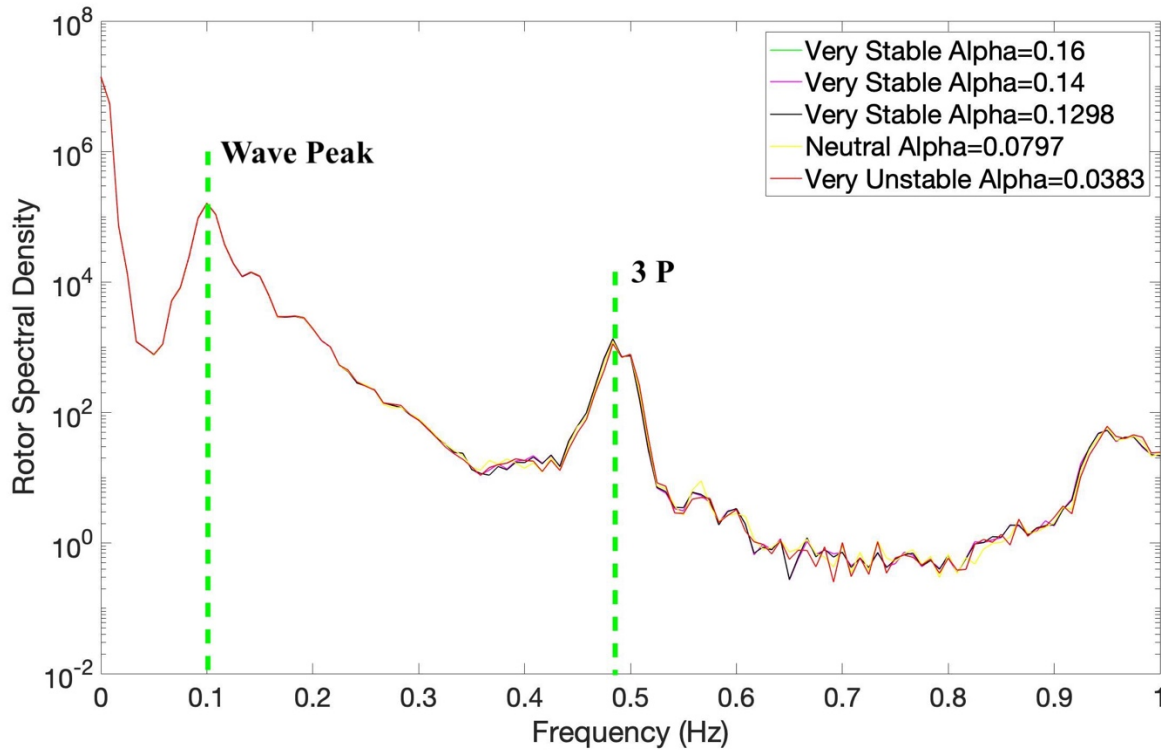


Figure 4.16 Normalized Rotor Damage Equivalent Loads under Each Stability Class for 8 m/s, 11.4 m/s and 15 m/s

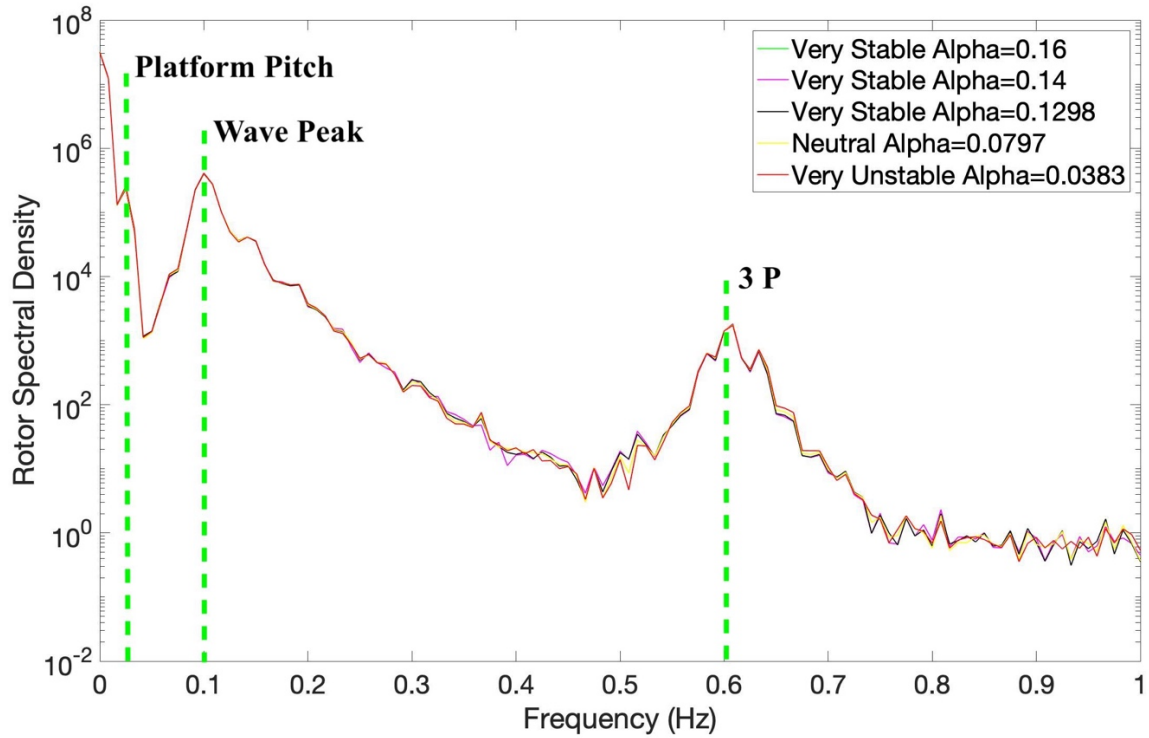
Table 4.13 Percentages of Rotor Damage Equivalent Load Relative to Neutral Stability

Atmospheric Stability	Rotor (%)		
	8 m/s	11.4 m/s	15 m/s
Very Stable $\alpha = 0.16$	99.605	165.378	182.588
Very Stable $\alpha = 0.14$	99.578	165.191	182.674
Very Stable $\alpha = 0.1298$	99.394	165.147	182.732
Neutral $\alpha = 0.0797$	100	165.694	182.806
Very Unstable $\alpha = 0.0383$	100.398	163.663	182.907

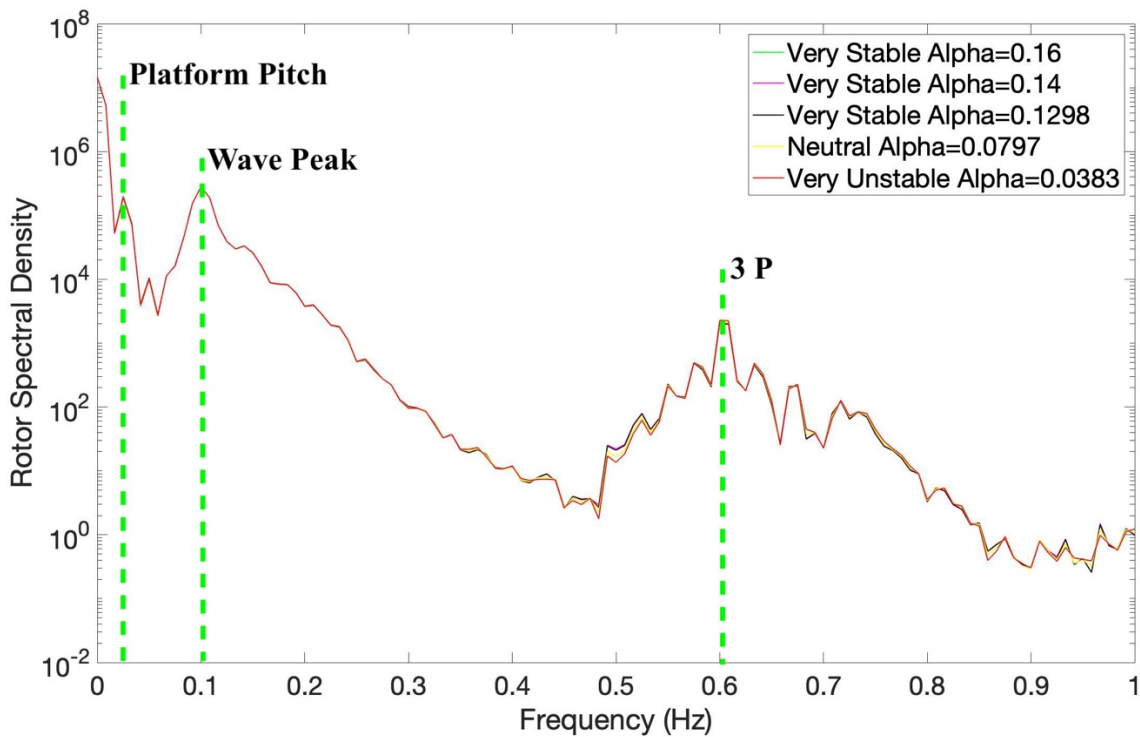
The rotor spectra at three different wind speeds are plotted in *Fig 4.17*. There is negligible difference in the energy content among these three stability classifications especially at the lower frequencies. The largest rotor loads energy content happens at wave eigenfrequency. Overall, the wind profile does not influence much rotor load and energy moment in this simulation.



(a)



(b)



(c)

Figure 4.17 Rotor Spectral Densities at 8 m/s (a), 11.4 (b) and 15 m/s (c) 4.6.8 Mooring Lines Loads and Moment

## 4.6.8 Translational Motion

There are six-degree of freedom motions induced by the wave and wind loadings on the floating wind turbine. Three of them are the translational motion: surge, sway and heave. A comparison of the maximum and minimum surge and sway motions and the spectral plots of them can be found below in *Fig. 4.18* to *Fig. 4.23*. When the wind turbines move along the positive direction of the axes, the translational displacement will get positive values, conversely, it will get negative values. In this thesis, the ‘maximum’ means the largest displacement in positive direction and the ‘minimum’ means the largest displacement in negative direction. From our results, we see that the surge motion has the largest displacements (about 30m at 15m/s, 35m at 11.4 m/s and 25m at 8m/s).

### Surge

In *Figure 4.18*, surge motion spectra at 15 m/s is shown where a new excitation appear at 0.033 Hz which coincides with the natural frequencies of platform roll and pitch (see *Table 4.8*). The maximum surge spectral density of 11.4 m/s is the highest among these three velocities at the same frequency interval as shown in *Fig. 4.18*. In terms of heave spectral density (*Figure 4.19*), there are no noticeable differences in the maximum or minimum heave displacements and heave spectra under each stability for below rated, rated and above rated mean wind speeds. Therefore, the magnitude of surge displacement mainly depends on hub height wind speed rather than wind profile slightly.

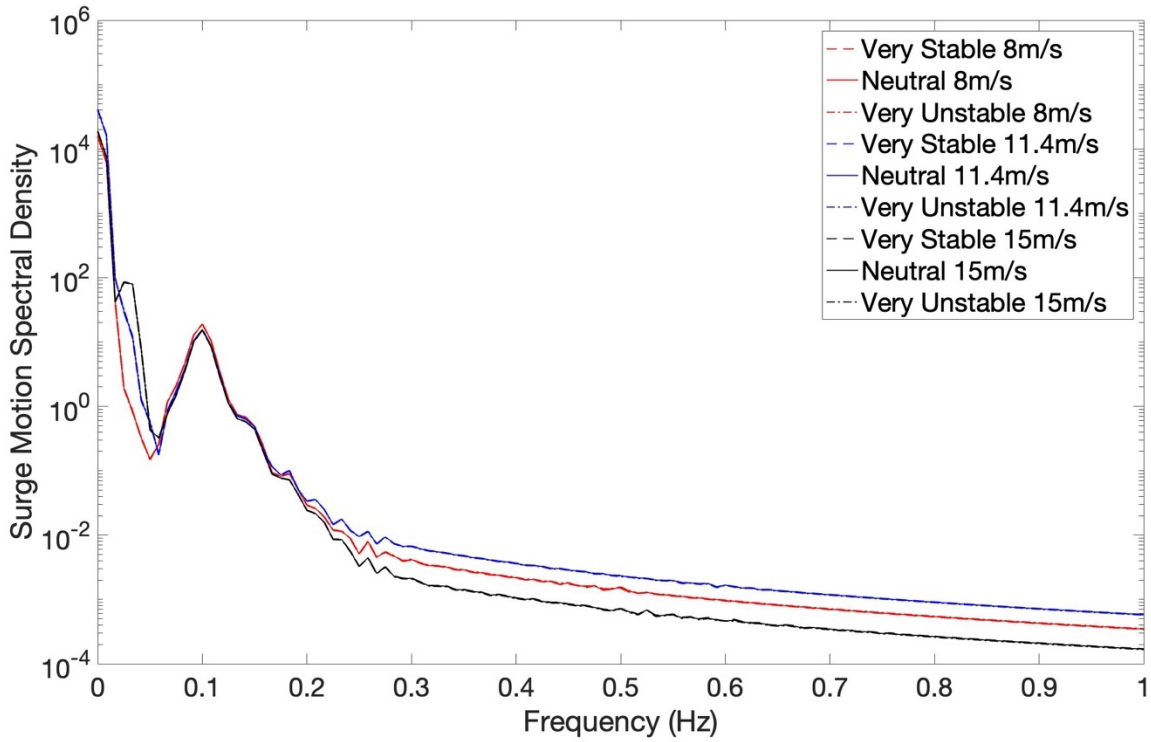


Figure 4.18 Surge Motion Spectral Densities at 8 m/s, 11.4 m/s and 15 m/s

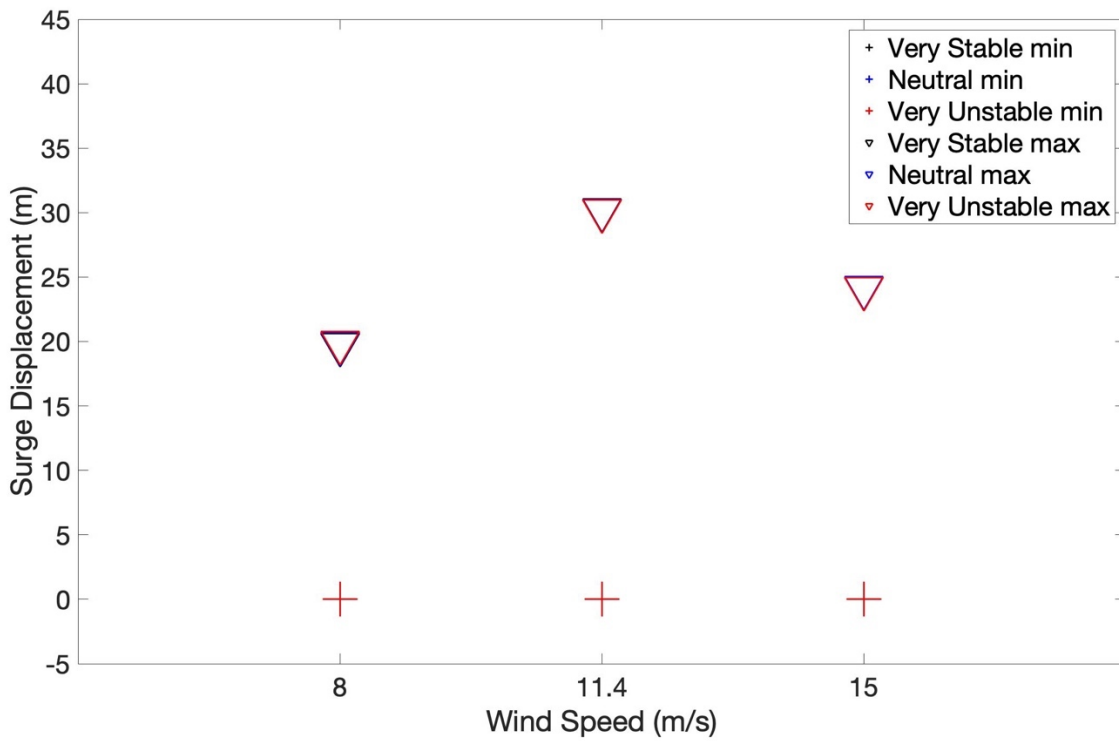


Figure 4.19 Comparison of Maximum and Minimum Surge Rotation under Each Stability for 8 m/s, 11.4 m/s and 15 m/s

## Sway

The spectral energy plots of sway motion show clear peaks at the wave excitation frequencies (0.1Hz) and an additional peak at 0.033Hz frequency (at 15 m/s) as well as at the 1P and 3P rotational frequencies in *Fig.4.20*. In which, the spectra of the sway motion which have similar decreasing trends at 8 m/s, 11.4 m/s and 15 m/s. The highest spectral energies are observed under very stable conditions for all of wind speeds. With the increasing of wind speed, the higher wind speed under very stable conditions gives significantly larger difference of energy among these three stability classifications, which coincides with the indication of *Figure 4.21*. The comparison of maximum and minimum sway motions is presented in *Figure 4.21*. Overall, the higher wind speed and very stable condition give the largest displacement, wind profile has slightly influence on the sway motion as well.

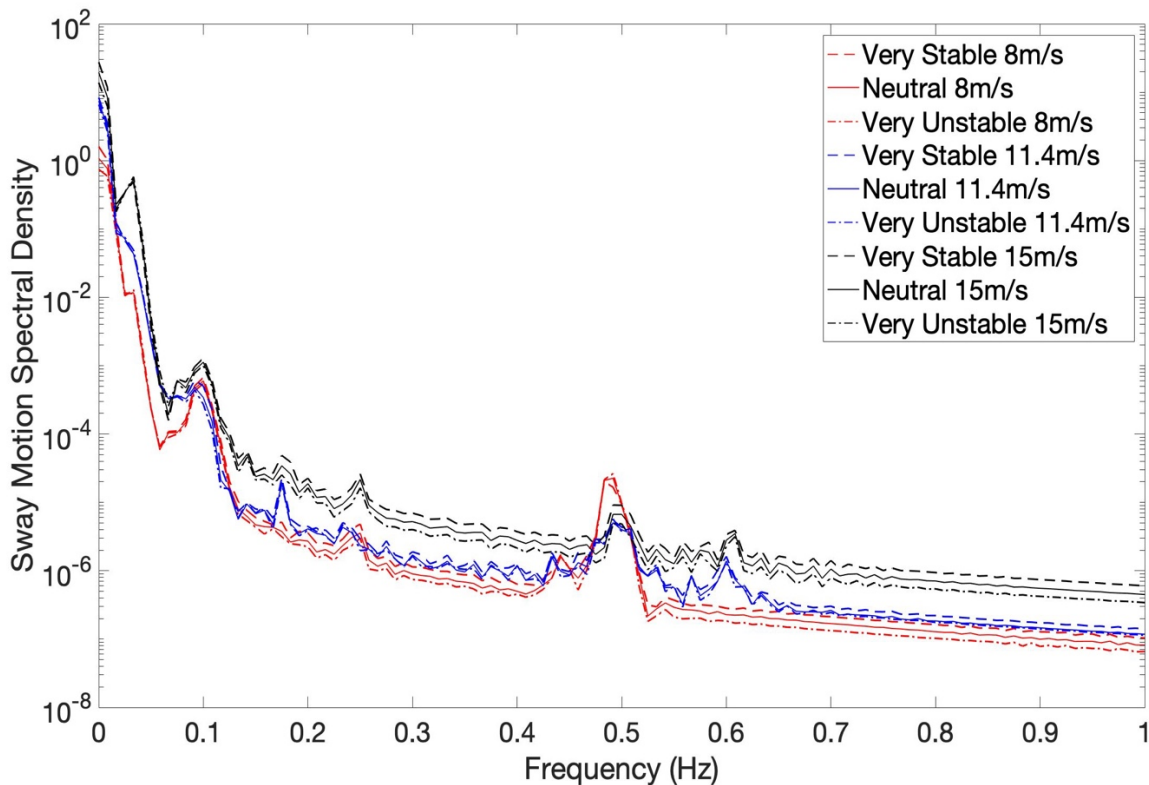


Figure 4.20 Sway Motion Spectral Densities at 8 m/s, 11.4 m/s and 15 m/s

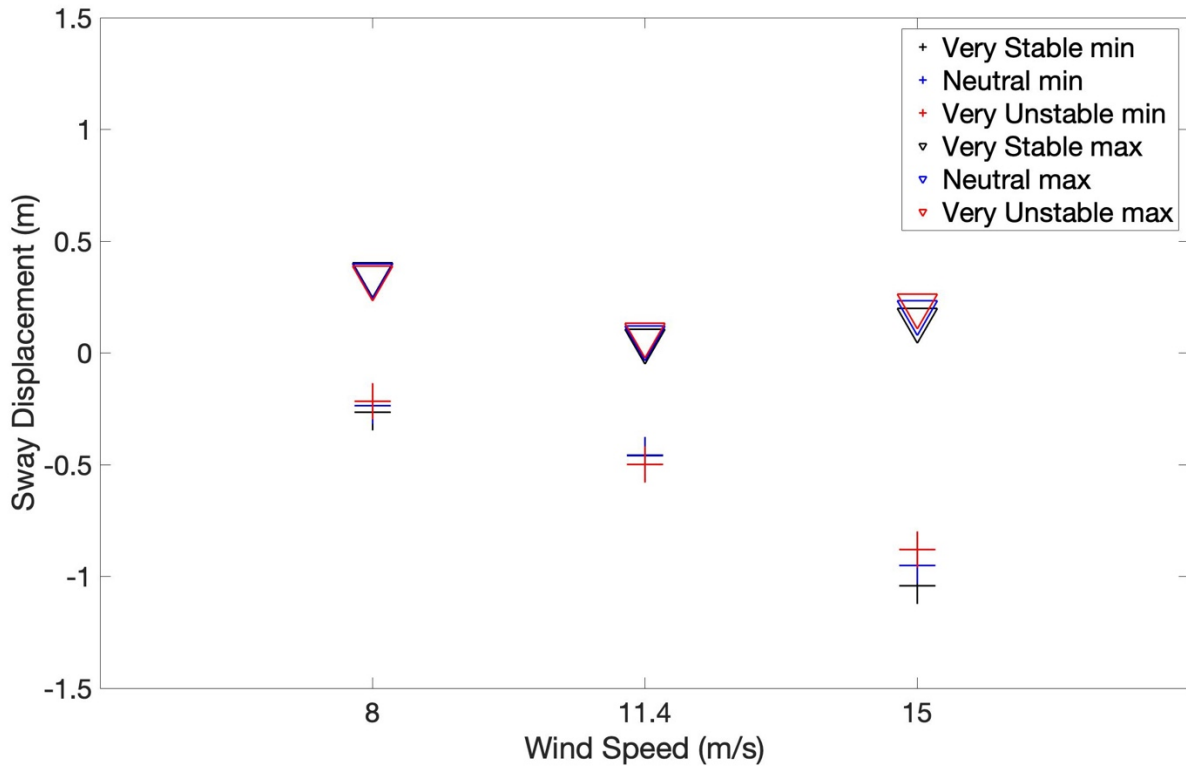


Figure 4.21 Comparison of Maximum and Minimum Sway Rotation under Each Stability for 8m/s, 11.4 m/s and 15 m/s

## Heave

For heave motion (see *Figure 4.22*) there is substantial differences in the spectral energy plots for varying wind speed and very little variance for varying wind profiles (see *Figure 4.23*). From *Figure 4.22* (black lines), there is a notable peak when the frequency is 0.033 Hz. The heave spectral moment of 15 m/s is the highest between the heave spectral density at 8 m/s and 11.4 m/s at the same frequency interval. We would like to say that the higher speed will produce more energy resulting in inducing higher displacements. However, in that three groups, each stability condition has something in common with the trend of heave spectral density for higher frequency. Therefore, heave motion strongly depends on hub height wind speeds. Overall, the main heave excitations happen at very low frequency (0.033Hz) or at the wave peak (0.1Hz). Wind profile has little influence on heave motion, because there is no too much difference between extreme values at *Figure 4.23*. In which the over rated wind speed responses larger surge motion energy spectral density.

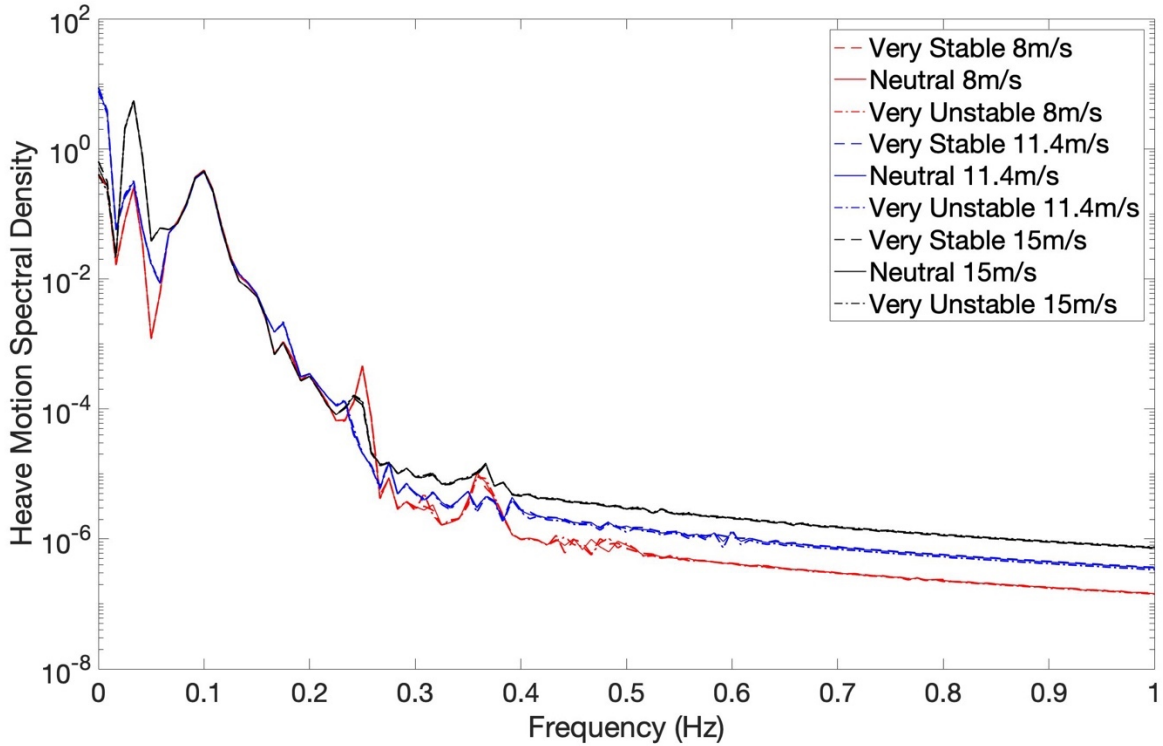


Figure 4.22 Heave Motion Spectral Densities at 8 m/s, 11.4 m/s and 15 m/s

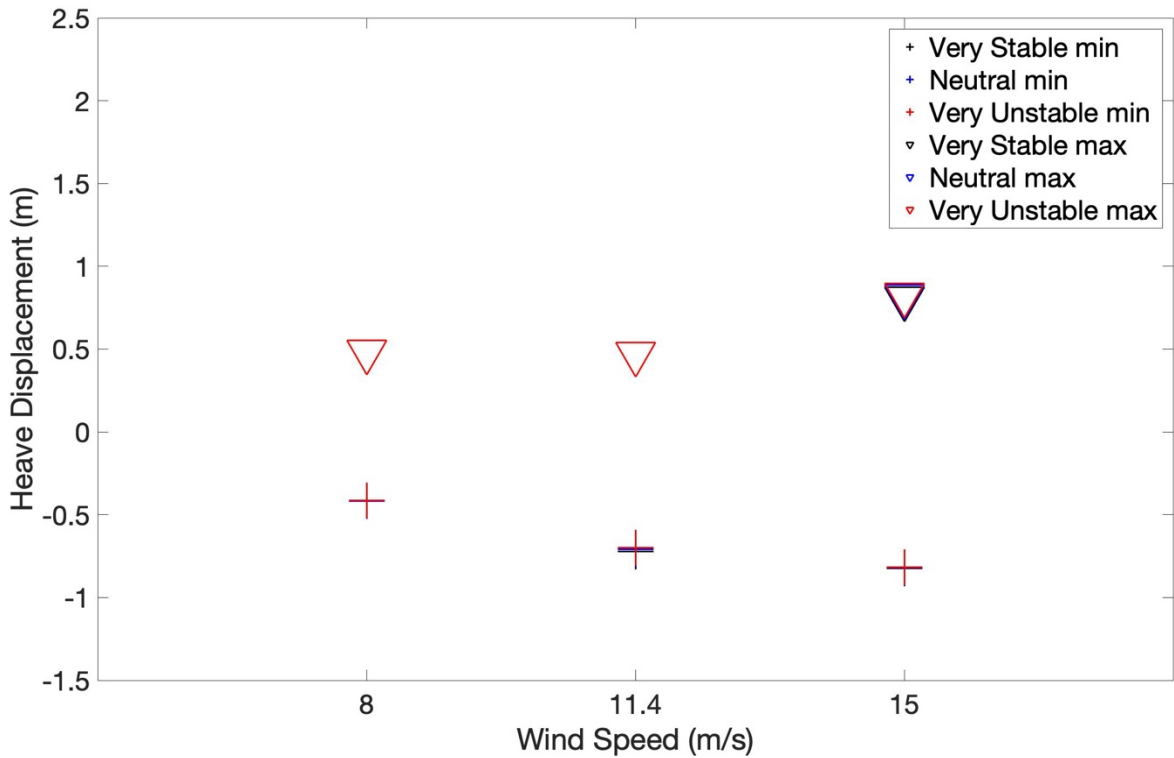


Figure 4.23 Comparison of Maximum and Minimum Heave Motion under Each Stability for 8m/s, 11.4 m/s and 15 m/s

## 4.6.9 Rotational Motion

Roll, pitch and yaw make up rotational motions. In the same manner with translational motion, the ‘maximum’ is the largest rotational degree of angle in positive direction and the ‘minimum’ is the largest rotational degree of angle in negative direction. The comparison of maximum and minimum rotational motions and spectra are presented below from *Figure 4.24* to *Figure 4.29*. It is thus evident that pitch motion has the largest rotations (about 10 degrees at 15 m/s, 7 degrees at 11.4 m/s and 4.5 degrees at 8 m/s).

### Roll

The values of ‘positive’ and ‘negative’ roll rotation under each stability at 15 m/s are approximately tripled than at 11.4 m/s and twice at 8 m/s from *Figure 4.25*. Furthermore, the roll motion with ‘maximum’ rotation at all of velocities will happen under very stable conditions, which is corresponding to roll motion energy spectrum (*Figure 4.24*). According to *Figure 4.24*, an increase in hub height wind speed tends to result in higher spectral density, i.e., higher energy. It is because that each black line (roll motion at 15 m/s) is almost above each yellow (roll motion at 11.4) and red (roll motion at 8 m/s) lines. In general, wind profile and hub high wind speed both have influence on roll motion. The roll motion spectral densities at 11.4 m/s and 15 m/s in *Figure 4.24*, there are new prominent peaks at 0.033Hz which is same with the natural frequencies of platform pitch and roll (see *Table 4.8*). The wave spectral peak, 1P and 3P generate significant roll motion energy as well for various mean wind speeds.

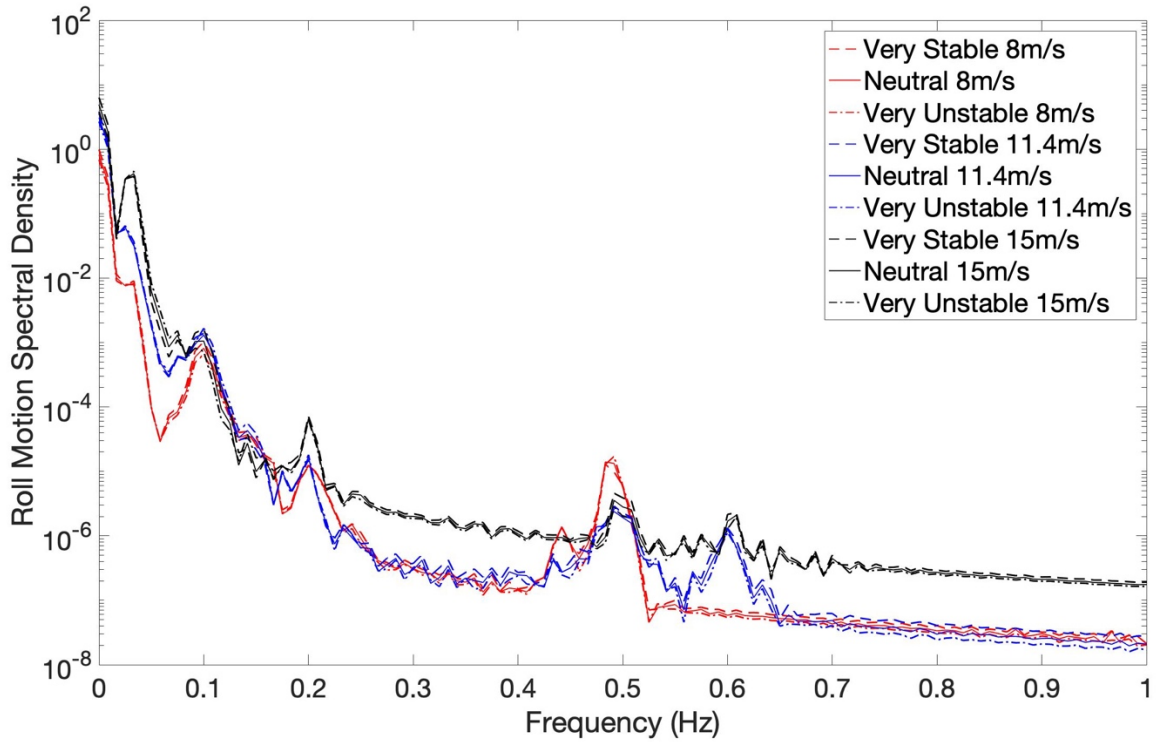


Figure 4.24 Roll Motion Spectral Densities at 8 m/s, 11.4 m/s and 15 m/s

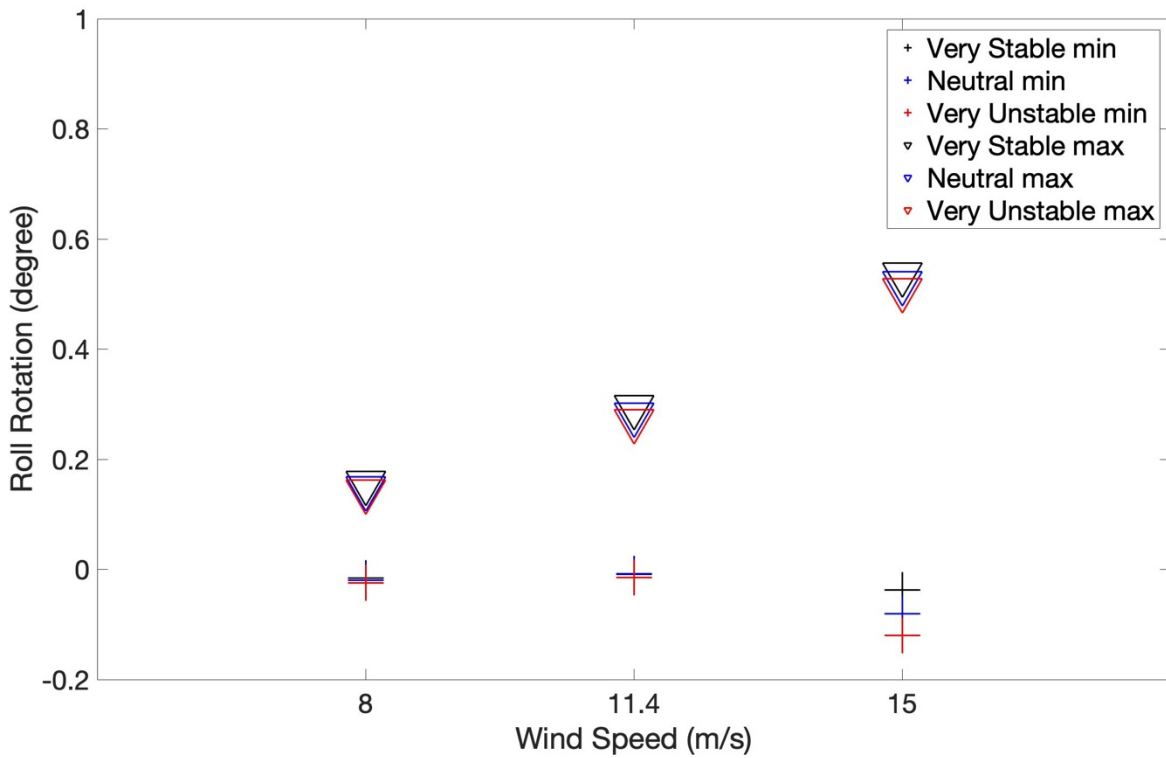


Figure 4.25 Comparison of Maximum and Minimum Roll Rotation under Each Stability for 8 m/s, 11.4 m/s and 15 m/s

## Yaw

*Figure 4.26* demonstrates various wind profiles resulting in small difference of yaw motions for each wind speed (8 m/s, 11.4m/s and 15 m/s). It is shown that very unstable responses the highest yaw motion spectral energy (shown in *Figure 4.26*) and induces maximum yaw rotation (shown in *Figure 4.27*) for all of wind speeds. There are substantial fluctuations in *Fig. 4.26*, and period witnesses peak differ in shape (width and height) for the spectra corresponding to different stability classes. Moreover, there are significant differences and fluctuations for yaw motion spectral energy at above rated wind speed. Thus, the combination of wind profile and wind speed are two of the major factors that could cause variation in the yaw motion (rotation). Besides, the wave peak gives the highest excitation, i.e. the wave effect is also an essential factor. We will further discuss yaw motion spectral densities (*Fig. 4.26*) in section 5.1. The result of comparison of maximum and minimum yaw rotations presents below in *Fig. 4.27* where the above rated wind speed generates largest yaw rotation.

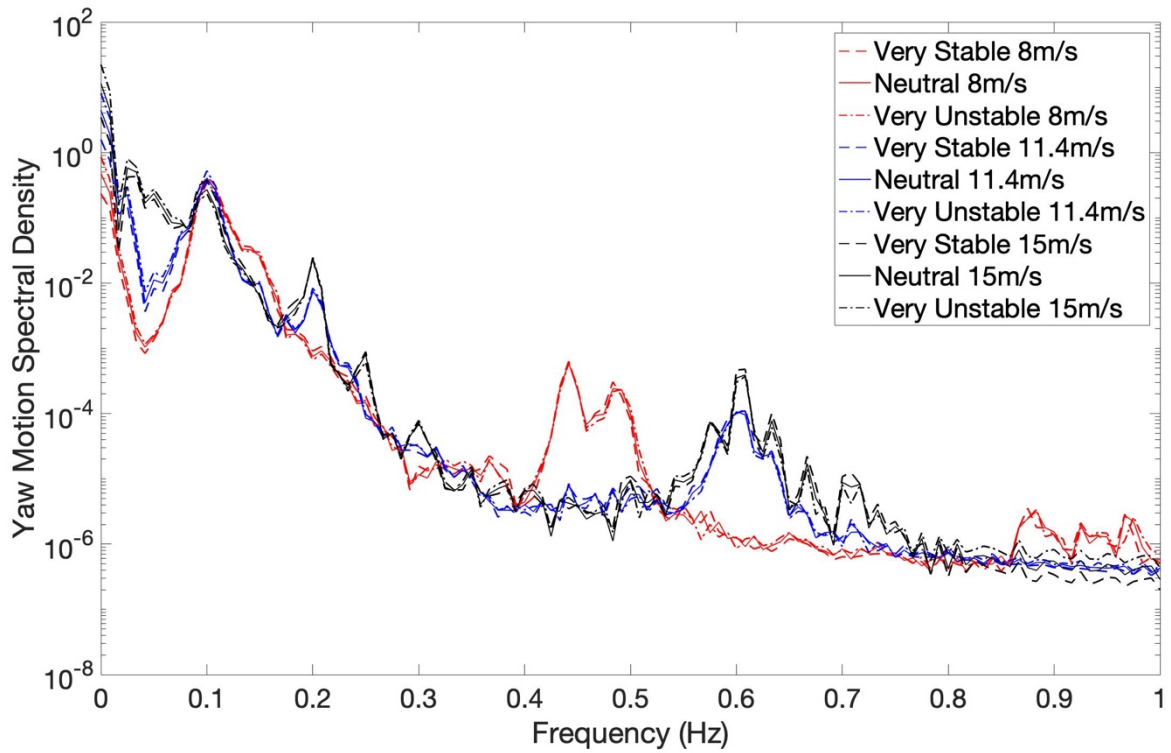


Figure 4.26 Yaw Motion Spectral Densities at 8 m/s, 11.4 m/s and 15 m/s

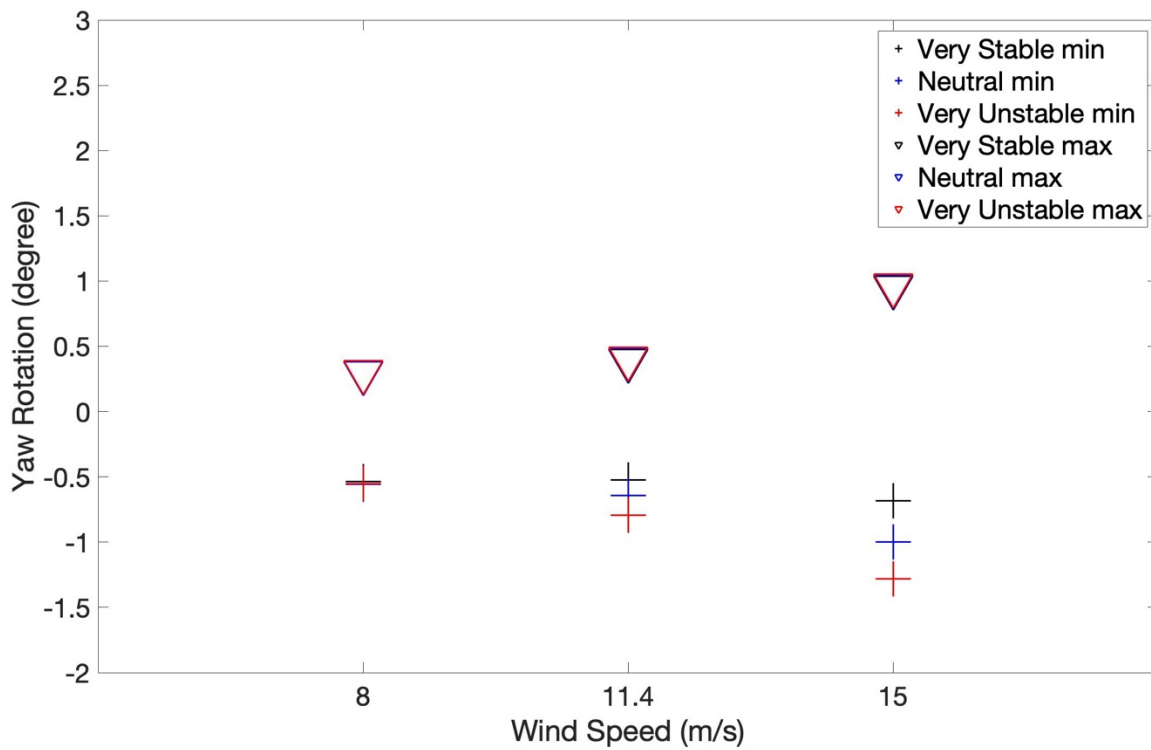
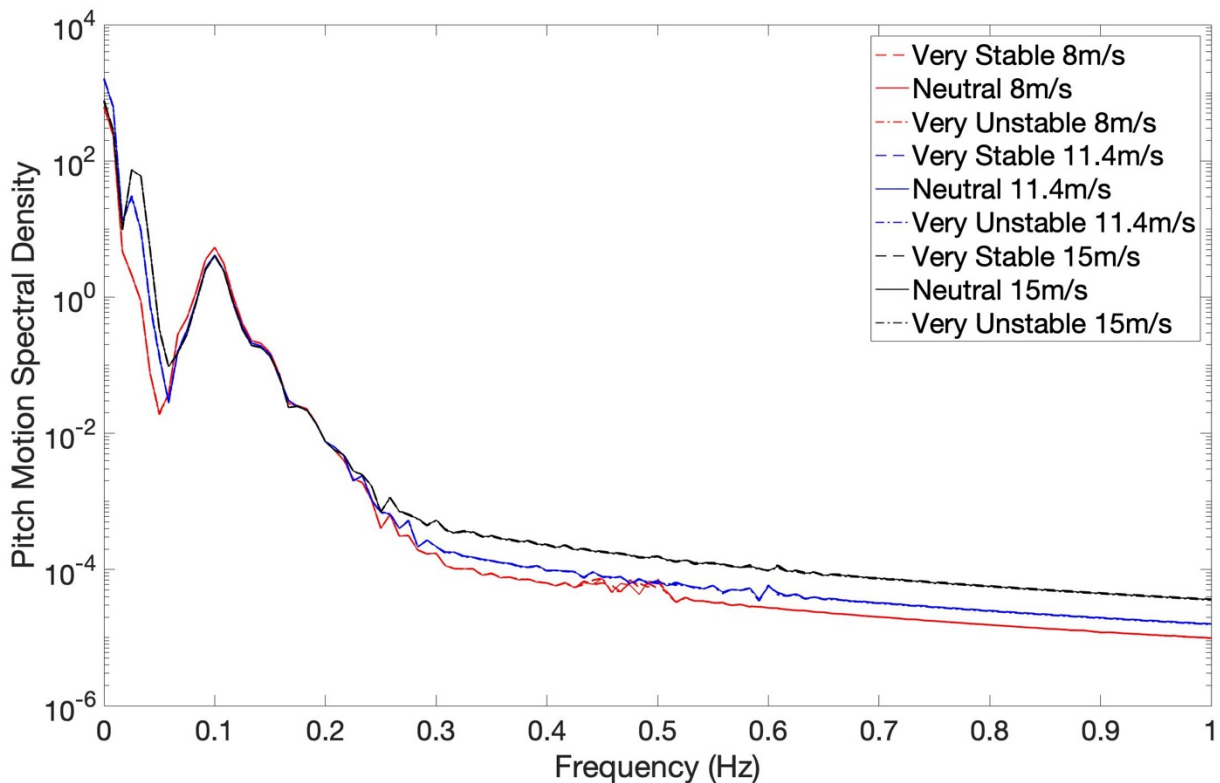


Figure 4.27 Comparison of Maximum and Minimum Yaw Rotation under Each Stability for 8m/s, 11.4 m/s and 15 m/s

## Pitch

In *Figure 4.28*, there is a notable difference of pitch spectral energy at 11.4 m/s and 15 m/s when the frequency is at 0.033 Hz which is coincide with the natural frequencies of platform pitch and roll (see *Table 4.8*). This finding is in agreement with the previous results of roll motion. The wave spectral peaks give higher excitations of pitch motion at various mean wind speeds, which are also observed in *Figure 4.28*. The maximum pitch spectral density of 15 m/s is the highest among these three velocities at the same frequency interval as shown in *Fig. 4.29*. That is to say, the higher wind speeds produce more energy resulting in inducing higher rotation about the z-axis for floating wind turbine. As this spectrum shown, each wind profile responses a similar trend of pitch motion spectral density for higher frequency as well as there is no notable difference under various wind profiles.



*Figure 4.28 Pitch Motion Spectral Densities at 8 m/s, 11.4 m/s and 15 m/s*

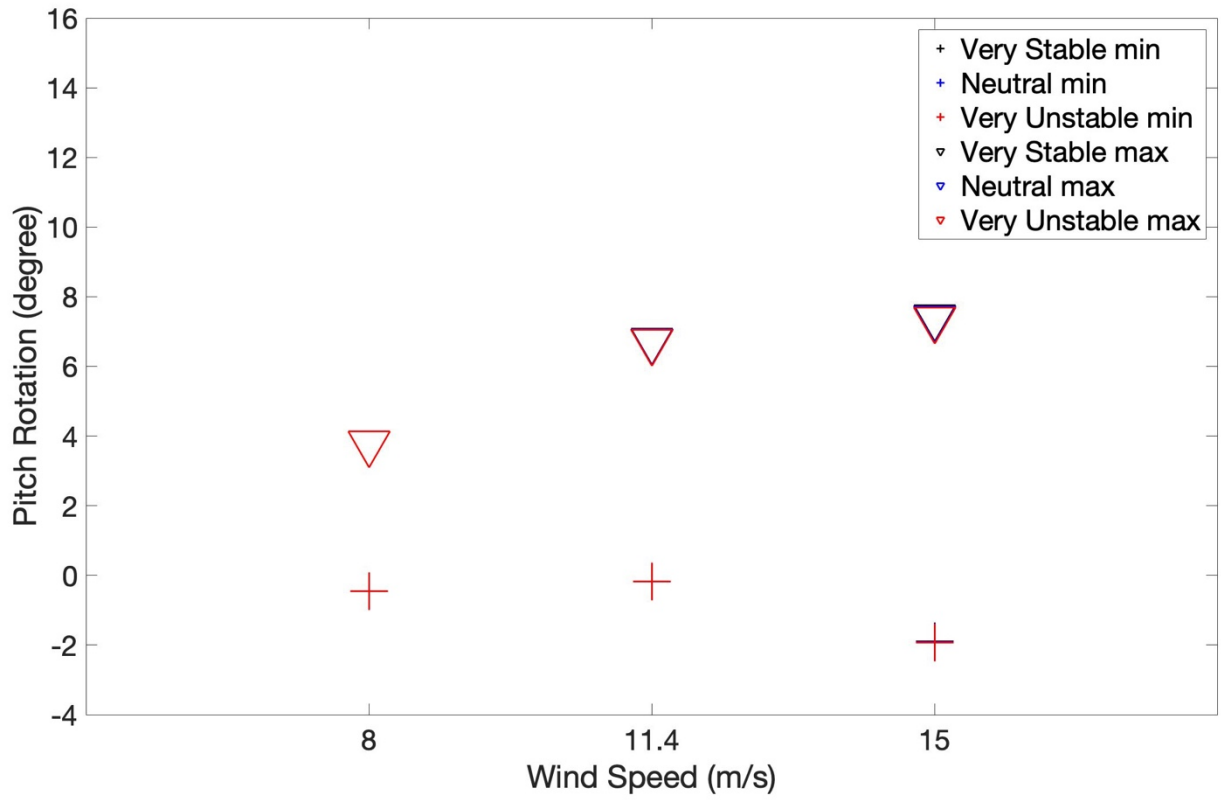


Figure 4.29 Comparison of Maximum and Minimum Pitch Rotation under Each Stability for 8 m/s, 11.4 m/s and 15 m/s

## **5. Discussion and Conclusion**

### **5.1 Discussion**

#### **5.1.1 Wind Turbine Damage Equivalent Loads**

In this thesis, we've assessed the sensitivity of damage equivalent loads of various wind turbine components to wind shear (mean wind profiles) and distinct hub height wind speeds (see chapter 4.6 and Appendix A). As power density spectra of mooring lines shown in Appendix A.1, there are a lot of distinct peaks at the frequencies from 0 to 1 Hz, also which are different to the other components (tower, blades and rotor). Wind profile and wind speeds are not the only unique factors that have effects on the DELs and motion of mooring lines, such as wave load and current load. Moreover, comparing the DELs of other turbine components, the mooring lines damage loads take up the smallest influence. Likewise, the wind profile influences the blades root edgewise fatigue damage loads very little. Thus, only the equivalent loads of tower base fore-aft, blade root flapwise, tower top and rotor will be further discussed in this chapter.

For tower base fore-aft loads, it can be seen that the rated wind speed causes the highest damage equivalent loads and the below rated wind speed generates the lowest fatigue loads. A Sathe et al. also observed similar results in their study that tower base fore-aft loads are the largest at rated wind speed as the rated power is produced and the pitching of the rotor blades induces a reduction of the loads, i.e. the turbine starts to pitch at the same time. [10] As such, Erin E. Bachynski and Lene Eliassen [28] recently indicated that there is a significant peak responses in pitch at lower frequency particularly for higher wind speed, although the tower base fore-aft bending moment primarily depends on wave eigenfrequency loading. This is also in

line with our results of power density spectra of tower base fore-aft bending moment. If the simulations are carried out without turbulence input, the result can be seen in *Figure 5.1*. Tower base fore-aft damage equivalent loads increases with increasing mean wind speed and the highest loads occur at above rated wind speed. This is consistent with the findings of M. C. Holtslag et al [27]. To compare with the spectra of tower base fore-aft moment with turbulence and without turbulence at 11.4 m/s (see *Figure 5.2*), we observe that the spectra of tower base fore-aft moment with turbulence has higher energy than the simulation without turbulence in the range from 0.3 Hz to 0.7 Hz. This results in higher tower base fore-aft loads with turbulence (see *Figure 4.3*) at rated wind speed than the loads without turbulence (see *Figure 5.1*). In Ref. [27], very unstable stratified induced the highest tower loads due to higher turbulence levels under unstable conditions. It is different with our results that the differences in the loads for tower base between different stability classifications are relatively small since the loads only vary by up to 2% considering the same wind speed (see *Figure 4.4* and *Table 4.9*). That is because we did simulations considering fixed turbulence levels and only varying the mean wind profile. Hence, we would like to say turbulence levels also cause tower base fore-aft damage loads, but this thesis does investigate this aspect. Generally, wind profile has little impact on tower base loads.

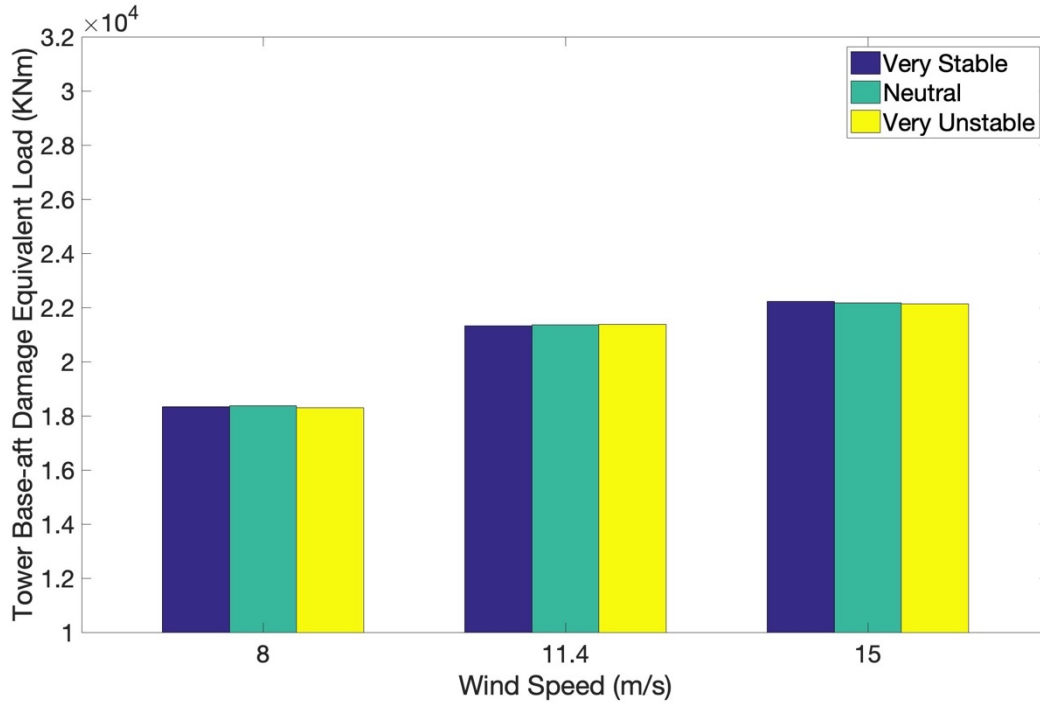


Figure 5.1 Tower Base Fore-Aft Damage Equivalent Loads without Turbulence under Each Stability for 8 m/s, 11.4 m/s and 15 m/s

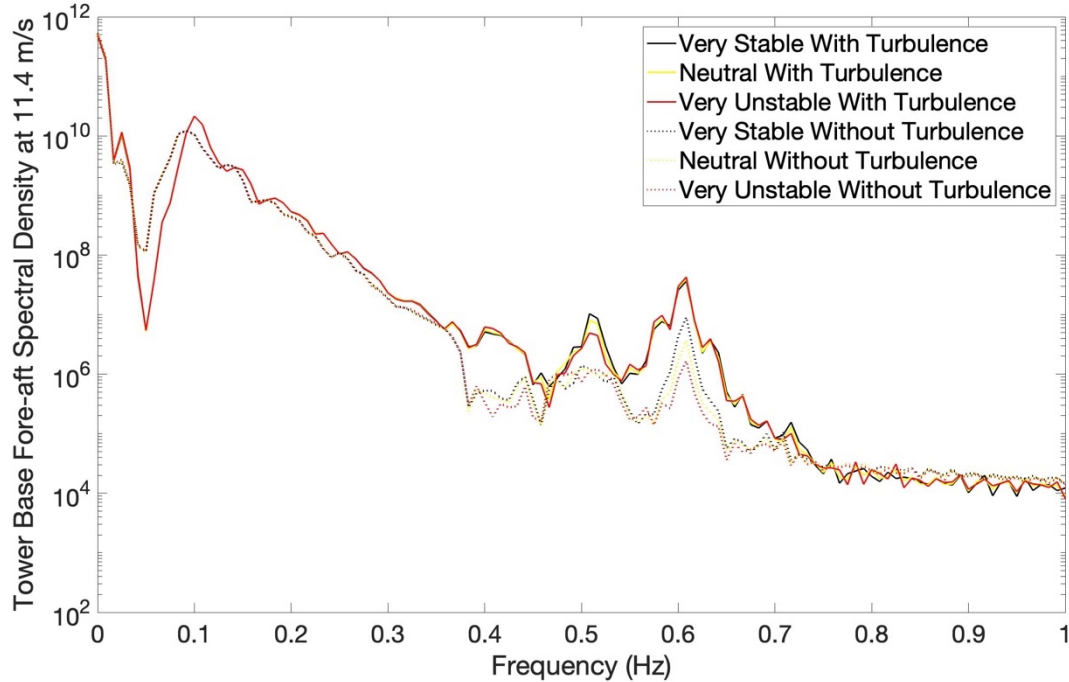


Figure 5.2 Comparison of Tower Base Fore-Aft Moment Spectral Densities with Turbulence and without Turbulence under Each Stability for 11.4 m/s

For the blade root flapwise equivalent load, the DELs are not predominantly influenced by wind profile at lower wind speed, whereas the variation in the loads will be up to more than 50% when the wind speed increases to over rated wind speed. In other words, the higher wind speed and more stable conditions will cause larger blade root flapwise loads. A. Sathe et al. also presented similar results in 2013. [10] In section 2.5.2, we hypothesize that the stability conditions from very unstable to very stable will exert increased the blades root flapwise loads. Similar behaviors were observed by A Eggers et al. stated in 2003 [25], by A. Sathe et al. in 2013 [10] and M. Kretschmer et al. in 2018 [26]. As can be seen, under very stable conditions, there is a larger wind gradient in Fig. 1 in Ref. [14] and Fig. 7 in Ref. [16]. Therefore, the wind profile under very stable conditions will generate larger loads on the blade root, this behavior causes larger damage equivalent loads on blades root in flapwise direction. In previous research, Eggers similarly stated that blades root flapwise load at very stable conditions is larger than very unstable conditions when turbulence intensity is equal to 0.12. [25] We also did the simulation for the assessment of blade root flapwise loads without turbulence (see *Figure A.1*), while the results show almost same tendency with the results with turbulence. In terms of turbulence input in this thesis, turbulence intensity (TI=0.12) is same for three seeds during the simulation running i.e. theoretically only wind profiles mainly affect blade root flapwise. A. Sathe et al. [10] presented the blades root flapwise loads were averaged out in the end due to the combined influence of wind profiles and turbulence. However, only wind profiles contribute to damage equivalent loads for blades root in flapwise direction in our simulation whose results should be same with the case of blades root flapwise loads without turbulence. This means that the result is reasonable to some extent, but this thesis does not account for whether the effect of turbulence on the blade root flapwise damage loads.

For rotor damage equivalent loads, there is a prominent increasing trend when mean wind speed increases from 8 m/s to 15 m/s. From the percentages of normalizing rotor equivalent loads to below rated wind speed under neutral condition in *Table 4.13*, the differences of the rotor loads comparing with rated wind speed are up to 65% and the above rated wind speed are up to 83%. The variation of rotor damage equivalent loads is highly dependent on mean wind speed. At 11.4 m/s, the rotor loads along the x-axis ( $M_x$ ) experience pitch loading as the rated power is produced and rotor rotational speed will be steady, which induces larger pitching moment, i.e. larger rotor loads in x-direction. This is in agreement with Ref. [25] where Eggers states the higher wind speed will exert higher pitching moment when shear exponent is equal to 0.28 (very stable conditions).

For tower top damage equivalent loads, similar trends with the rotor equivalent loads are observed, however the difference between with both cases is that increasing wind shear results in lower tower top torsion loads. We also did assessment of tower top equivalent loads without turbulence input (see *Figure 5.3*). The loads without turbulence are up to 50% smaller than the loads with turbulence when considering the same wind speed. Comparing *Figure 4.12* and *Figure 5.3*, the large tower top damage equivalent loads tend to occur at very unstable conditions considering the same wind speed. From the result of tower top loads without turbulence at 8 m/s, the loads at very stable conditions is the highest. Thus, power spectral densities of tower top equivalent loads with turbulence and without turbulence for different mean wind speeds are compared in order to verify above results and shown in *Fig. 5.4*. An important observation from *Figure 5.4*, is that all of the power spectral densities of tower top torsion damage equivalent loads with turbulence are higher than the loads without turbulence at higher frequency. In particular at 8 m/s (see *Figure 5.4 (a)*), there are significant differences of tower top torsion spectral densities between these

two cases. Moreover, the rotational frequency (3P) responses the highest excitation of tower top loads without turbulence under very stable conditions. Nonetheless, the 3P causes tower top fatigue loads which are less, comparing the loads which are induced by combination of strong wind speed and strong unstable conditions (larger turbulent energy). The inclusion of turbulence has a large influence on the tower top torsion as we see a reduction (up to 50%) in the tower top torn DEL's without turbulence. Therefore, we can see the very stable conditions lead to the highest DELs of tower top torsion without turbulence conditions at 8 m/s. Overall, the DELs of tower top depended strongly on wind profile and turbulent wind input.

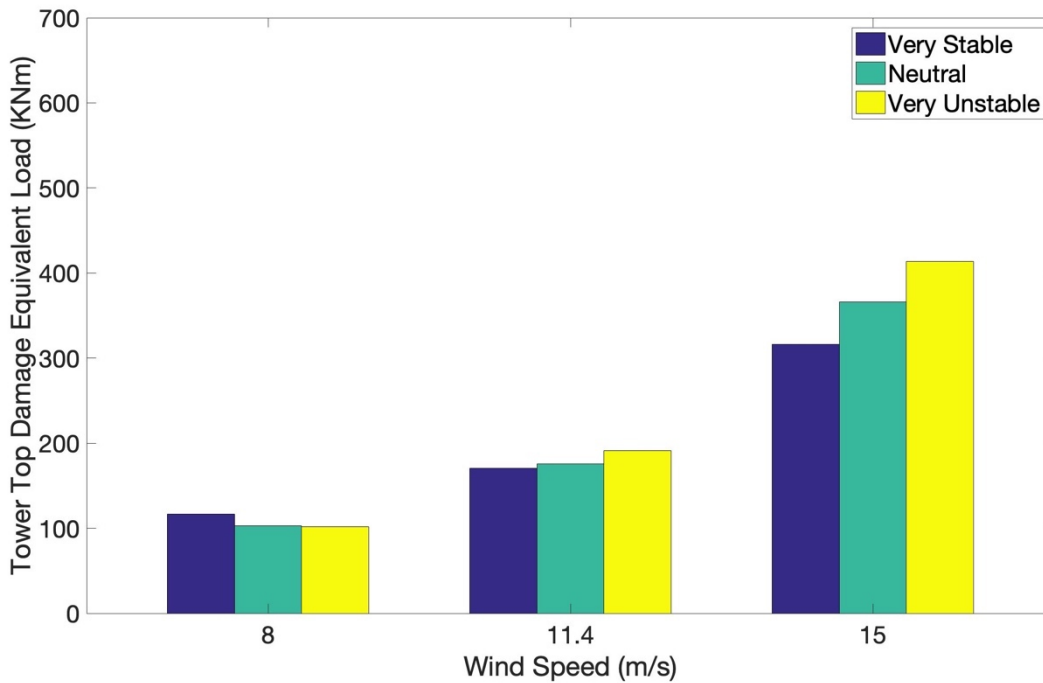
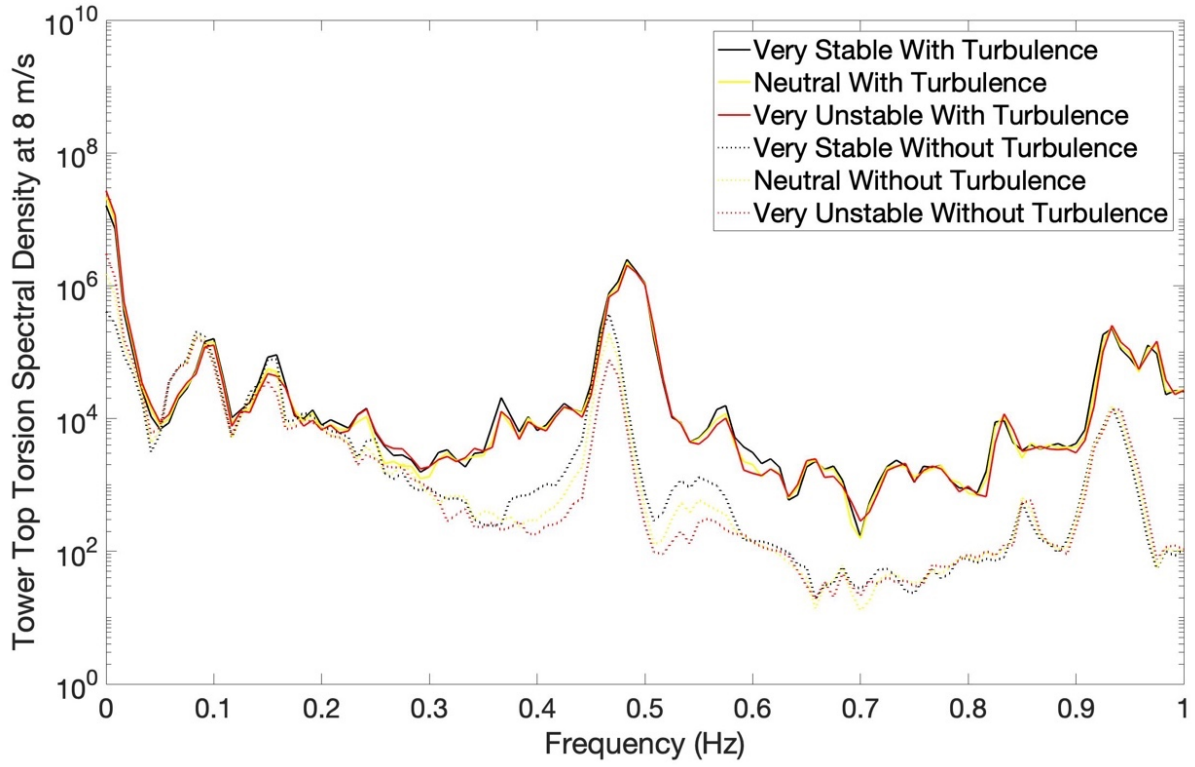
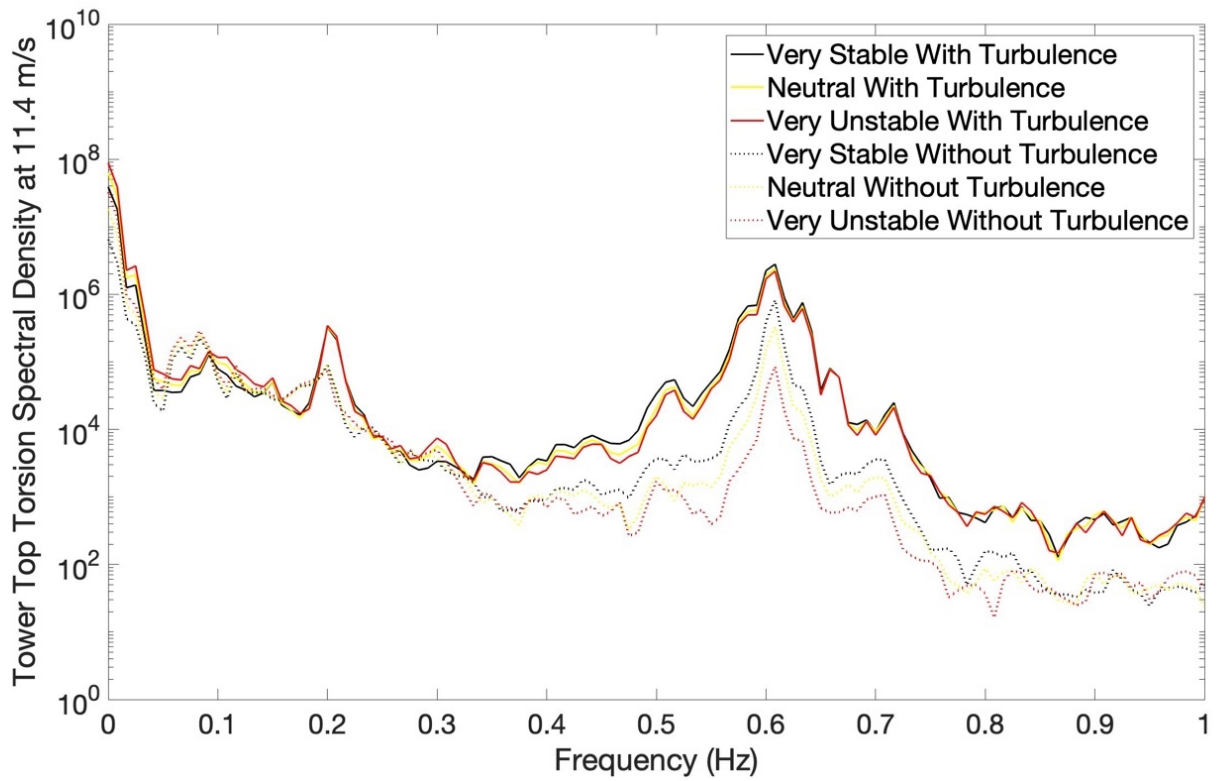


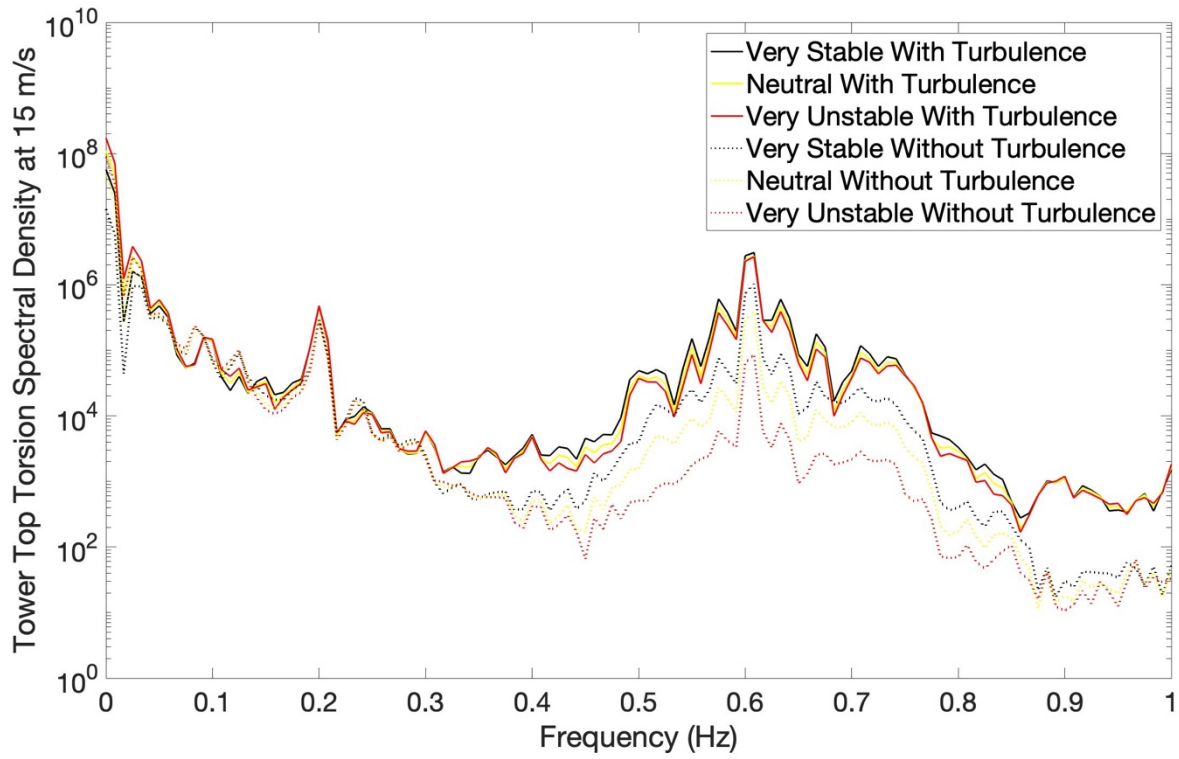
Figure 5.3 Tower Top Damage Equivalent Loads without Turbulence under Each Stability for 8 m/s, 11.4 m/s and 15 m/s



(a)



(b)



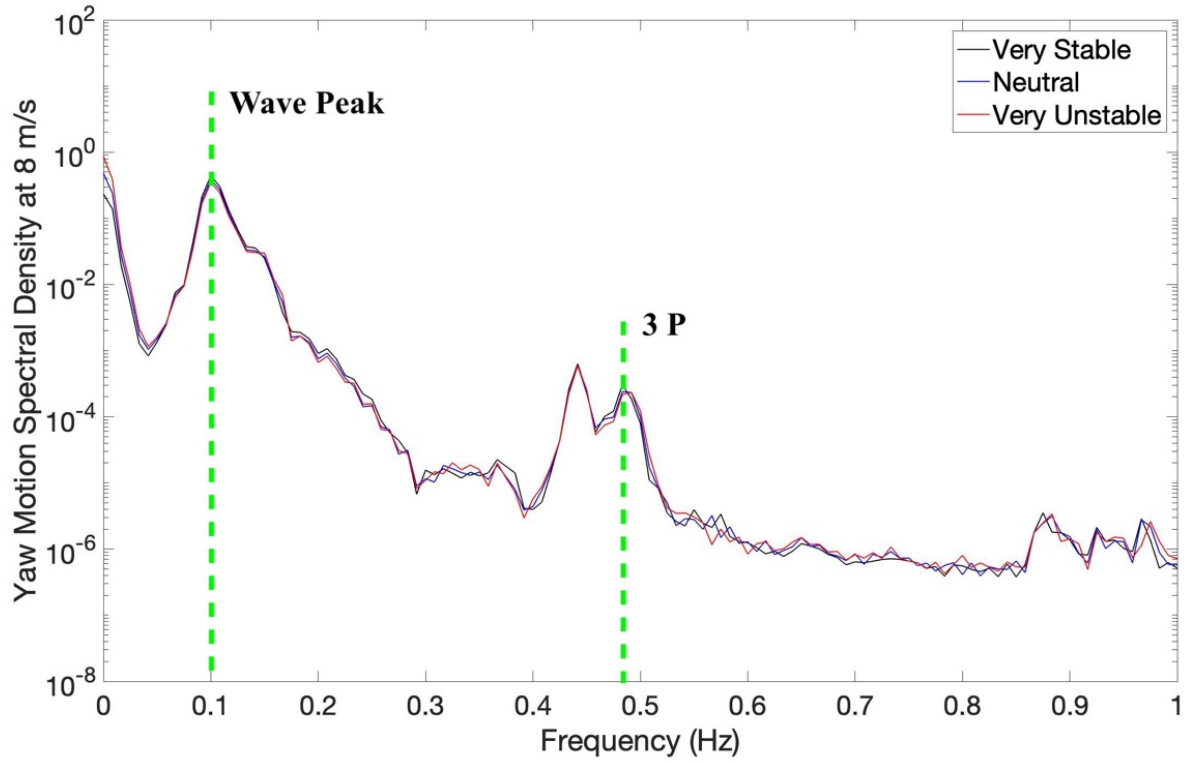
(c)

Figure 5.4 Comparison of Tower Top Spectral Densities with Turbulence and without Turbulence at 8 m/s (a), 11.4 m/s (b) and 15 m/s (c)

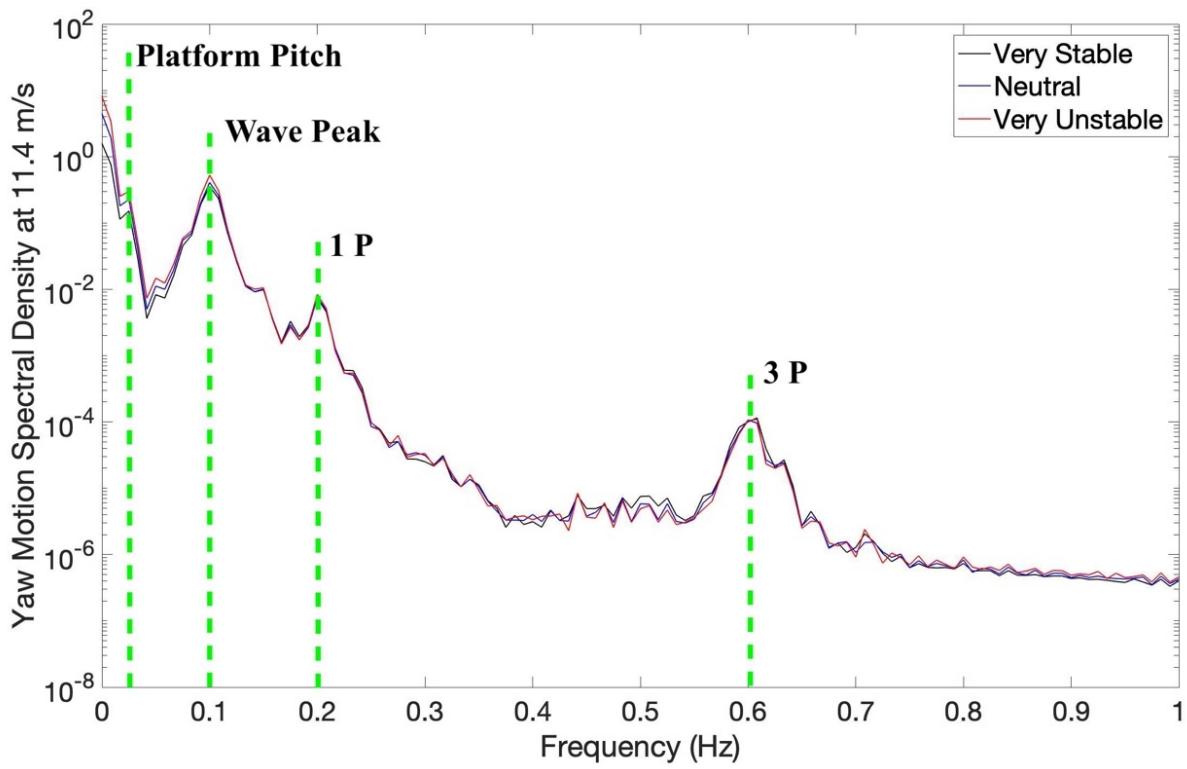
## 5.1.2 Wind Turbine Motions

We observed that there are some complicated fluctuations in *Figure 4.35* as well as the differences of maximum negative values of yaw rotations are up to 80% for various stabilities classifications (see *Figure 4.36*). Hence, the yaw motion spectral densities varying mean wind speeds are respectively shown in *Figure 5.5* in order to further analyze how does wind profiles influence the yaw motion.

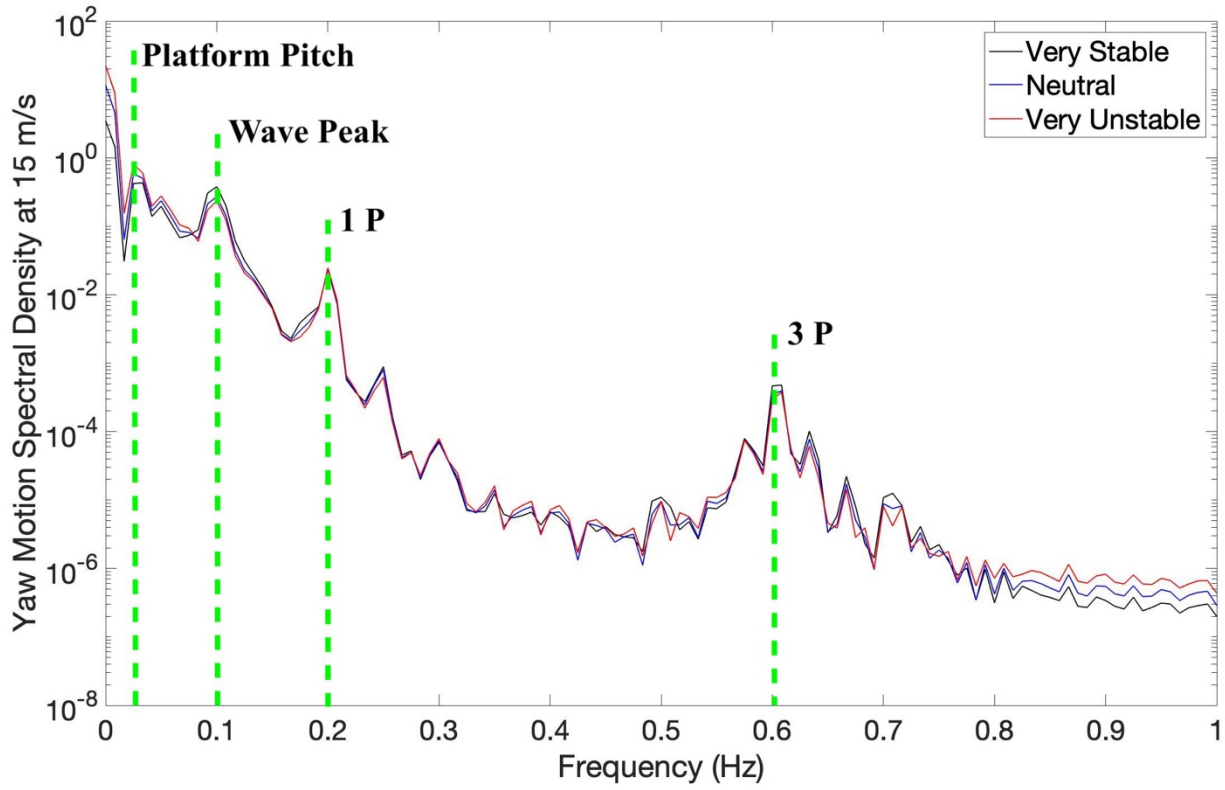
It is found that wind profiles have little impact on wind turbine yaw motion at these three wind speeds in *Figure 5.5*, since there are no significant differences of yaw motion spectral densities due to various wind profiles. In addition to above rated wind speed (see *Figure 5.5 (c)*), very unstable conditions give the highest energy at higher frequency. This is in line with the results of comparison of maximum and minimum yaw rotations in *Figure 4.36*. Overall, the main excitations at 8 m/s are wave peak and 1P rotational frequency but extra two peaks inducing by platform pitch and 1P are observed at 11.4 m/s and 15 m/s.



(a)



(b)



(c)

Figure 5.5 Yaw Motion Spectral Densities under Each Stabilities at 8 m/s (a), 11.4 m/s (b) and 15 m/s (c)

## 5.2 Conclusion

The effects of varying wind shear on the simulated loads (DELs) and motions of 5 MW offshore floating wind turbines (spar) have been investigated in this thesis. There are six representative wind turbine components (tower base, blades root flapwise, blades root edgewise, rotor, tower top and mooring lines) as well as six motions (surge, sway, heave, roll, pitch and yaw). These were respectively assessed and the analyzed loads and motions were determined for different mean wind profiles.

In general, the tower base fore-aft experienced the highest damage equivalent loads as well as blade root flapwise had the second largest damage loads. By comparing each turbine component case for various mean wind speed, all DELs were significantly dependent on hub height wind speeds. It is found that increasing mean wind speeds caused increasing damage fatigue loads, except for the tower base fore-aft where the largest fatigue loads were observed at rated wind speed because of a decrease of loads resulting from the pitching of blades rotor above 11.4 m/s (rated wind speed). The influences of different wind shear due to different stability classifications (very stable, neutral and very unstable) on blades root in the flapwise direction and tower top torsion were significant. The blades root flapwise damage equivalent loads decreased when the wind shear changes from very stable to very unstable. The very stable conditions have a larger wind gradient, i.e. larger wind shear (wind profile). That is, the wind profile has predominant impact on the fatigue loads of blades root flapwise. Conversely, the tower top torsion damage equivalent loads increased when the wind shear changed from very stable condition to very unstable condition for a fixed turbulence level.

Regarding the wind turbine motions, increasing wind speed caused an obvious increase in the heave motion, roll motion and pitch motion as well as a slight increase in sway. However, the surge motion excited the highest energy at rated wind speed (11.4 m/s). The values of sway and roll motions will become the largest under very stable conditions. Hence, the motions of sway and roll motions were influenced by a combination of mean wind speed and wind profile. The surge, heave and pitch motion were only dependent on various mean wind speed. The yaw motion for wind turbine was also slightly influenced with difference in mean wind speed and wind profile.

### **5.3 Future Work**

This thesis has provided preliminary study on how the wind profile and wind speed affect the loads and motions of offshore wind turbine. There may be some defects due to limiting time. Therefore, the following work is suggested for future work:

- 1) To accurately classify the stability conditions from three stability classes to seven stability classes including very stable, stable, weakly stable, neutral, weakly unstable, unstable and very unstable, the influence of wind profile could be further performed
- 2) Taking account for turbulence effect by using either various turbulence intensity or turbulence model such as Mann model to analyze atmospheric stability effect
- 3) Increasing simulation length from 600s to 3600s in order to get more realistic simulation results
- 4) Comparing with other floating wind turbines with different foundation like tension leg platform or fixed wind turbines like monopile

## Reference

1. Official FINO3. - FINO - research platforms in the North Sea and the Baltic 2018 [Available from: <https://www.fino3.de/en/fino3>].
2. Kindler D. 20 Months of Wind Data from the FINO3 Meteorological Mast. FINO Conference Hamburg: GL Garrad Hassan; 2011.
3. Fabre S, Stickland M, Scanlon T, Oldroyd A, Kindler D, Quail F. Measurement and simulation of the flow field around the FINO 3 triangular lattice meteorological mast. *Journal of Wind Engineering and Industrial Aerodynamics*. 2014;130:99-107.
4. Külpmann A. Case Study of Mesoscale Windfluctuations during Cold Air Outbreaks: Carl von Ossietzky Universität Oldenburg; 2017.
5. Obhrai C, Kalvig S, Gudmestad OT, editors. A review of current guidelines and research on wind modelling for the design of offshore wind turbines. The Twenty-second International Offshore and Polar Engineering Conference; 2012: International Society of Offshore and Polar Engineers.
6. Hayden BP, Pielke RA. Planetary boundary layer. *Planetary boundary layer* 2018.
7. Stull RB. An introduction to boundary layer meteorology. The Netherlands: Kluwer Academic; 1988. 670 p.
8. Wagner D. Evolution and Properties of Low Level Jet Events above the Southern North Sea. Oldenburg: Carl von Ossietzky University of Oldenburg; 2017.
9. Obhrai C. Improved Design Criteria and Forecast for Energy Yield from Offshore Wind Turbine. University of Stavanger; StormGeo Control in a Changing Environment; 2011.

10. Sathe A, Mann J, Barlas T, Bierbooms W, van Bussel G. Influence of atmospheric stability on wind turbine loads. *Wind Energy*. 2013;16(7):1013-32.
11. Venkatram A. Estimating the Monin-Obukhov length in the stable boundary layer for dispersion calculations. *Boundary-Layer Meteorology*. 1980;19(4):481-5.
12. Lee JA, Hacker JP, Delle Monache L, Kosović B, Clifton A, Vandenberghe F, et al. Improving Wind Predictions in the Marine Atmospheric Boundary Layer through Parameter Estimation in a Single-Column Model. *Monthly Weather Review*. 2017;145(1):5-24.
13. IEC61440-1. Wind turbines-Part 1: Design requirements. 2005.
14. Sathe A, Bierbooms W, editors. Influence of different wind profiles due to varying atmospheric stability on the fatigue life of wind turbines. *Journal of Physics: Conference Series*; 2007: IOP Publishing.
15. Sathe A, Gryning SE, Peña A. Comparison of the atmospheric stability and wind profiles at two wind farm sites over a long marine fetch in the North Sea. *Wind Energy*. 2011;14(6):767-80.
16. Gryning S-E, Batchvarova E, Brümmer B, Jørgensen H, Larsen S. On the extension of the wind profile over homogeneous terrain beyond the surface boundary layer. *Boundary-Layer Meteorology*. 2007;124(2):251-68.
17. Olaofe ZO. A surface-layer wind speed correction: A case-study of Darling station. *Renewable Energy*. 2016;93:228-44.
18. Peña A, Gryning S-E, Hasager CB. Measurements and modelling of the wind speed profile in the marine atmospheric boundary layer. *Boundary-Layer Meteorology*. 2008;129(3):479-95.

19. Holtslag M, Bierbooms W, van Bussel G. Extending the diabatic surface layer wind shear profile for offshore wind energy. *Renewable Energy*. 2017;101:96-110.
20. Ragan P, Manuel L. Comparing estimates of wind turbine fatigue loads using time-domain and spectral methods. *Wind engineering*. 2007;31(2):83-99.
21. Tran T, Kim D, Song J. Computational Fluid Dynamic Analysis of a Floating Offshore Wind Turbine Experiencing Platform Pitching Motion, *Energies*, 7, 5011–5026. 2014.
22. Putri RM. A Study of the Coherences of Turbulent Wind on a Floating Offshore Wind Turbine: University of Stavanger, Norway; 2016.
23. Jonkman J, Musial W. Offshore code comparison collaboration (OC3) for IEA Wind Task 23 offshore wind technology and deployment. National Renewable Energy Lab.(NREL), Golden, CO (United States); 2010.
24. Lalanne C. Mechanical vibration and shock analysis, fatigue damage: John Wiley & Sons; 2010.
25. Eggers A, Digumarthi R, Chaney K, editors. Wind shear and turbulence effects on rotor fatigue and loads control. 41st Aerospace Sciences Meeting and Exhibit; 2003.
26. Kretschmer M, Schwede F, Guzmán RF, Lott S, Cheng P, editors. Influence of atmospheric stability on the load spectra of wind turbines at alpha ventus. *Journal of Physics: Conference Series*; 2018: IOP Publishing.
27. Holtslag M, Bierbooms W, van Bussel G. Wind turbine fatigue loads as a function of atmospheric conditions offshore. *Wind Energy*. 2016;19(10):1917-32.
28. Bachynski EE, Eliassen L. The effects of coherent structures on the global response of floating offshore wind turbines. *Wind Energy*. 2019;22(2):219-38.

## Appendix A

### A.1 Mooring Lines Loads

There are three mooring lines in the OC3 floating wind turbine. The mooring line 1 is located at the back of wind turbine whose direction is same with wave and wind direction, the mooring line 2 and 3 are located at the sides of floating wind turbine as shown in *Figure 3.1*. Thus, mooring line 2 and 3 should have similar results because of symmetric location.

*Figures from A.1 to A.3* present the mooring lines loads (tension) at wind speeds 8 m/s, 11.4 m/s and 15 m/s respectively. All of mooring lines damage equivalent loads at 11.4 m/s are highest among these three wind speeds. *Figure A.2* and *Figure A.3* show the similarity of DELs between them, this corresponds to the preliminary interpretation. However, the mooring line 1 obtains significant fluctuations of DELs experienced various wind profiles.

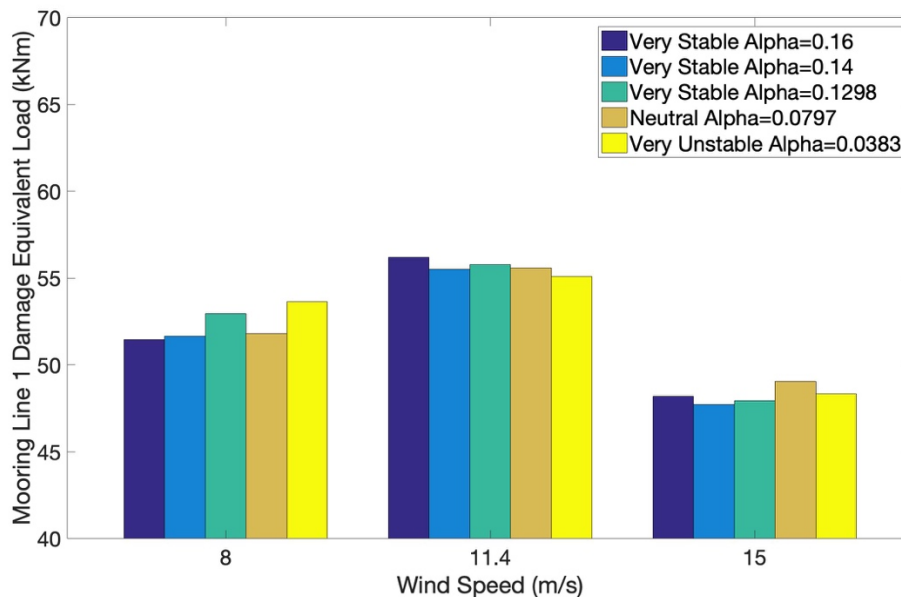


*Figure A.1* Mooring Line 1 Damage Equivalent Loads under Each Stability Class for 8 m/s, 11.4 m/s and 15 m/s

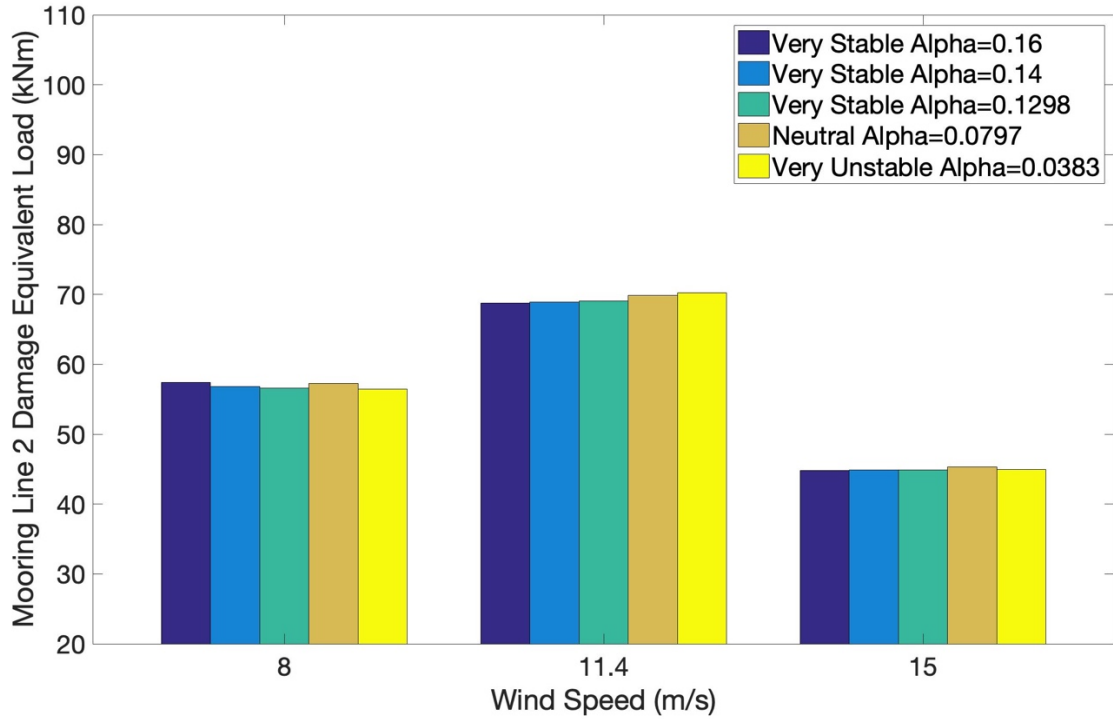


Figure A.2 Mooring Line 2 Damage Equivalent Loads under Each Stability Class for 8 m/s, 11.4 m/s and 15 m/s

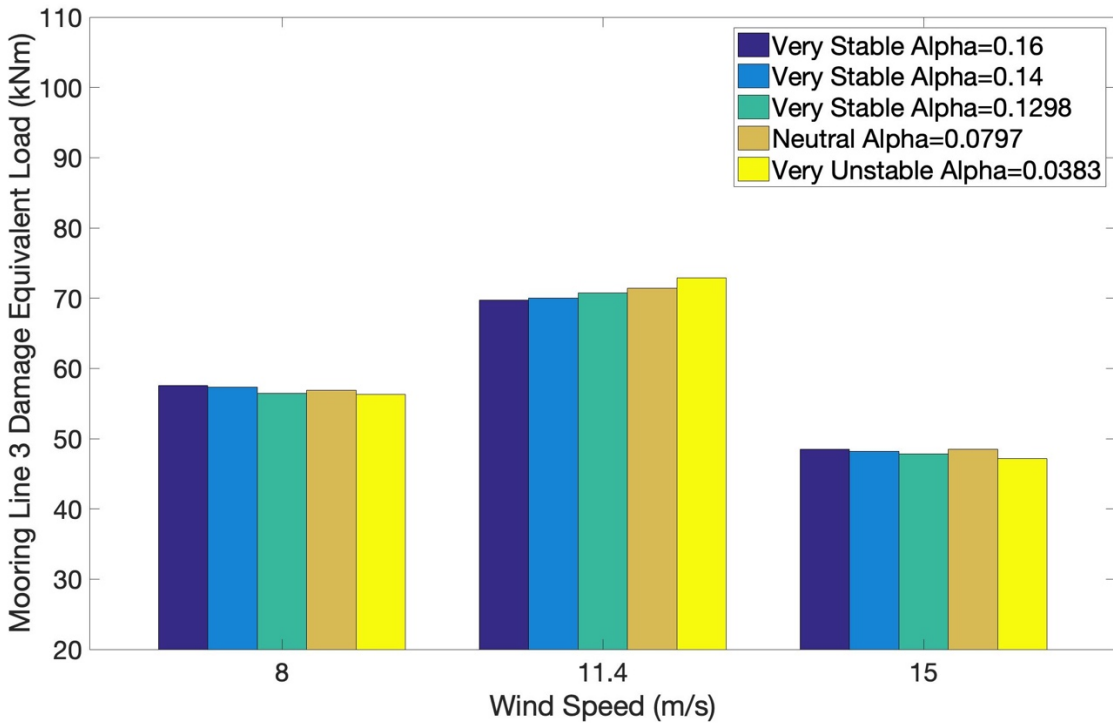
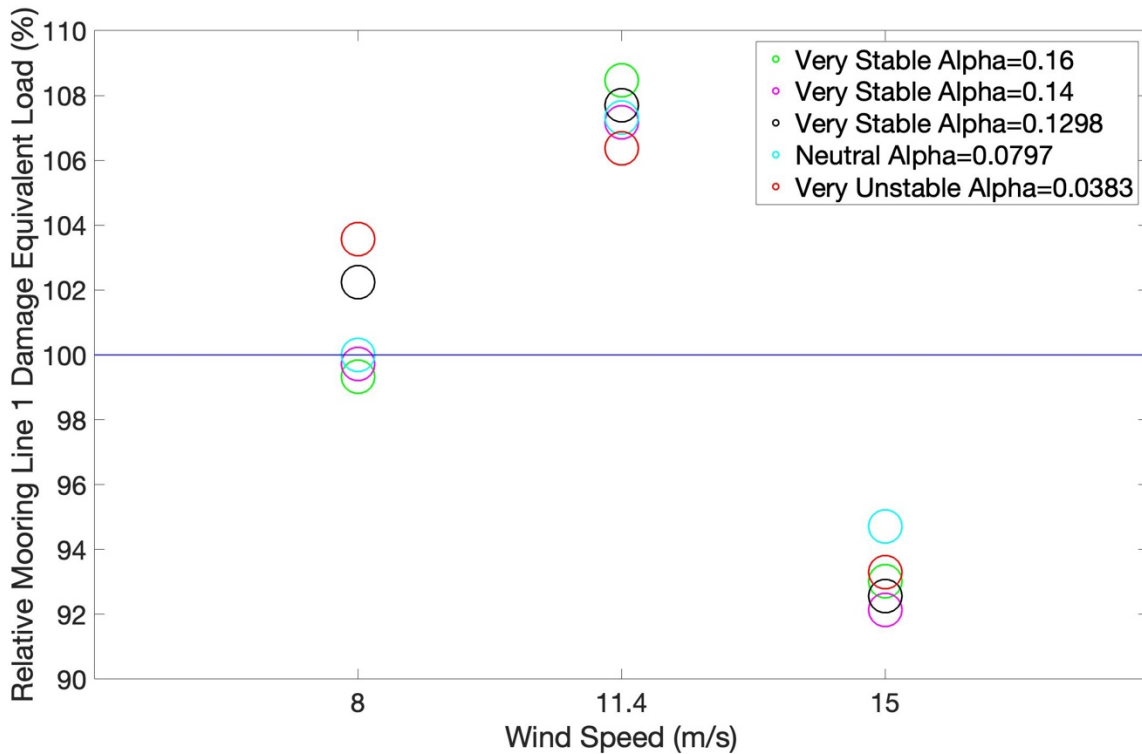


Figure A.3 Mooring Line 3 Damage Equivalent Loads under Each Stability Class for 8 m/s, 11.4 m/s and 15 m/s

Relative equivalent loads of mooring line 1, 2 and 3 are shown in from *Fig. A.4* to *Fig. A.6*, and the percentages are also shown in *Table A.1*. The majority of differences are less than 3% between varying wind profiles. Whereas, the normalized mooring line 2 and 3 equivalent loads to neutral conditions at 8 m/s have very significant differences (up to 20%) as well as the differences for mooring line 1 are up to approximately 8%. In general, the wind profile exerts little impact while the mean wind speed contributes much influence on mooring line fatigue loads.



*Figure A.4 Normalized Mooring Line 1 Damage Equivalent Loads under Each Stability Class for 8 m/s, 11.4 m/s and 15 m/s*

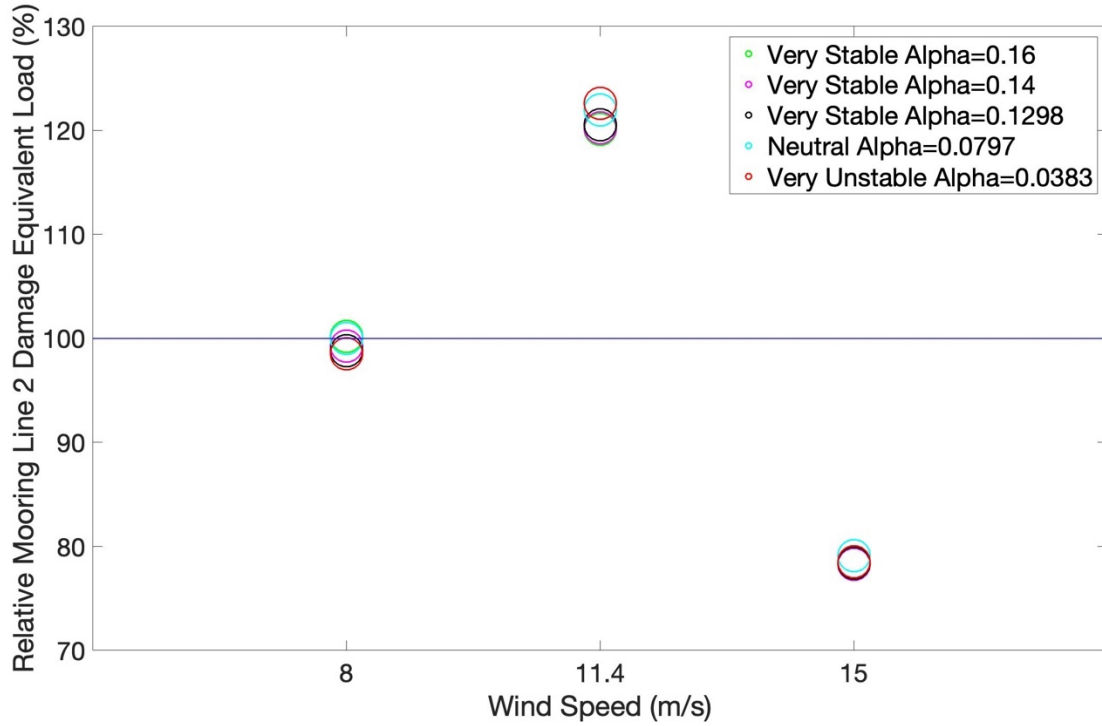


Figure A.5 Normalized Mooring Line 2 Damage Equivalent Loads under Each Stability Class for 8 m/s, 11.4 m/s and 15 m/s

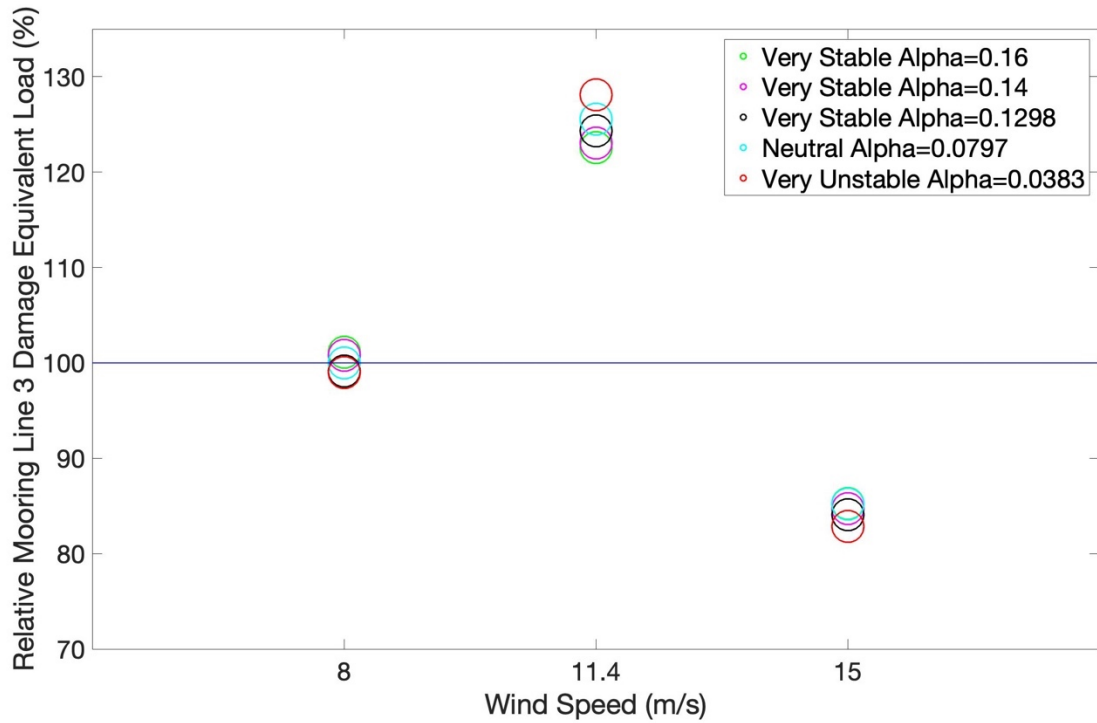
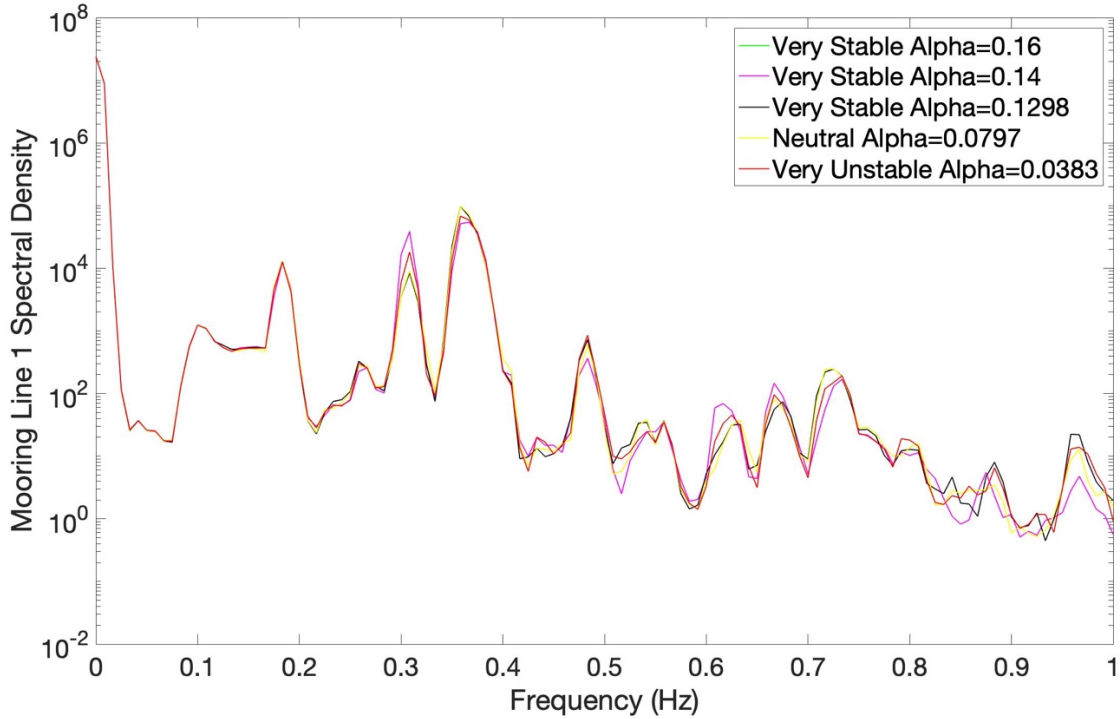


Figure A.6 Normalized Mooring Line 3 Damage Equivalent Loads under Each Stability Class for 8 m/s, 11.4 m/s and 15 m/s

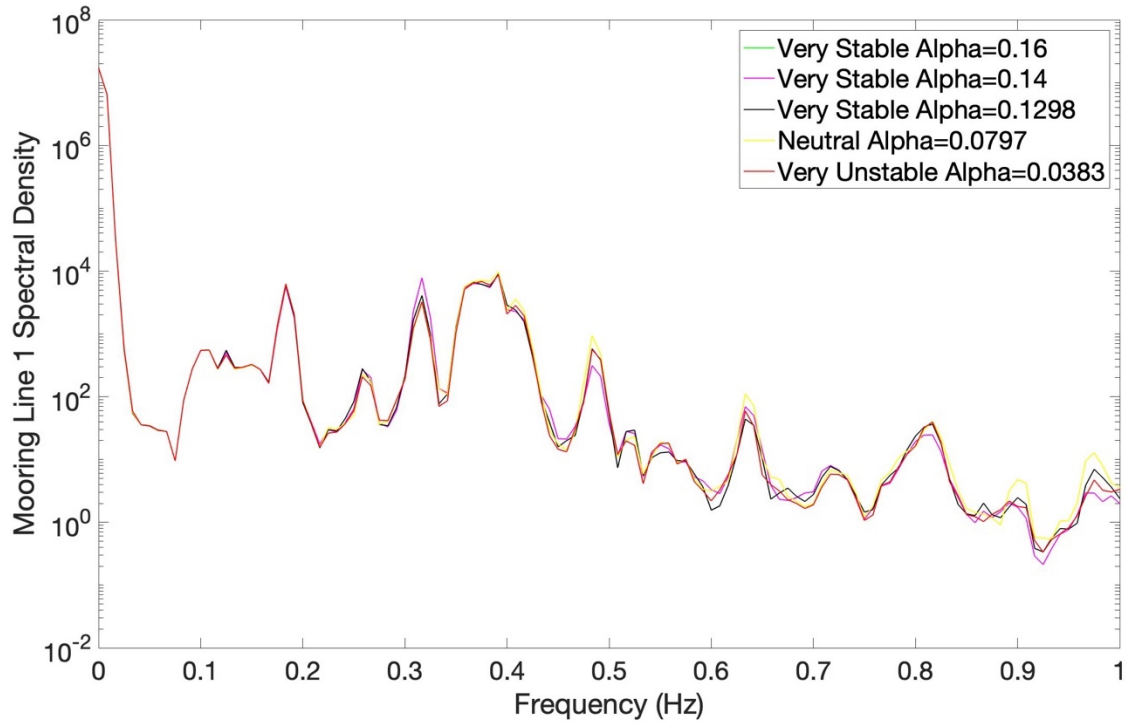
Table A.1 Percentages of Mooring Line Damage Equivalent Loads Relative to Neutral Stability

Atmospheric Stability	Mooring Line 1 (%)			Mooring Line 2 (%)			Mooring Line 3 (%)		
	8 m/s	11.4 m/s	15 m/s	8 m/s	11.4 m/s	15 m/s	8 m/s	11.4 m/s	15 m/s
Very Stable $\alpha = 0.16$	99.335	108.475	93.021	100.178	120.084	78.267	101.120	122.545	85.267
Very Stable $\alpha = 0.14$	99.728	107.178	92.130	99.251	120.260	78.303	100.822	123.022	84.722
Very Stable $\alpha = 0.1298$	102.251	107.694	92.560	98.807	120.541	78.386	99.168	124.345	84.083
Neutral $\alpha = 0.0797$	100	107.320	94.707	100	121.953	79.095	100	125.524	85.207
Very Unstable $\alpha = 0.0383$	103.573	106.372	93.299	98.503	122.606	78.519	99.009	128.127	82.869

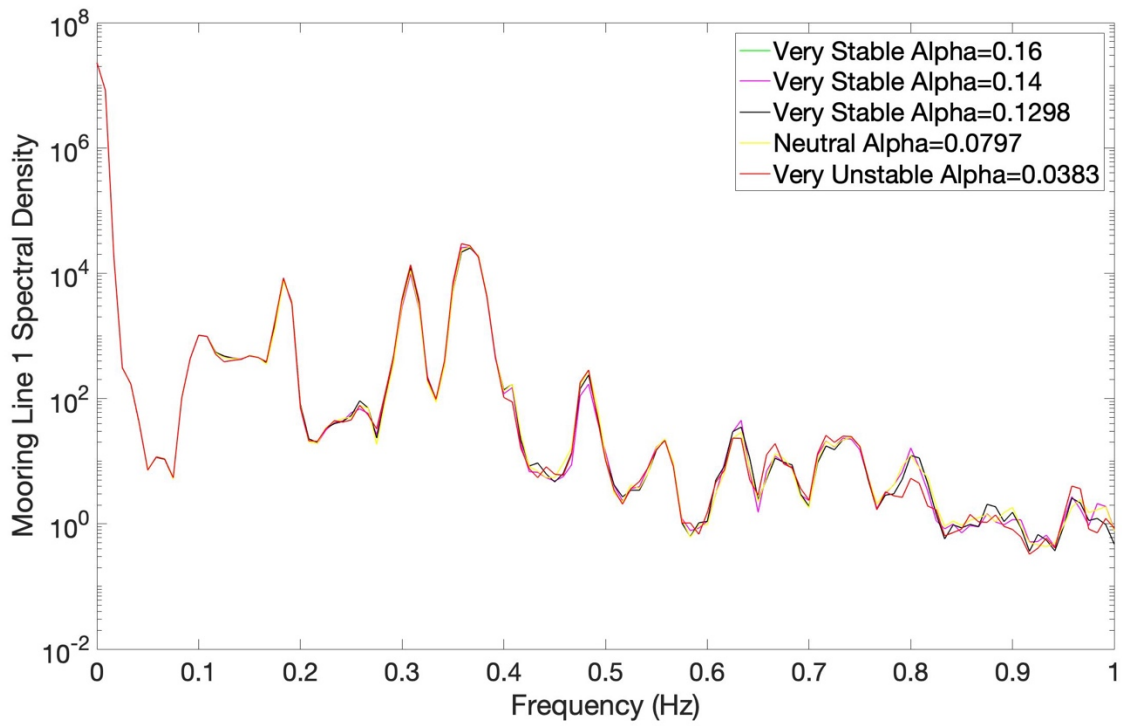
The similar *Figures* from *A.7* to *A.9* demonstrate the tension spectral densities of three mooring lines at the three different wind velocities which show very little variations with respect to varying wind shear. The spectra of mooring line 2 and mooring line 3 have almost same fluctuation trend because of their symmetric positions.



(a)

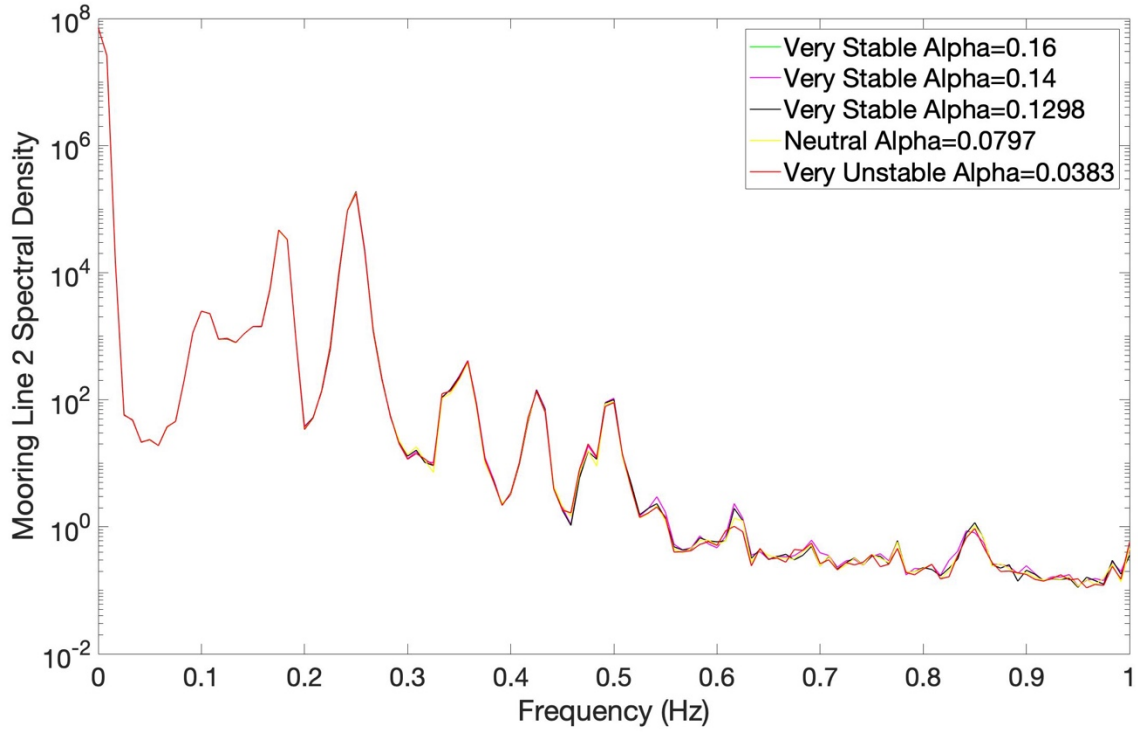


(b)

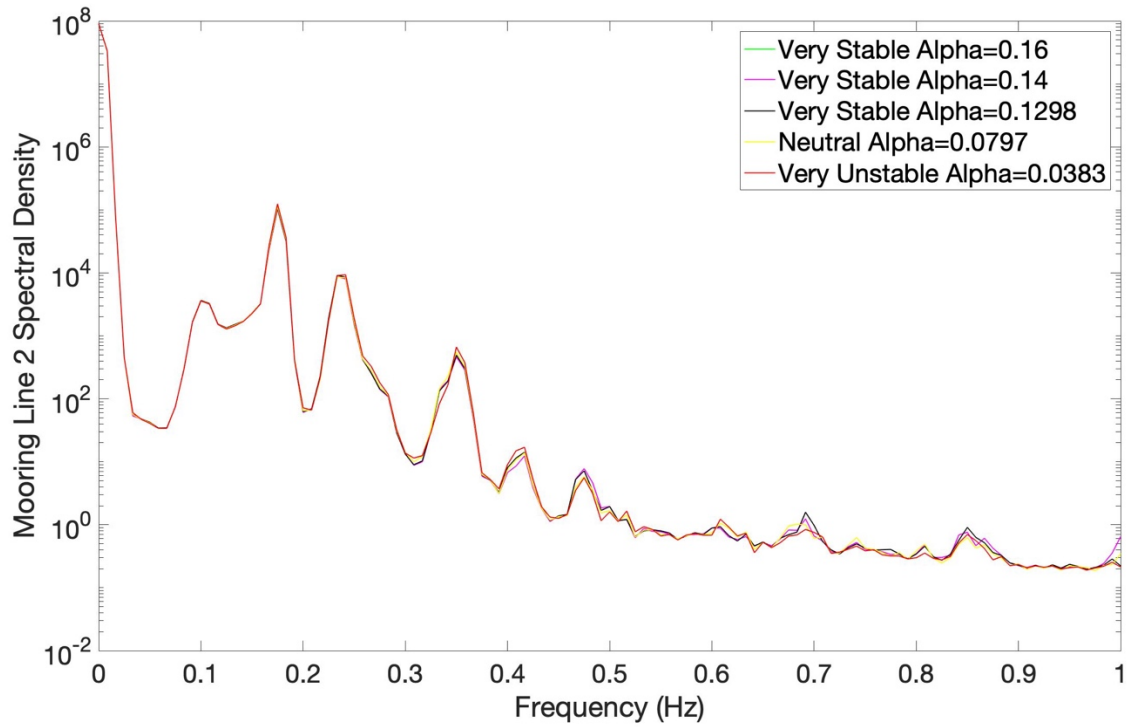


(c)

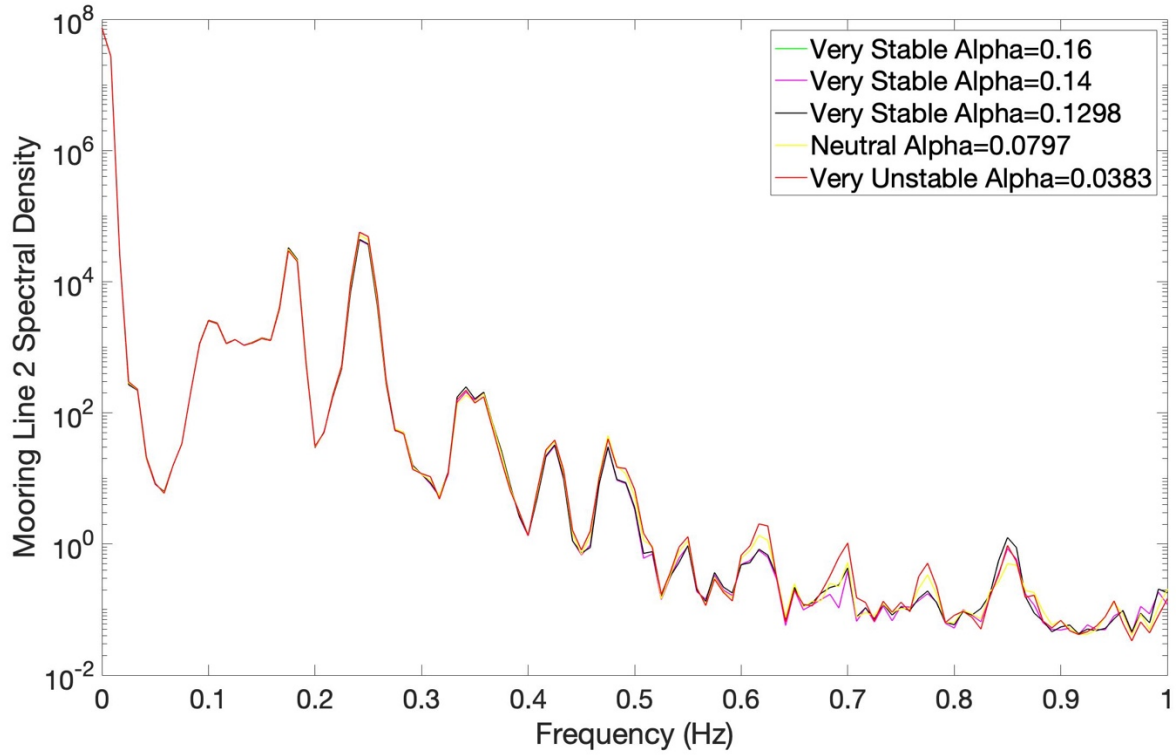
Figure A.7 Mooring Line 1 Tension Spectral Densities at 8 m/s (a), 11.4 m/s (b) and 15 m/s (c)



(a)

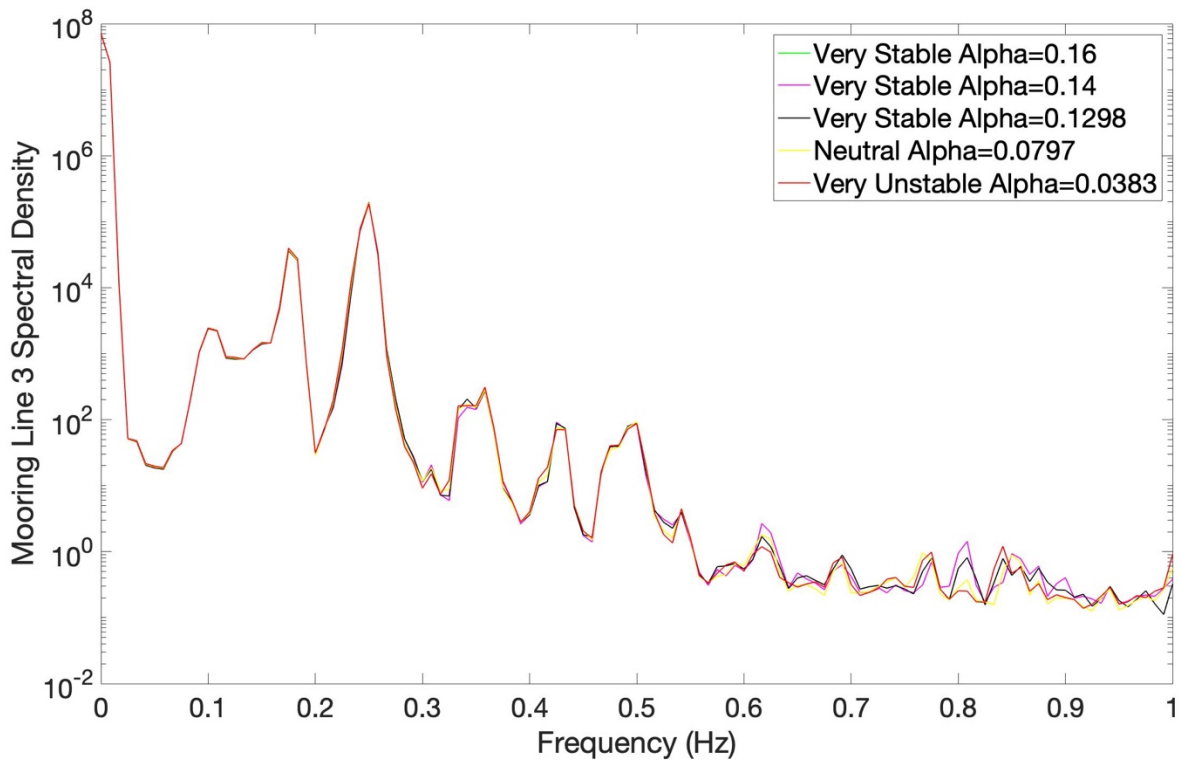


(b)

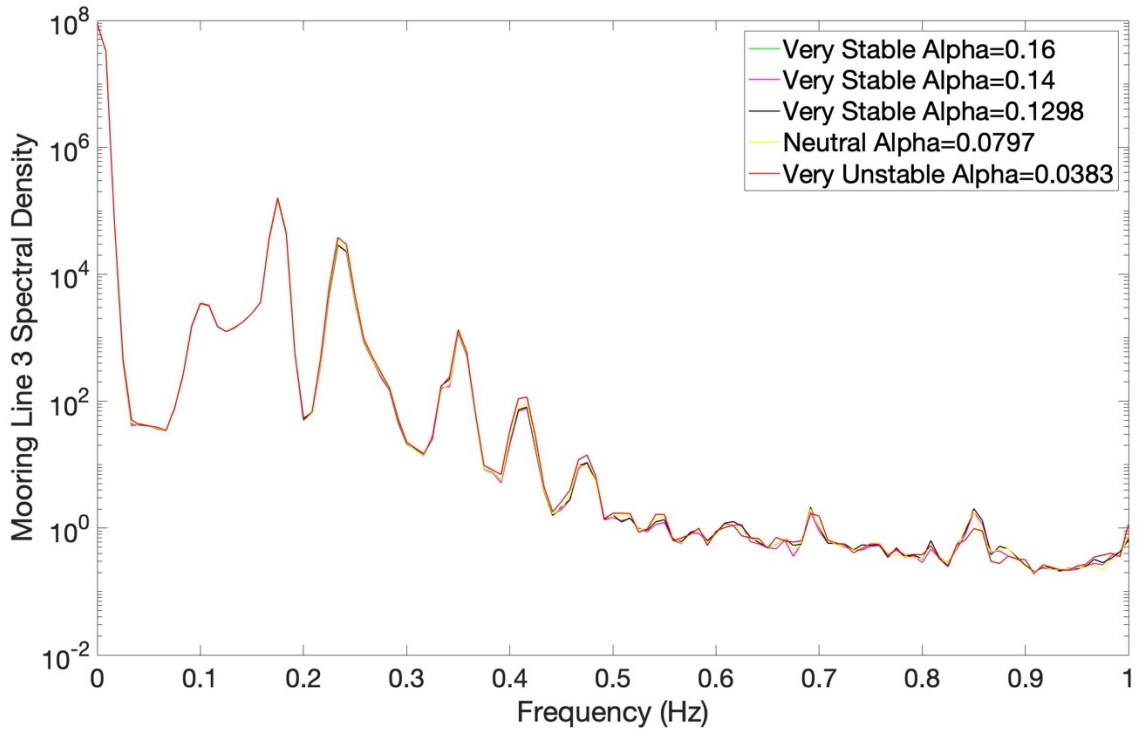


(c)

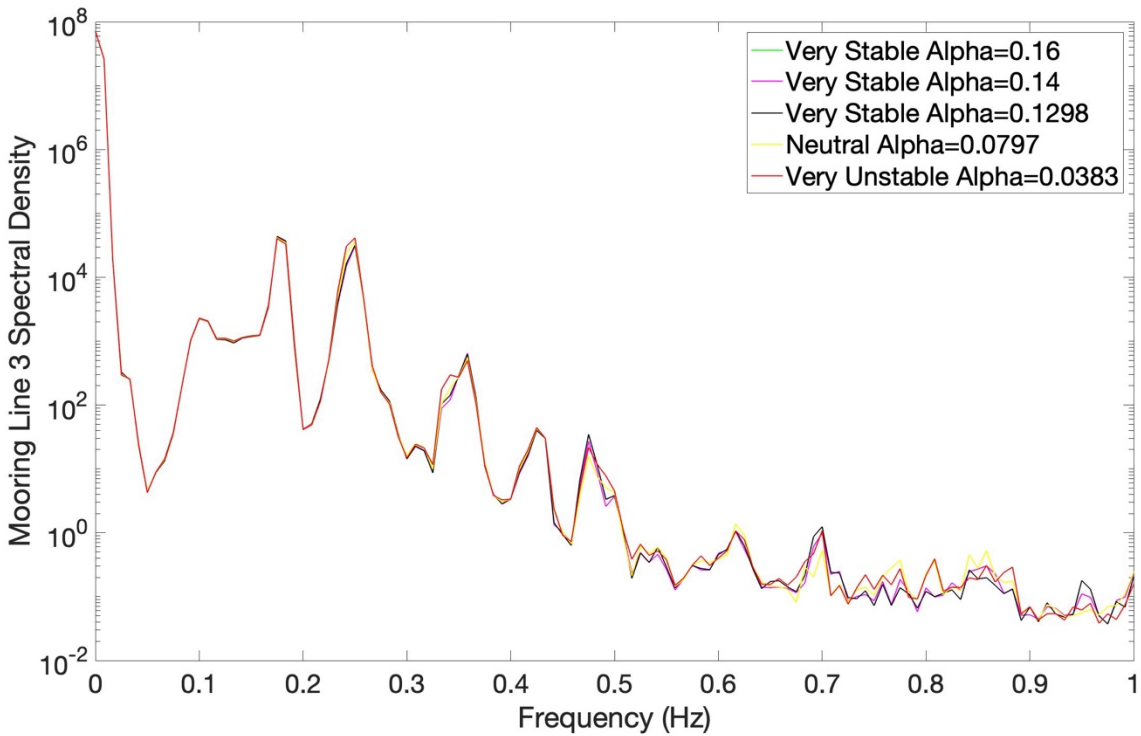
Figure A.8 Mooring Line 2 Tension Spectral Densities at 8 m/s (a), 11.4 m/s (b) and 15 m/s (c)



(a)



(b)



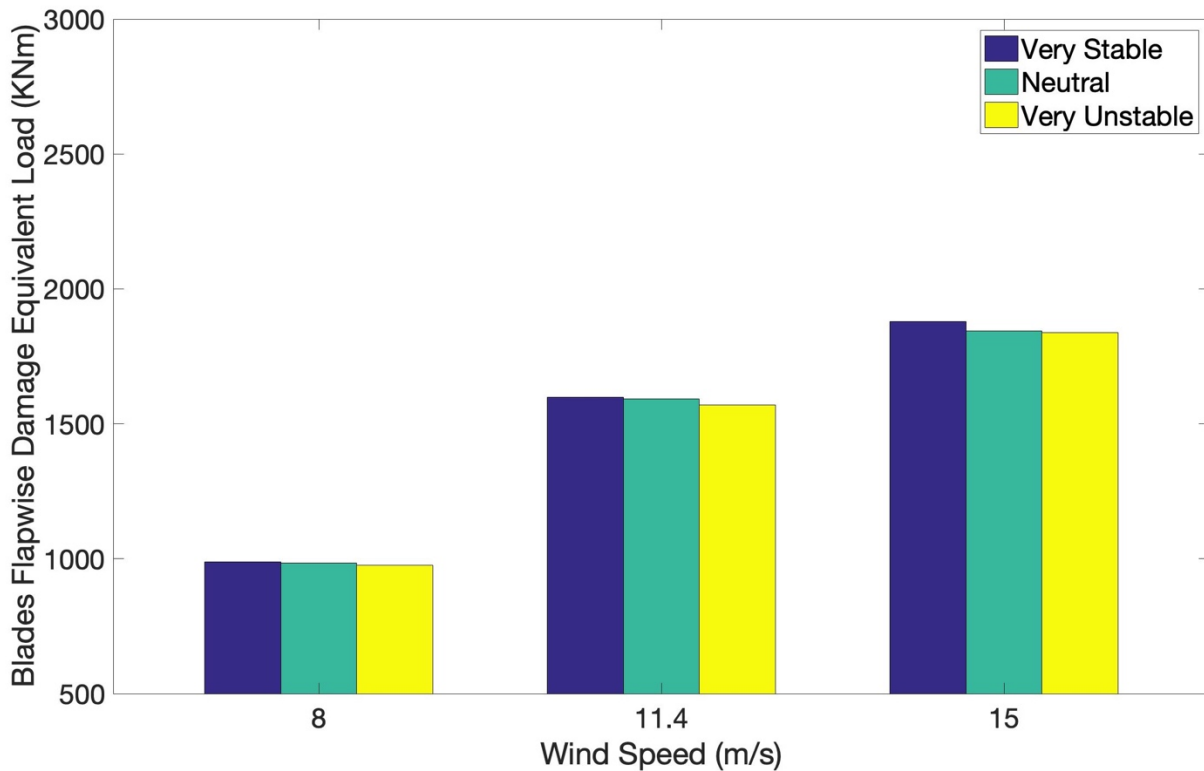
(c)

Figure A.9 Mooring Line 3 Tension Spectral Densities at 8 m/s (a), 11.4 m/s (b) and 15 m/s (c)

## A.2 The Results of Simulation without Turbulence

### A.2.1 Damage Equivalent loads

We also did simulation for offshore wind turbine damage equivalent loads without turbulence. The results of the DELs of blades root flapwise (*Figure A.10*), blades root edgewise (*Figure A.11*), rotor (*Figure A.12*) and mooring lines (*Figure A.13*, *Figure A.14* and *Figure A.15*) are almost same with the results of the loads with turbulence.



*Figure A.10 Blades Root Flapwise Damage Equivalent Loads without Turbulence under Each Stability for 8 m/s, 11.4 m/s and 15 m/s*

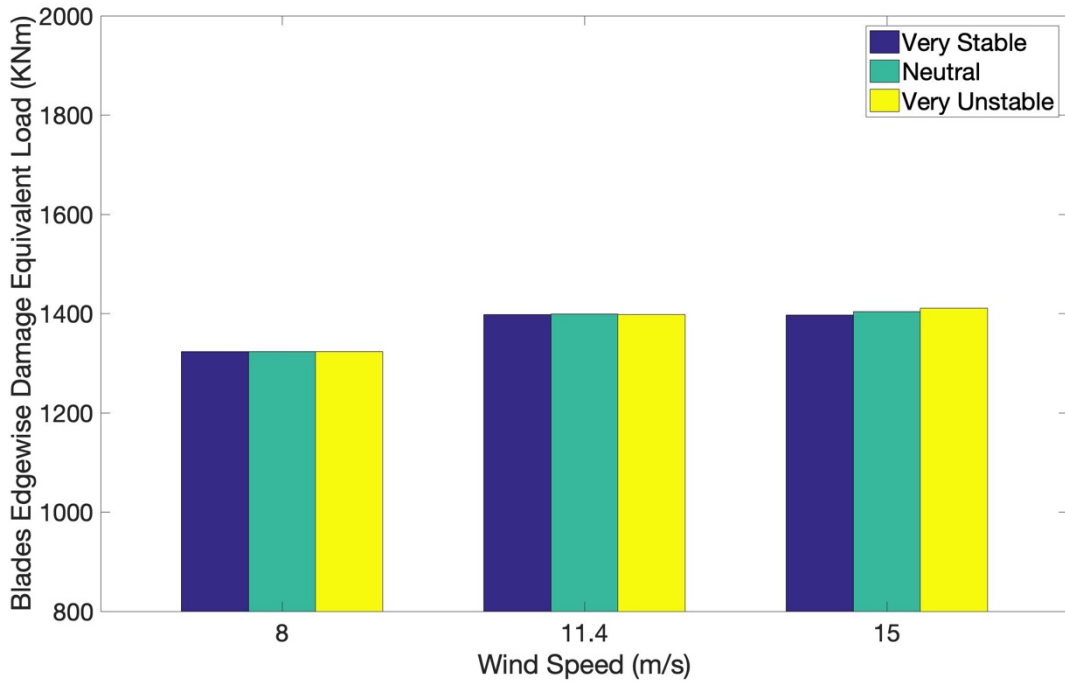


Figure A.11 Blades Root Edgewise Damage Equivalent Loads without Turbulence under Each Stability for 8 m/s, 11.4 m/s and 15 m/s

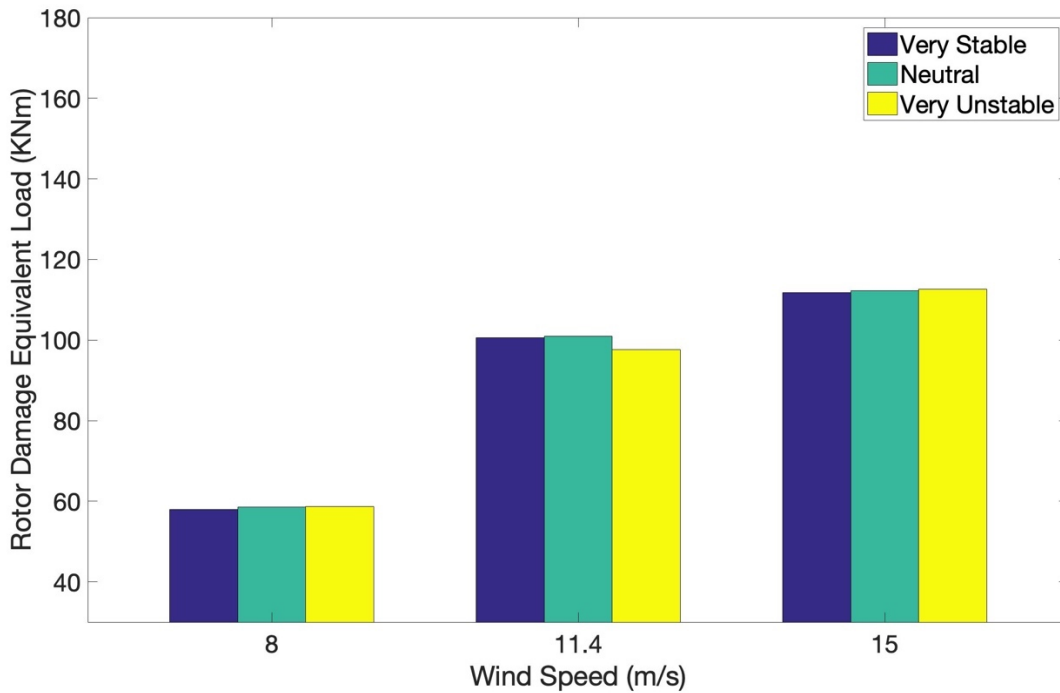


Figure A.12 Rotor Damage Equivalent Loads without Turbulence under Each Stability for 8 m/s, 11.4 m/s and 15 m/s

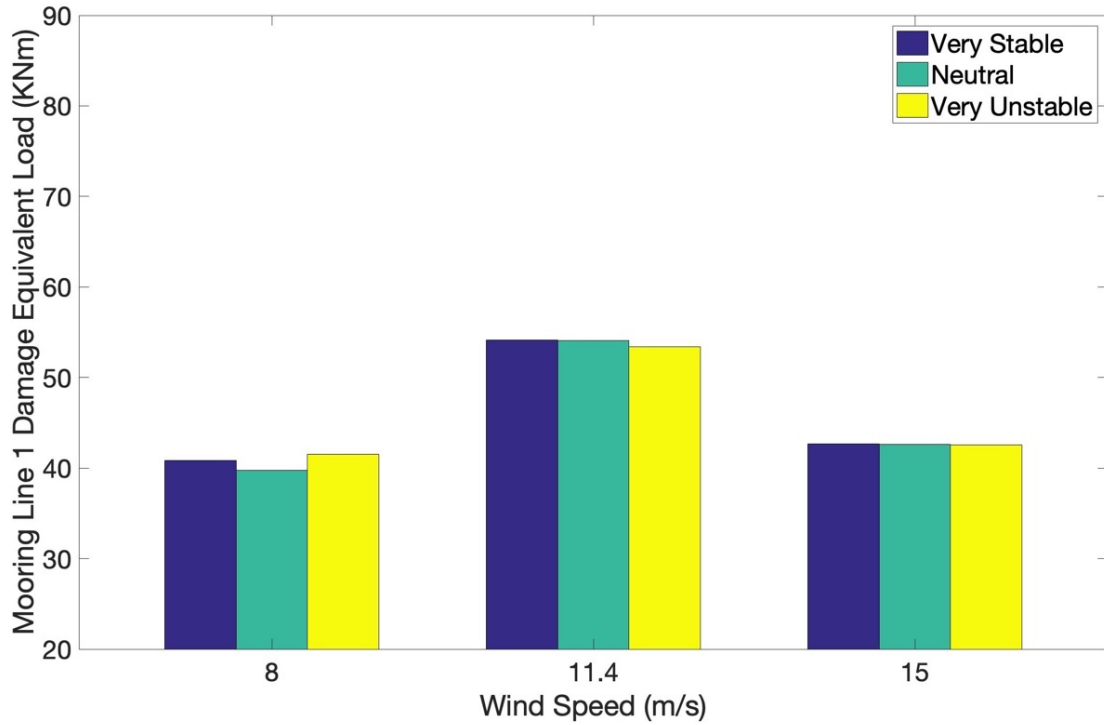


Figure A.13 Mooring Line 1 Damage Equivalent Loads without Turbulence under Each Stability for 8 m/s, 11.4 m/s and 15 m/s

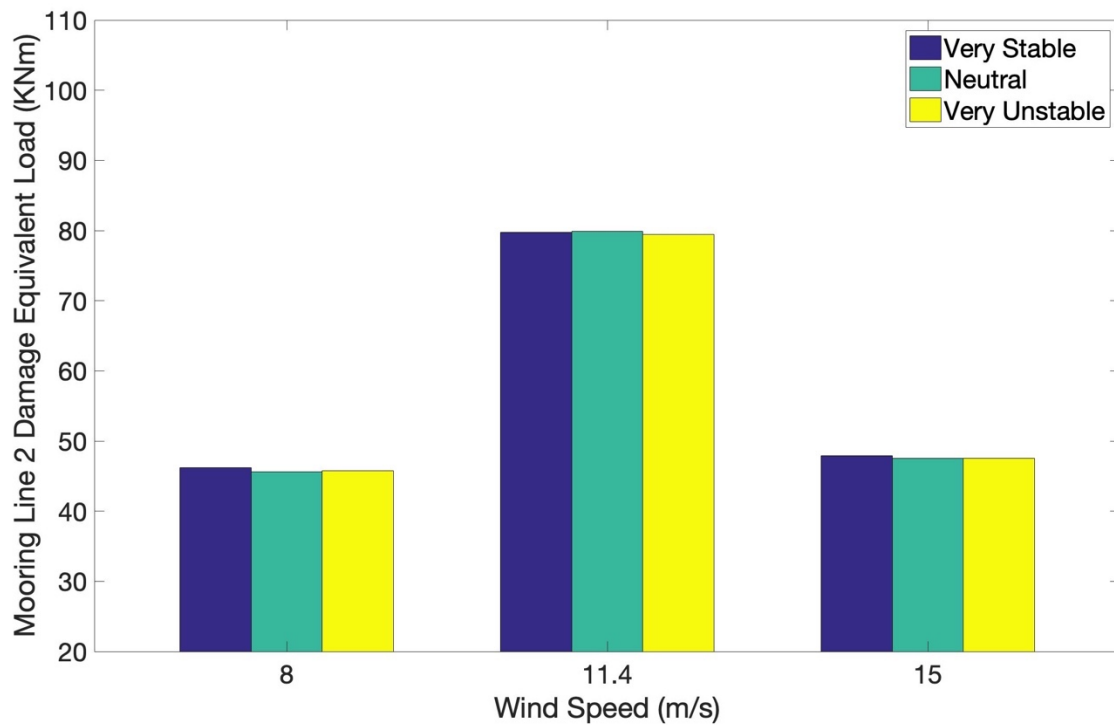
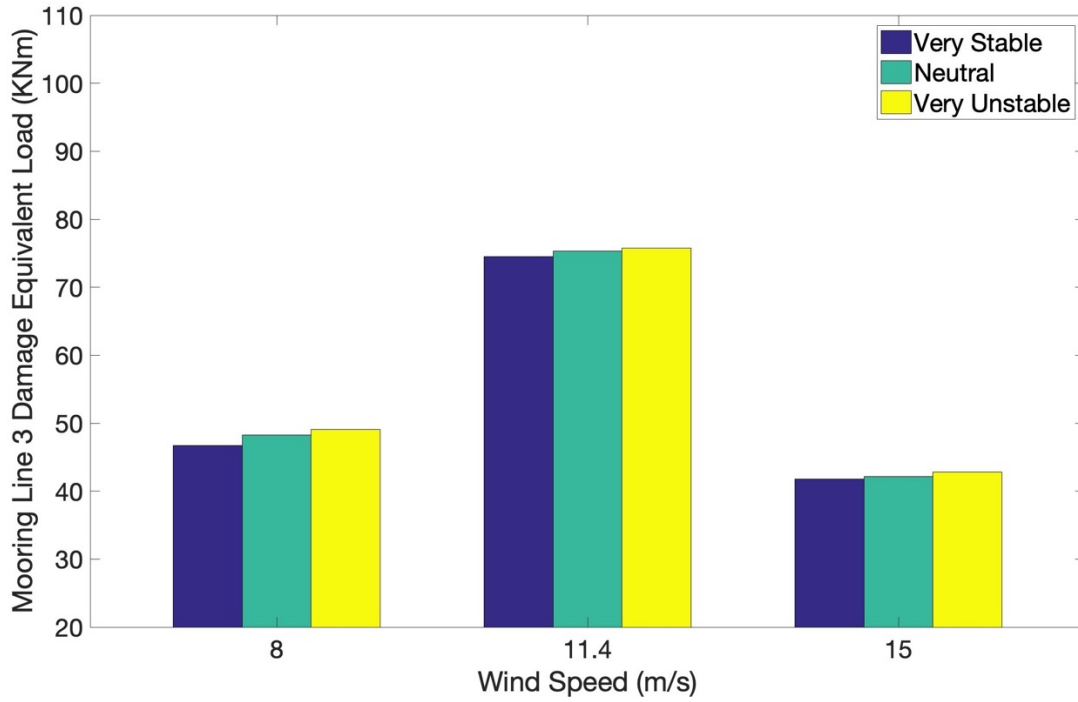


Figure A.14 Mooring Line 2 Damage Equivalent Loads without Turbulence under Each Stability for 8 m/s, 11.4 m/s and 15 m/s



*Figure A.15 Mooring Line 3 Damage Equivalent Loads without Turbulence under Each Stability for 8 m/s, 11.4 m/s and 15 m/s*

## A.2.2 Comparison of Tower Base Fore-Aft Moment

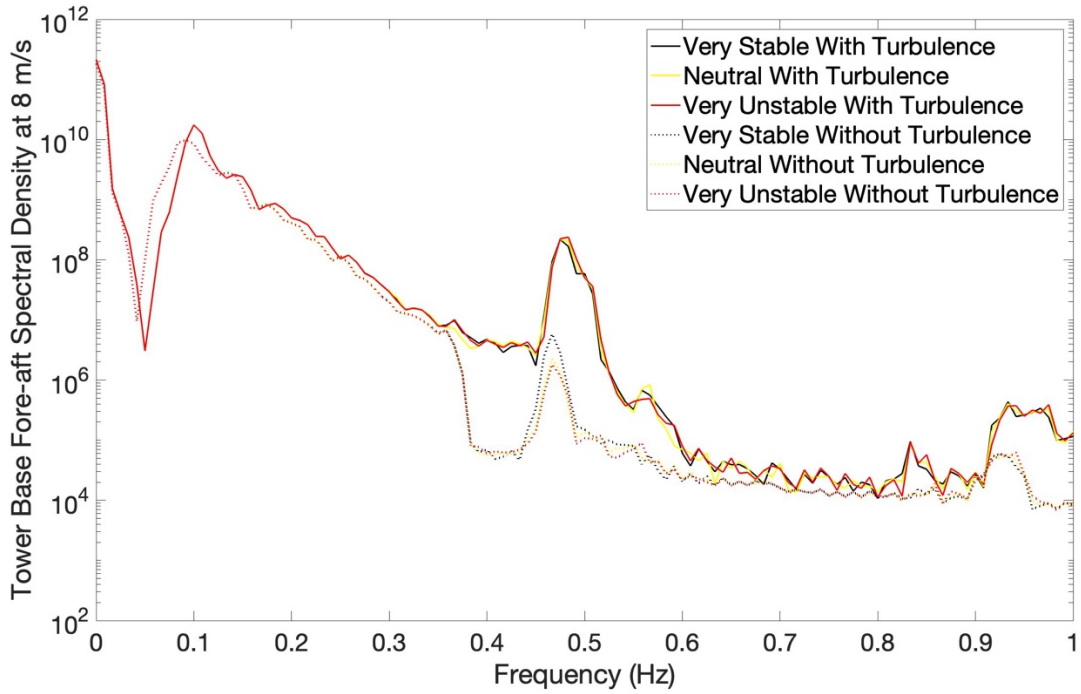


Figure A.16 Comparison of Tower Base Fore-Aft Moment Spectral Densities with Turbulence and without Turbulence under Each Stability for 8 m/s

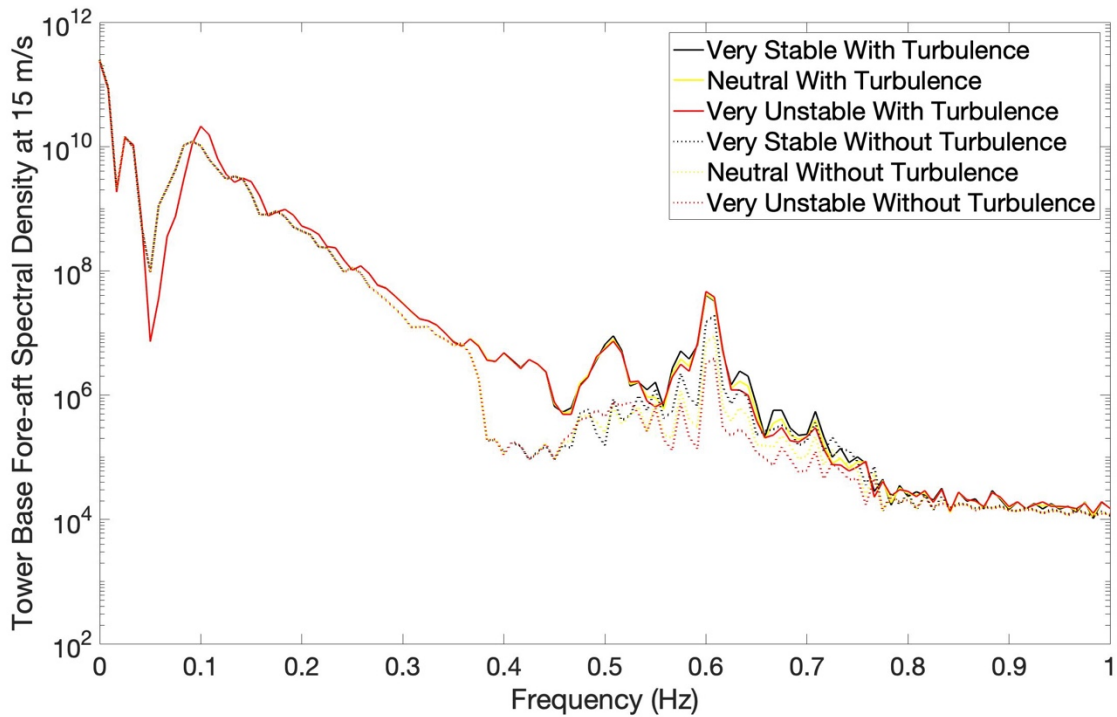


Figure A.17 Comparison of Tower Base Fore-Aft Moment Spectral Densities with Turbulence and without Turbulence under Each Stability for 15 m/s